MAPPING WHEAT WATER USE, YIELD GAP AND PRODUCTIVITY BASED ON CLIMATE AND SATELLITE DATA IN THE BERG RIVER CATCHMENT

JOSEPH TAUYANARWO MAZANGO
(MSc AGRICULTURAL ENGINEERING - IRRIGATION OPTION)

Thesis presented in partial fulfilment of the requirements for the degree of

Master of Science (in Geoinformatics)

in the Faculty of Science at Stellenbosch University

SUPERVISOR: DR Z MÜNCH

December 2020

DEPARTMENT OF GEOGRAPHY AND ENVIRONMENTAL STUDIES

DECLARATION

By submitting this report electronically, I declare that the entirety of the work contained therein is my own, original work, that I am the sole author thereof (save to the extent explicitly otherwise stated), that reproduction and publication thereof by Stellenbosch University will not infringe any third party rights and that I have not previously in its entirety or in part submitted it for obtaining any qualification.

Date: 26th October 2020

SUMMARY

The world population is forecast to increase substantially in the coming decades and doubling of current food production to meet expected demand is envisaged. The Western Cape (WC) of South Africa (SA) is a dryland winter wheat production area with average yield levels below the national average. It was important to ascertain whether the current wheat production levels are optimal or potential exists to increase yields. The study intended to establish wheat yields, estimate seasonal water use and subsequently compute study area wheat yield gaps and water productivity. The study was implemented in part of the Berg river catchment area for the 2016 season winter wheat crop. The Penman Monteith (PM) and Hargreaves Samani (HS) reference ET_0 were compiled and computed respectively using Python scripts and compiled into a Julian day (JD) indexed databases. The daily distributed reference crop evapotranspiration ET_{0PM} and ET_{0HS} surfaces were interpolated using the spline with tension interpolator implemented in ArcMap. Seasonal distributed wheat crop water use (ET_c) was determined from Sentinel 2 (S_2) and Landsat 8 (L_8) NDVI modelled crop coefficients and ET_0. Wheat crop yield surfaces were modelled from L_8 and S_2 scenes of the 4th and 5th of August 2016 respectively. From the statistical analysis of validated yield data, the within study area, regional and globally benchmarked wheat yield gaps were estimated.

The at-station generated ET_{0HS} were validated based on ET_{0PM} using the absolute and relative difference statistical measures. The results indicated that climate station ET_{0HS} deviated from the monthly ET_{0PM} values in the year 2016 with the magnitude of the differences higher in some stations and certain months. Although the ET_{0HS} and ET_{0PM} were generally in close range of each other, the ET_{0HS} values were consistently higher in nearly all the months, except in January, March and December. The climate station ET_{0HS} and ET_{0PM} differences although large in absolute terms had a low annual RMSE of 0.426 mm.day^{-1}. The averaged percent relative difference (RD %) indicated that ET_{0HS} estimates were within 20% of the ET_{0PM}. The results indicate that the ET_{0HS} adequately estimates reference crop evapotranspiration in the study area. Both the S_2 and L_8 based crop coefficients (K_{cS2} and K_{cL8}) were low at the start of the season at 0.236 and 0.185 level, and increased to a maximum of 0.954 and 0.66 mm.day^{-1} by mid-season on JD 217, respectively. Thereafter the K_c values decreased. The computed seasonal K_{cS2} and K_{cL8} values and plotted curves conform to those indicated in the literature, validating the NDVI based K_c in crop water use estimation studies. However, the K_{cS2} had consistently higher values than those estimated using the Landsat 8 NDVI (K_{cL8}).

The seasonal wheat crop water use patterns indicated that the ET_{0HS} and the K_{cS2} based ET_c consistently overestimated crop water use when compared to the ET_{0PM} and K_{cL8} based crop ET_c.

Study area wide crop water use data based on PM and HS methodologies, and S_2 and L_8 modelled K_c were extracted using the zonal statistic as table tool in ArcMap. The median statistic values indicated that the season wheat crop water use was generally low and less than the expected values cited in literature. This was likely due to the drought conditions during the 2016 winter wheat growing season. The range in ET_c values obtained were due to differences observed at the level of ET_0 and K_c computation. The L_8 modelled crop coefficients had lower values than the S_2 coefficients. In addition, the ET_{0HS} had consistently higher vales than the ET_{0PM}.

The best wheat yield metrics were obtained from the L_8 based wheat yield maximum statistic with RMSE less than one t.ha^{-1} while the corresponding S_2 based wheat yield estimate showed a RMSE of 3 t.ha^{-1}. The mean wheat yield for S_2 was relatively more accurate than the L_8 sensor based wheat yield mean statistic with lower RMSE of 1.408 compared to 1.865 t.ha^{-1}. For both S_2 and L_8 the median maximum yield statistic results were higher than the corresponding mean of the maximum statistic values.

The mean-based within study area wheat yield gaps gave comparable results using S_2 and L_8 imagery of 1.51 and 1.78 t.ha^{-1} respectively. Similarly the median-based statistic was computed giving yield gaps of 1.36 and 1.47 t.ha^{-1} respectively. These were compared with yield gaps obtained using mean SA irrigated, SA dryland and Northern Cape irrigated wheat study area median of maximum zonal statistics of 2.39, -1.51 and 3.65 t.ha^{-1} respectively. These results indicated that the study area had yields that were higher than the national dryland average and that an additional 3.65 t.ha^{-1} to current yield level could be attained in the WC with irrigation.

The observed study area water productivity metrics of 0.39 to 0.43 kg.m^{-3} established using the L_8 yields to ET_{cPML8} and ET_{cHSL8} mean statistics respectively, indicated the existence of wheat production augmentation potential considering the possible 2kg.m^{-3} attained in high wheat production regions. The corresponding S_2 yield to ET_{cPMS2} and ET_{cHSS2} WP were 1.89 and 1.79 kg.m^{-3} respectively, which was more than 4 times the L_8 estimates. The study results showcased the utility of geographic information systems (GIS), remote sensing (RS) and tabular climate data in determining wheat water use and yield characteristics. The crop performance characterisation has been specified in United Nations sustainable development goals (SDGs). Studies of this nature are important decision support tools in the planning and management for sustainable irrigation projects to meet the escalating world food demand.

Keywords:

Wheat production, crop water use, evapotranspiration, water productivity, crop yield, yield gap.

OPSOMMING

Daar word voorspel dat die wêreldbevolking in die komende dekades aansienlik sal toeneem en dat die huidige voedselproduksie sal moet verdubbel om aan die verwagte aanvraag te voldoen. Die Wes-Kaap (WK) van Suid-Afrika (SA) is 'n droëland-winterkoringproduksiegebied met 'n gemiddelde opbrengsvlak onder die nasionale gemiddelde. Dit is dus belangrik om vas te stel of die huidige koringproduksievlakke optimaal is en of daar potensiaal is om opbrengste te verhoog. Die studie het ten doel gehad om koringopbrengste te bepaal, seisoenale watergebruik te skat en vervolgens koringopbrengskoers en waterproduktiwiteit in die studiegebied te bereken. Die studie is uitgevoer in 'n gedeelte van die Bergrivier-opvanggebied vir die winterkoringoes van 2016. Die verwysingsevapotranspirasie ET_0 van Penman Monteith (PM) en Hargreaves Samani (HS) is met behulp van Python-kode bereken en saamgestel in 'n databasis op Juliaanse dag (JD) geïndekseer. Daaglikse verspreide verwysingsevapotranspirasie oppervlaktes (ET_{0PM}- en ET_{0HS}) is geïnterpoleer met behulp van die spline met spanningsinterpolator in ArcMap sagteware. Seisoenale verspreide koringgewaswaterverbruik (ET_c) is bereken vanaf Sentinel 2 (S_2) en Landsat 8 (L_8) NDVI-gemodelleerde gewaskoëffisiënte en ET_0. Koringoes-opbrengsoppervlaktes is gemodelleer vanaf L_8- en S_2-beelde van 4 en 5 Augustus 2016 onderskeidelik. Uit die statistiese ontleding van gevalideerde opbrengsdata is die gapings binne die studiegebied, streeks- en wêreldwye maatstaf vir koringopbrengskoerse geskat.

Die per-stasie gegenereerde ET_{0HS} is bekragtig deur middle van ET_{0PM} absolute en relatiewe verskilstatistieke. Die resultate het aangedui dat die klimaatstasie ET_{0HS} afwyk van die maandelikse ET_{0PM}-waardes in 2016 met die omvang van die verskille hoër in sommige stasies en sekere maande. Alhoewel die ET_{0HS} en ET_{0PM} oor die algemeen naby mekaar was, was die ET_{0HS}-waardes in alle maande hoër, behalwe in Januarie, Maart en Desember. Die klimaatstasie ET_{0HS}- en ET_{0PM}-verskille, hoewel groot in absolute terme, was die jaarlikse RMSE van 0.426 mm.dag^{-1} laag. Die gemiddelde persentasie relatiewe verskil (RD%) het aangedui dat ET_{0HS}-ramings binne 20% van die ET_{0PM} was. Die resultate dui aan dat die ET_{0HS} die evapotranspirasie van gewasse in die studiegebied voldoende skat. Beide die S_2- en L_8-gebaseerde gewaskoëffisiënte (K_{cS2} en K_{cL8}) was laag aan die begin van die seisoen, en het op JD217 onderskeidelik tot 'n maksimum van 0.954 en 0.66 mm.dag^{-1} in die midseisoen toegeneem. Daarna het die K_c-waardes afgeneem. Die berekende seisoenale K_{cS2}- en K_{cL8}-waardes en kurwes stem ooreen met die aangedui in die literatuur, wat bevestig dat NDVI-gebaseerde K_c gebruik kan word in beramingsstudies vir gewaswatergebruik. Die K_{cS2} het egter deurgaans hoër waardes gehad as wat geskat is met behulp van die Landsat 8 NDVI (K_{cL8}).

Die seisoenale watergebruikspatrone vir koringgewasse het aangedui dat die ET_{0HS} en die K_{cS2}-gebaseerde ET_c die gewaswatergebruik konsekwent oorskat het in vergelyking met die ET_{0PM}- en K_{cL8}-gebaseerde ET_c. Sonestatistieke is gebruik om die maksimum-, minimum-, mediaan- en gemiddelde seisoengewaswatergebruikswaardes te bereken vanaf die PM en HS modelle met beide S_2 en L_8 sensors vir die koringgroeiseisoen in 2016. Die mediaanstatistiek het aangedui dat die seisoenale gebruik van koringgewasse laag was en minder as die verwagte waardes wat in die literatuur genoem word. Dit was waarskynlik as gevolg van die droogtetoestande gedurende die 2016 winter koringgroeiseisoen. Die verskeidenheid in ET_c-waardes wat verkry is, was as gevolg van verskille waargeneem op die vlak van ET_0- en K_c-berekening met laer waardes vir die L_8-gemodelleerde gewaskoëffisiënte as die S_2-gebaseerde koëffisiënte. Daarbenewens het die ET_{0HS} deurgaans hoër waardes gehad as die ET_{0PM}.

Die beste statistieke vir koringopbrengste is verkry vanaf die maksimum L_8-gebaseerde koringopbrengstes met RMSE minder as een $t.ha^{-1}$, terwyl die ooreenstemmende S_2-gebaseerde koringopbrengskatting 'n RMSE van 3 $t.ha^{-1}$ getoon het. Die gemiddelde koringopbrengs vir S_2 was relatief meer akkuraat as die L_8-gemiddelde statistiek met 'n laer RMSE van 1.408 $t.ha^{-1}$ vergeleke met 1.865 $t.ha^{-1}$. Vir beide S_2 en L_8 was die mediaan van die maksimum opbrengs statistieke resultate hoër as die ooreenstemmende gemiddelde van die maksimum statistiese waardes. Die gemiddeld-gebaseerde koringopbrengskoers in die studiegebied het vergelykbare resultate gelewer met behulp van S_2- en L_8-beelde van onderskeidelik 1.51 en 1.78 $t.ha^{-1}$. Net so is die mediaan-gebaseerde statistiek bereken, wat opbrengingskoers van onderskeidelik 1.36 en 1.47 $t.ha^{-1}$ gegee het. Hierdie waardes is vergelyk met opbrengskoers wat verkry is met gemiddelde SA besproeiings-, SA droëland- en Noord-Kaapse besproeiingskoringstudiegebied, gemiddeld van maksimum sonestatistieke van onderskeidelik 2.39, 1.51 en 3.65 $t.ha^{-1}$. Hierdie resultate het aangedui dat die opbrengste vir die studiearea hoër was as die nasionale droëlandgemiddelde en dat 'n addisionele 3.65 $t.ha^{-1}$ tot die huidige opbrengsvlak vir die studiegebied bygevoeg sou kon word onder besproeiing. Die waargenome waterproduktiwiteit statistiek vir die studiegebied van 0.39 tot 0.43 $kg.m^{-3}$, bepaal vanaf die L_8-opbrengste en onderskeidelik ET_{cPML8} en ET_{cHSL8}-gemiddelde statistieke, het die potensiaal van addisionele koringproduksie aangedui, met inagname van die moontlike 2 $kg.m^{-3}$ wat in hoë koringproduksiestreke verkry word. Die ooreenstemmende waterproduktiwiteit vanaf S_2-opbrengs en onderskeidelik ET_{cPMS2} en ET_{cHSS2} was 1.89 en 1.79 $kg.m^{-3}$, meer as vier keer die L_8-ramings. Alhoewel die resultate beïnvloed is deur sensoreienskappe en opbrengsmodel, het sommige van die resultate 'n akkurate uitbeelding van die studiegebied se koring watergebruik, waterproduktiwiteit en opbrengsvlakke aangedui. Die studie het dus die gebruik van geografiese inligtingstelsels (GIS), afstandwaarneming (RS) en getabuleerde klimaatdata bevestig in die bepaling van die koringoes prestasie-eienskappe in die

studiegebied, soos gespesifiseer in die Verenigde Nasies se doelwitte vir volhoubare ontwikkeling (SDG's). Studies van hierdie aard is belangrike hulpmiddels vir besluitneming in die beplanning en bestuur van volhoubare besproeiingsprojekte om in die toenemende wêreldaanvraag na voedsel te voorsien.

Trefwoorde:

Koringproduksie, gewaswatergebruik, evapotranspirasie, gewasproduktiwiteit, gewasopbrengs, opbrengsgaping.

ACKNOWLEDGEMENTS

I sincerely thank:

1. The almighty God who in his grace has shown his benevolence and allowed me to make this output a reality against all odds.

2. The SU, particularly Professor Adriaan van Niekerk for my admission as a special student and subsequently as researcher and notably the staff in the Department of Geography and Environmental studies for a job well done in the realisation of this study. The experience gained is suggestive of a growth trajectory of the University and the Geo-Informatics section in the Department.

3. The staff in the CGA contributed immensely for the hands-on skills acquisition in GIS and RS by attending to my numerous requests and impromptu visits to their offices in between regular subject matter sessions. Special mention Professor Adriaan van Niekerk and Mr P K Poona for facilitating extra practical sessions through Khaleed Balim.

4. Dr J Kemp & Dr H de Klerk for well-run courses.

5. Professor Adriaan van Niekerk & Dr Zahn Munch for financial assistance. The assistance rendered is greatly appreciated. Please continue doing this to all who will come knocking at your doors I do pray.

6. My supervisor Dr Zahn Munch mere words cannot express my gratitude, you stood your ground and implemented a plan, despite the ardour associated with project conception and execution and my occasional hesitations, you remained firm and steered me on. It's only due to a premonition equivalent hunch that made you believe in the viability of my study even at the conception phase when I was still revolving in circles. She critically nudged me on when I was faltering and feeling exasperated. Her encouragement and steadfastness under unfamiliar and difficult academic and trying financial situation I went through respectively has earned her a nickname, 'my iron lady" of Stellenbosch. You did well. By his grace the Almighty God has seen it fit to bless her efforts and mine by ensuring the successful completion of this phase for a purpose. He has created a holy launch pad from which further academic escalations will be made. To the faculty lecturers, your work was well administered, and your expressed desires that I complete the current phase of my research have been satisfied. I bear witness going forwards of your dedication to work by replicating your styles and research thrust.

7. The external examiner for the detailed critic, that gave birth to the current study report.

8. My family your loss in contact time with me was worth it. My mother Mrs Francisca Masheka and David Mazango, this output was due to you, and through your prayers. My late father Albert Tauyanarwo Masheka this output imprints his name through his projeny at Stellenbosch University and is suggestive of the potential he had, had he been exposed similarly. My children do your bit and become academics of repute.

CONTENTS

TABLES

FIGURES

ACRONYMS AND ABBREVIATIONS

A. D.	anno domini
APAR	Absorbed photosynthetic active radiation
ARC	Agricultural Research Council
ARM	Atmosphere Radiation Measurement
ATCOR2	Atmospheric and topographic correction 2
B_{4L8}	Landsat8 Band4
B_{5L8}	Landsat8 Band5
B_{1MODIS}	MODIS Band1
B_{2MODIS}	MODIS Band2
B_{4S2}	Sentinel2 Band4
B_{8S2}	Sentinel2 Band 8
B_{8AS2}	Sentinel2 Band8A
B	Satellite sensor band
BEWAB	BEsproeiingsWAterBestuursprogram
B.C	Before Christ
BC	Blaney & Criddle
B/C	Benefit cost ratios
BR	Bowen Ratio
CGA	Centre for Geographic Analysis
CSIR	Council for Scientific and Industrial Research
$WP_{yL8/ETcHSL8}$	Water productivity from Wheat yield L_8 based (y_{L8}) to ET_{cHSL8}
$WP_{yL8/ETcPML8}$	Water productivity from Wheat yield L_8 based(y_{S2}) to ET_{cPML8}
$WP_{YS2/ETcHSS2}$	Water productivity from Wheat yield S_2 based (y_{S2}) to ET_{cHSS2}
$WP_{YS2/ETcPMS2}$	Water productivity from Wheat yield S_2based (y_{L8}) to ET_{cPM}
C_3	C3 pathway to fix carbon (3-carbon molecule)
C_4	C4 pathway to fix carbon (4-carbon molecule)
cwu	Season crop water use
DA	Department of Agriculture
DEADP	Department of Environment Affairs and Development Planning
DEM	Digital elevation model
DN	Digital number
DWAF	Department of Water Affairs and Forestry

EEFlux	Google Earth Engine Evapotranspiration Flux
EM	Electromagnetic spectrum
EOS	End of season
EROS	Earth resources observation satellites
ET	Evapotranspiration (units are mm.day^{-1})
ET_c	Crop water use / Crop water requirements
ET_{cPML8}	Crop water use based on the PM at 30 m SR and $K_{c\ L8}$
ET_{cHSL8}	Crop water use based on the HS at 30 m SR and $K_{c\ L8}$
ET_{cPMS2}	Crop water use based on the PM at 10 m SR and $K_{c\ S2}$
ET_{cHSS2}	Crop water use based on the HS at 10 m SR and $K_{c\ S2}$
ET_0	Crop reference evapotranspiration
$ET_{0HS\ S2}$	Hargreaves Samani ET_0 at 10 m Spatial Resolution
$ET_{0HS\ L8}$	Hargreaves Samani ET_0 at 30 m Spatial Resolution
ET_{0j}	Reference evapotranspiration on Julian day j
ET_{0PMS2}	Penman Monteith ET_0 at 10 m Spatial Resolution
$ET_{0PM\ L8}$	Penman Monteith ET_0 at 30 m Spatial Resolution
ESA	European Space Agency
EVI	Enhanced vegetation index
FAO	Food and Agricultural Organization of the United Nations
FAS	Foreign Agricultural Services
Fc	Fractional canopy cover
FID	Field Identifier (unique identifier of an object in ArcGIS)
FPCIG	Focus module of the PC Geomatica software
GIS	Geographic Information Systems
GNSS	Global Navigation Satellite Systems
GPS	Global Positioning Systems
GTZ	German Technical Co-operation Agency (Gesellschaft für Technische Zusammenarbeit)
ha	Hectare
HH	Horizontal sent horizontal receive (wavelength polarisation)
HI	Harvest index
HS	Hargreaves & Samani
HV	Horizontal sent and vertical receive (wavelength polarisation)
IMF	International Monetary Fund
ILWIS	Integrated land and water information system

IPAD	International Production Assessment Division
IPC	Irrigation project cycle
IPCM	Irrigation project cycle management
IRR	Internal rate of return
K_{cL8}	Crop coefficient modelled from L_8, NDVI
K_{cS2}	Crop coefficient modelled from S_2, NDVI
kg	Kilogram
$kg.m^{-3}$	Kilograms per cubic meter (water productivity)
LAI	Leaf area index
l	Litre
L_8	Landsat 8 thematic mapper
LiDAR	Light detection and ranging
MAD	Management allowable depletion
m.a.s.l	Meters above sea level
METRIC	Mapping for evapotranspiration with internalized calibration
MTL	Landsat metadata file
MODIS	Moderate resolution imaging spectro radiometer
MOST	Monin–Obukhov (M–O) similarity theory
NDVI	Normalised difference vegetation index
$NDVI_{L8}$	Normalised difference vegetation index based on L_8 bands
$NDVI_{S2}$	Normalised difference vegetation index based on S_2 bands
NIR	Near infrared radiation
NPV	Net present value
OGA	Office of global analysis (USDA)
obs	observation
P	Penman
PA	Precision agriculture
PAR	Photosynthetic active radiation
PC	Project cycle
PCIGM	PCI Geomatica software
PCM	Project cycle management
PM	Penman Monteith
P-T	Priestley and Taylor
Ra	Radiation
RADAR	Radio azimuth direction and ranging

Rh_{min}	Minimum humidity
Rh_{max}	Maximum humidity
R_s	Solar radiation energy
RS	Remote sensing
RMSE	Root mean square error
RUE	Radiation use efficiency
SA	South Africa
SABI	Suid Afrikaanse besproeiingsinstituut
SAGIS	South African grain information system
SAVI	Soil adjusted vegetation index
SDGs	Sustainable development goals
SR	Spatial resolution
S_2	Sentinel 2 satellite
SEB	Surface energy balance
SEBAL	Surface energy balance algorithm for land
SEBI	Surface energy balance index
SEBS	Surface energy balance systems
SOS	Start of season
sp	species
SUDEM	Stellenbosch University digital elevation model
SVAT	Soil vegetation atmosphere transfer model
SWAT	Soil and water assessment tool
t	Tonne
$t.ha^{-1}$	Tonne per hectare (crop yield)
$t.mm^{-1}.ha^{-1}$	Tonne per mm per hectare (water productivity)
T_{mean}	Average temperature
T_{min}	Minimum temperature
T_{max}	Maximum temperature
UN	United Nations
USAID	United States Agency for International Development
USDA	United States Department of Agriculture
USGS	United States Geological Services
VH	Vertical sent and horizontal receive (wavelength polarisation)
VI	Vegetation index

VV	Vertical sent vertical receive (wavelength polarisation)
WC	Western Cape
WDRVI	Wide dynamic range vegetation index
WOFOST	World food studies
XML	Extensible mark-up language, text-based database (notepad)
Y_{L8}	Wheat yield based on L_8 at 30 m SR
Y_{S2}	Wheat yield based on S_2 at 10 m SR
Y_p	Yield potential

CHAPTER 1: WATER PRODUCTIVITY MAPPING USING GEOGRAPHICAL INFORMATION SYSTEMS AND REMOTE SENSING TECHNOLOGIES

1.1 BACKGROUND

The aggregate world population is rising (Cleland 2013) whereas food production growth rates are stagnating. Plateauing and declining food production rates characterise agricultural production in many regions of the world, e.g. France (Schauberger et al. 2018) and Germany (van Wart et al. 2013). The demand for agricultural products is driven by population growth, dietary shifts to animal products and crop based fuel production (Hoogeveen et al. 2009; Schulze 2016; Tilman et al. 2017). Although the average global population growth rates are decreasing there are regions where the declines still imply considerable population increases. According to Alexandratos & Bruinsma (2012), in the recent past Sub Saharan Africa (SSA) region population growth rate of 2.8 percent is forecast to decline to a still high 1.9 percent rate by 2050. The average global growth rate of 1.6 percent is expected to decline to 0.55 percent per year by 2050. In the period 1950 to 2010 the SSA population increased 4.6 times compared to European and worldwide population increases of 135 and 272 percent respectively (Cleland 2013). South Africa is located in the SSA region hence is expected to undergo similar demographic changes projected for the region. These envisaged aggregate population increases translate into escalating food demand.

Human diets strongly rely on wheat (Triticum aestivum L.), maize (Zea mays L.) and rice (Oryiza sativum L.) (Neumann et al. 2010) and given population growth more of these cereals will have to be produced. Increasing cereal production is associated with challenges in many regions of the world due to declining fresh water supplies, increasing non-agricultural water demands and downstream environmental requirements (Clark & Tilman 2017). Annual wheat production in South Africa (SA) lags domestic wheat consumption and imports of 2.0 million tonnes (t) were forecast for 2018 (Maluleke 2018). Past wheat production trends indicated rising overall SA average wheat production levels, at 1.11 and 3.57 tonnes per hectare (t.ha^{-1}) produced in 1989/90 and 2014/15, respectively, with the Western Cape (WC) province producing 1.62 and 2.95 t.ha^{-1} in the corresponding periods (OGA 2015). However, these SA wheat production rates are less than half the yield rates of major wheat producing countries e.g. Germany and France (van Wart et al. 2013; Schauberger et al. 2018). Furthermore, the SA wheat cultivated area has fluctuated widely in the past, with 2 million ha under wheat production in 1973/74, and in 1991/92 had declined to 700 000 ha. A severe drought coupled with government incentives resulted in wheat field

conversion to grazing pasture and natural grazing (Meyer et al. 2015). This resulted in wheat imports valued at 5 million US dollars.

Currently about 2.5 % WC cultivated area is irrigated (Vink & Tregurtha 2005). The irrigated crops include vegetables, deciduous fruits and vineyards with limited areas of irrigated wheat. Evidence of centre pivot irrigation is available on satellite imagery. According to a WEB, downloaded SAGL statistics only 1.456 % of the total WC wheat cultivated area was under irrigation in 2014/15 (SAGL 2020). This indicate that irrigation is not a widespread activity in the area. Traditionally wheat production in the WC has been dryland based, and dependant on winter rainfall. The WC dryland wheat yields' historical variability has been ascribed to unsteady and highly inconsistent winter rainfall patterns (IPAD 2013). In view of the historical wheat production variability mentioned, one could postulate that supplementary wheat irrigation could potentially contribute to wheat yield increases and stabilization. However, the realisation of irrigation benefits in the WC depends on freshwater supplies. Irrigation water resources are negatively impacted by recurrent droughts, increasing water usage competition from urban and industrial areas coupled with environmental requirements (DEADP. 2012b & 2013).

Irrigation is globally rated as the largest fresh water user, at an annual abstraction rate of seventy percent. Due to increasing non-agricultural competitive water demands, future freshwater resources availability for irrigation purposes is expected to decline (Schulze 2016). At the global scale irrigated agriculture is carried out on 17% of cropped land and contributes 40% of total food production (Siebert et al. 2005). Irrigation water use is estimated at over 70% of global freshwater withdrawals (Zaussinger et al. 2019) while in SA about 62% is used (DWAF 2004). The history of water resources development in the WC province and the developed capacities is outlined in the DWAF 2013 annual report (DWA F 2013).

The ~300 km Berg river which originates in the Groot Drakenstein mountains near the town of Franschhoek, drains a catchment area of ~9000 km^2 and is the principal source of fresh water in the study area (DWAF 2004). Several dams have been constructed on the Berg river which include the Berg river dam commissioned in 2008 (Water Wheel 2008) with a capacity of 130 010 mega litres. The Voëlvlei dam with capacity of 164 095 mega litres, commissioned in 1952 (DWAF 2013) marked the commencement of large water infrastructure projects in the WC. Despite the available water storage infrastructure in the WC the frequently occurring droughts of prolonged duration have further exacerbated fresh water availability. According to the Department of Environment Affairs and Development Planning (DEADP), climate change induced temperature rise has increased droughts occurrences in the region (DEADP. 2012b & 2013) The decade prior to the wet winter seasons of 2018 and 2019, the WC experienced a prolonged dry spell and WC

dams only reached 60% of their full capacity despite the high fresh-water inflows experienced in the previous three winter seasons (Archer et al. 2019).

In addition to climate change challenges that negatively impact freshwater resources development, irrigation technology utilization involves the use of scarce capital resources and hence the need for appraisal to ascertain project viability before implementation (Baum 1978; Youker 1989; Gittinger 1984). Irrigation projects are appraised based on the broad field of project cycle management's (PCM) feasibility stages (Baum 1978). The PCM for irrigation projects require intensive data inputs from a considerable range of scientific disciplines that include among others agronomy, land and water, and their physical and chemical attributes respectively, climatology, engineering and economics (Savva & Frenken 2002). The operational use of the emerging sciences of geographic information systems (GIS) and remote sensing (RS) are expected to play increasing roles in the provisioning and integrated analysis of these data. The current study intended to determine the study area wheat crop water use performance parameters from tabular climate and RS data sets, and to partially establish yield potential, water consumptive use and productivity which are required when appraising projects. These principles recommended by Baum (1978) at the World Bank among others are deemed appropriate.

The PCM stages include the pre-feasibility stages, feasibility, implementation, monitoring and evaluation (Baum 1978; Gittinger 1984). Each PCM stage requires that decisions are made with regard to passing a project to the next stage or that it is eliminated based on technical, economic and or financial viability criteria. RS data sets are consistent and can be used over large study areas as opposed to depending solely on farmers' reported yields (Bastiaanssen & Bos 1999; Blatchford et al. 2019). Enhanced data quality ensures the integrity of investigations and the authenticity of decisions arrived at in the respective PCM stages. As noted by Bastiaanssen & Bos (1999), the data requirements will of necessity gravitate towards the use of GIS and RS to objectively identify and characterise the pertinent project variables for regional based irrigation studies. These data include the landform (topography) or appropriately modelled digital elevation models (DEM) for irrigation system designs and implementation (Maune 2011), yield modelling to estimate crop yield potential, water productivity and value of current production (Bastiaanssen & Bos 1999; Boogaard et al. 2013). Irrigation design is an engineering science that deals with the routing and sizing of water conveyance, distribution infrastructure and infield water application machinery and equipment, based on project area topography and cropping pattern's peak water requirements (Savva & Frenken 2002; SABI 2017). Economic and/or financial appraisal is carried out at the feasibility stage where the project net present values (NPV), the benefit cost ratios (B/C) and the

internal rate of return (IRR) are calculated (Baum 1978; Gittinger 1984; Youker 1989; Ward et al. 1991) based on which projects are rated.

The monitoring and evaluation phase is continuously carried out throughout the project cycle stages of pre-feasibility, feasibility (designs and appraisal) and irrigation scheduling (operational) by incorporating best practices acquired through experience in previous cycles. The success or failure of irrigation systems have been reportedly observed to depend on several factors chief among which are, the irrigation system used, system design quality and users' ability to operate the irrigation systems, project cropping pattern and produce market prices. The wheat yield performance indicator is specified by the United Nations (UN) sustainable development goals (SDGs) which stipulated that agricultural productivity should be doubled by 2030 and water use efficiency must substantially increase (Blatchford et al. 2019). The methodologies to estimate wheat water use, yields and gap, and thereafter water productivity are reviewed in Chapter 2. The importance of the performance variables are briefly outlined below and references texts and manuals by   Baum (1978); Gittinger (1984); Youker (1989); Ward et al. (1991) among others on economic project appraisal and irrigation designs are recommended.

Irrigation project designs are based on peak crop water requirements (SABI 2017). The forecasted daily crop water requirements are required as a basis for water rights application from the Department of Water Affairs (DWA) and should the irrigation scheme involve pumping, to estimate annual energy costs. Wheat yield estimates are necessary in computing the current value of production to give the "without" project income, an opportunity cost (Gittinger 1984) that is deductible from the irrigation gross project income. The "with" project income is estimated from the expected yield under irrigation and the market value. The difference between the "with" and the "without" project incomes is the gross income to irrigation use. These projected incomes can then be rated as incremental yield value based on the within study area or global based yield gaps (Lobell 2013). Traditional agronomic site trials generate point specific yield data that cannot be up scaled to characterize regional yields due to the non-representativeness of sites in the spatial and temporal domains. The projected world food requirements (Alexandratos & Bruinsma 2012) versus the required production intensification challenges that do not entail negative environmental impacts (Tilman et al. 2002) are dealt with in the research problem section.

1.2   RESEARCH PROBLEM

The growing world population requires food production augmentation, and it is unclear how this will be achieved. Dryland wheat production is the traditional and dominant wheat production system in the WC with current statistics indicating that only 2.5 % of cultivated area is irrigated (Vink & Tregurtha 2005). From a literature search made, wheat irrigation is not documented for

the WC, but evidence from satellite imagery indicates centre pivot foot prints. This might indicate that irrigation is not a widespread activity in the area. Investigating irrigation-based wheat production intensification opportunities in the WC could be justified on the basis that current production is predominantly rainfed and varies widely as a function of rainfall. The WC dryland wheat yields' historical variability has been ascribed to unsteady and highly inconsistent winter rainfall patterns (IPAD 2013). In combination with sustainable agricultural practices supplementary irrigation is expected to reduce yield fluctuations and augment yields. There is therefore a need to investigate the viability of irrigating wheat in the WC. Irrigation technology utilisation involves huge capital investments to acquire equipment and machinery, installation and operation, which must be offset by projected yield increases. Irrigation development is typically evaluated based on the PCM framework as proposed by Baum 1978 among others. Sustainability in irrigation projects is assured if the PCM procedures are judiciously followed at feasibility and relevant decisions undertaken. The estimation of study area data requirements for implementing a PCM based appraisal formed the basis of this enquiry. To satisfy the above criteria wheat crop water requirements and production potential were investigated using GIS, RS technologies (Bastiaanssen & Bos 1999).

The water storage infrastructure in the Berg river experiences pressure from escalating abstraction of fresh water for domestic, agricultural and industrial use, exacerbated by the reduced inflows into the Berg river dams due to prolonged droughts now occurring more frequently (Archer et al. 2019). The current scenario in the WC of decreasing fresh water supplies versus increased freshwater demand in non-agricultural activities necessitates a more detailed and critical scrutiny of costs and benefits when appraising the potential of irrigation use. Further expansion in agricultural water use in the WC is only justifiable based on water availability and irrigation viability. The continued availability of satellite technology and improvements in processing software, coupled with free data access policies of the major satellite image data archivers, and usage of accurate models can facilitates the determination of crop water use and yield estimates at increasing spatial and temporal scales (Lobell et al. 2003). In 2008, the United States Geological survey department (USGS) decided to make the entire archive of Landsat satellite data, available at no charge to the research community (http://landsat.usgs.gov/). A similar policy has been adopted by the European space agency (ESA) for Sentinel data. Improvements in pre-processing algorithms to geographically register images is enhancing the utility of remotely sensed data in the objective and precise determination of vegetation indices (VI), which can be used to estimate wheat yields and water use crop coefficients at pixel level (Lobell et al. 2003; Calera et al. 2017). Irrigation systems project cycle management require data at increasing temporal and spatial scales

to facilitate timely intervention in inputs application, chief among which is water for sustainable crop production intensification purposes (Tilman 2002; Calera et al. 2017).

The irrigation project cycle management stages utilize basin scale preliminary estimates of reference climate evaporative demand followed by detailed stages where annual project area crop water requirements are outlined , from which the peak crop water requirements can be ascertained and annual energy consumption estimated (Savva & Frenken 2002). Additional data requirements cover agronomic aspects in crop selection and annual cropping pattern which depend on the project area climate, physical and chemical properties of soils and water available and expected yields. The project is evaluated based on the difference in income between the current production levels to the value of expected project crop yields (Gittinger 1984). It is proposed to use the yield gap analysis concept (Lobell 2013, Sosibo et al, 2016) to estimate study area wheat production potential.

Given these data requirements, the following research questions were formulated: -

1. How accurate is the estimated wheat crop water use and yields based on remote sensing and available climate station data when compared with available within study area ground truth data?

2. Can these available variables (RS data sets and climate data) be used to accurately determine the study area wheat yield potential and wheat water productivity levels?

3. Can a yield model developed using a coarse spatial resolution accurately determine yields using higher spatial resolutions sensor data?

4. To what extend can the modelled yields facilitate the estimation of the within study area and globally benchmarked wheat yield gaps?

1.3   RESEARCH AIM AND OBJECTIVES

The aim of this study is to characterise and establish current crop water use, wheat yield and yield gaps, as well as water productivity, thereby demonstrating the potential utility of GIS and RS in provisioning critical data inputs required in irrigation project cycle management (PCM) (Baum 1978).

In order to address the research questions in Section 1.1 the following aims / objectives were proposed:-

1. Generate study area reference crop water requirements surfaces using tabular climate station data.

   The specific objectives were to

    a. determine the ET_{0HS} based on climatic data using Python scripts

    b. interpolate the ET_{0PM} and ET_{0HS} surface using the spline with tension interpolator implemented in ArcMap using an Arcpy scripts.

2. Compute the study area seasonal wheat water use surfaces for the WC, 2016 wheat growing season.

The specific objectives were to

    a. use ArcMap and PCIGM software and developed Python scripts in the processing of satellite imagery DN values to ground reflectance and thereafter the computation of NDVI,

    b. model crop coefficients(K_c) from NDVI, and

    c. computation of the wheat season crop water use (ET_c)based on Python Scripts in ArcMap.

3. Model the study area wheat yields using an empirical formulation applied on wheat normalised difference vegetation index (NDVI) at flowering stage as proposed by Mashaba et al. (2017).

4. Determine the water productivities based on modelled wheat yields and ET_c surfaces respectively.

5. Establish the study area wheat yield gap based on the mean yield and the 95th percentile yield values of the L_8 and S_2 modelled yields respectively (Lobel 2013) and from global based mean yields comparison as suggested by Sosibo et al. (2016) among others.

1.4   RESEARCH DESIGN

This was a quantitative study based on physical and empirical models to map the distributed winter wheat crop water use and yields for the 2016 winter wheat growing season, from satellite and climate data. The current study uses climate data and remotely sensed data sets from S_2 and L_8 satellites. The models used in the derivation of crop water use and crop yield estimates are based on NDVI, as outlined in the research flow diagram seen in Figure 1.1.
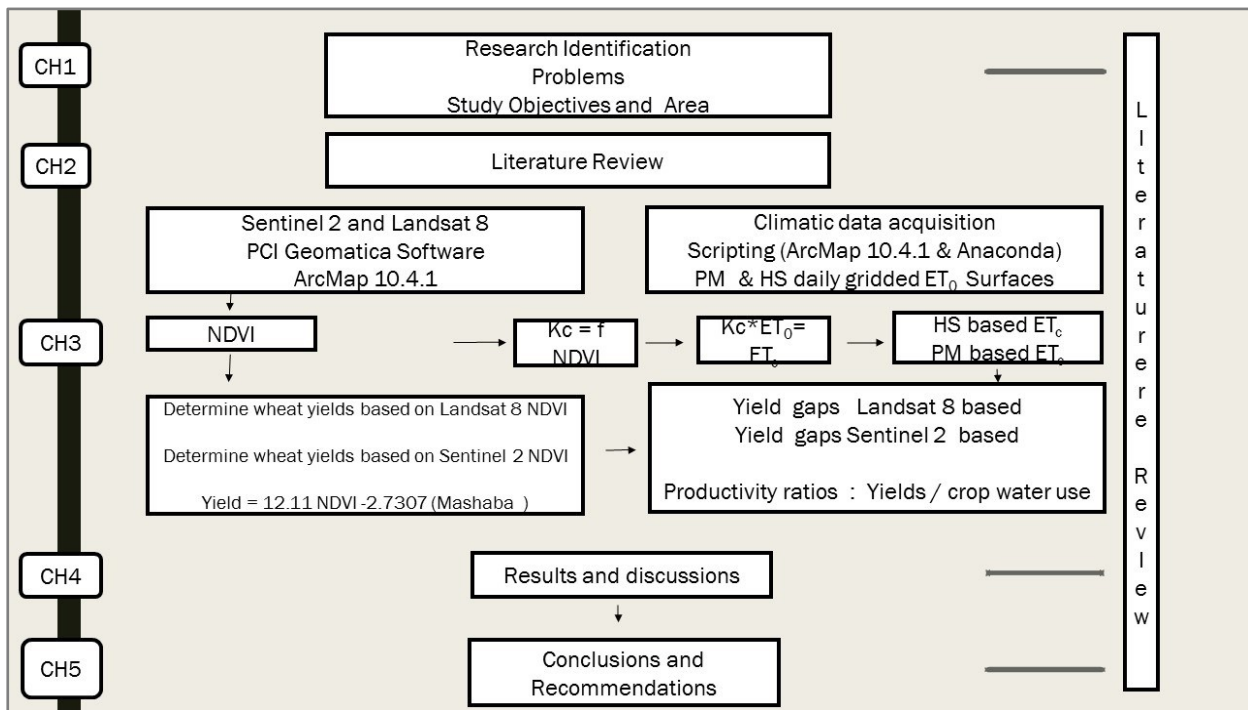
Figure 1.1 Research flow diagram

As outlined in the research flow diagram Figure 1.1, Chapter 1 details the study background, the research problem, research aims and objectives, the research framework and study area. The literature review is presented in Chapter 2. It includes the theoretical and practical aspects of the methodologies in use to estimate crop water requirements, wheat yield, water productivity and the wheat yield gap. The literature review is meant to enlighten the reader of the methodologies used in determining crop water use and yields, and to justify the selection of methodologies chosen in the current study. In Chapter 3 the methodologies used are presented, including the specific steps and procedures taken in carrying out the research. The results are presented in Chapter 4. In Chapter 5, based on the research findings, the results are discussed and conclusions made including proposals to upscale the enquiry in future research at a more advanced level suggested.

CHAPTER 2: LITERATURE REVIEW

The literature review introduces the importance of irrigation project appraisal for sustainable development. Irrigation project cycle management (IPCM) is a data intensive activity requiring inputs from a range of disciplines that include among others agronomy, climatology, engineering and economics (Savva & Frenken 2002; SABI 2017). The general data requirements for the specific stages of the irrigation project cycle (IPC) will be outlined followed by the literature review of the methodologies used in the current study. The study methodologies that are traditionally used in the generation of time series data will also be covered, including those that can be utilised on GIS platforms with inputs from RS data. Available methodologies as identified in the literature will be reviewed with respect to suitability of use in the current study. Physically based, analytical and empirical methods or combinations thereof will be covered. Data relevancy in IPCM stages per section will be introduced, followed by methodological reviews of the approaches in use to quantify the respective variables and ascertain the strengths and weaknesses of the methodologies, and including where applicable observational technologies employed. Finally, a general review of GIS and RS technology will be presented with emphasis on use in the agricultural sciences generally and more specifically project cycle (PC) data provisioning. The literature review chapter is structured into six sections, covering irrigation project cycle management, technological advances in GIS and RS technology, crop water used, wheat yield, yield gap and closure, and finally water productivity.

2.1 IRRIGATION DEVELOPMENT APPRAISAL

Irrigation is the artificial application of water to the soil to primarily meet the water needs of growing crops in addition to water supplied from effective rainfall and available soil profile moisture (Reinders 2011; Bjorneberg 2013). Irrigation water use is estimated at over 70% of global freshwater withdrawals (Zaussinger et al. 2019). Irrigation methods are broadly classified as surface, overhead and micro irrigation with some authors suggesting a fourth, sub-irrigation which involves raising the water table to near the root zone using ditches or subsurface drains (Savva & Frenken 2002; Reinders 2010; Bjorneberg 2013). Overhead and micro irrigation systems are more efficient with the latter having the highest water application efficiencies but is more capital intensive (SABI 2017).

According to Youker (1989) many international funded projects have failed to bear fruit in about two thirds of projects attempted. This has been attributed to hurriedly construed projects that are implemented without adequate scrutiny. Irrigated agriculture involves huge capital outlays, and consequently has to be appraised. Ideally implemented irrigation projects are required to have

passed sets of technical, economic and financial evaluative criteria that ensures technical and economic and or financial feasibility (Gittinger 1984; Youker 1989). Economic appraisal is carried out for national or multilateral funded projects whereas private / individual investments only require financial measures of viability. While there are many variables utilised in a full-scale irrigation project appraisal, the current research is limited to a one year (2016) snapshot characterisation of wheat crop and water performance variables i.e. actual wheat water consumptive use and yield, yield gaps and wheat water productivity. The proposed research variables were deemed adequate to establish the existence of wheat production potential in the study area. This was arrived at on the basis that current wheat crop yields are the primary input when computing the "without" project levels of production and income. Economic feasibility appraisals are primarily based on the difference using shadow prizes, between current production levels which is referred to as the "without" project, and the production level after project implementation which is called the "with" project scenario and the associated project capital and overhead costs (Gittinger 1984). The broad range of project feasibility variables discussed here, serves to outline the scope of issues included in a full scale irrigation project appraisal.

The cyclic nature of irrigation project investments over time was noted by Baum (1978). Since then the concept has evolved to the current analytical framework called project cycle management (PCM) which has been adopted by the development community e.g. United States Agency for International Development (USAID), German Technical Cooperation Agency (GTZ), the World bank and International Monetary Fund (IMF) to ensure worldwide sustainable irrigated agriculture development. The irrigation sector's overarching aims are the optimal irrigation water use for sustainable production of adequate human feed, fibre and energy requirements in the current complex world scenarios of increasing world populations. This in turn is coupled to the declining freshwater water for agriculture given increasing urban water requirements and global warming induced droughts (Tilman 2002; Schulze 2016). Statistical projections suggest that the world population is due to surpass the 9.8 billion level in 2050 from 2.5 billion in 1950 with SA's expected population increasing to 72 million by 2050 (Alexandratos & Bruinsma 2012). The population escalation implies augmentation in feed, food and energy requirements that can only be met by the increased use of irrigated agriculture. Rainfall volatility due to global warming poses real risks in dryland wheat production in the WC (Schulze 2016; Archer et al. 2019) hence the thrust in irrigation technology usage. However, historical evidence has indicated the negative environmental impacts attributable to irrigated agriculture.

Jacobsen & Adams (1958) noted, based on archaeological evidence and historical records, that wheat yield declined by 98% in 2100 B.C. when compared to yields in the year 3500 B.C, for

the Sumerian region of Iraq. Barley yields displayed a similar pattern whereby yields originally at 2537 l.ha^{-1} in 2400 B.C. declined to 897 l.ha^{-1} by 1700 B.C. They concluded that salinity was a major contributory factor in the wheat and barley yield reduction that possibly lead to the collapse of the Sumerian civilisation. The emerging and increasing non-agricultural competitive demands for water in the urban sector, freshwater fisheries and in the protection of natural ecosystems are further challenges to the continued and expanded use of fresh water in irrigation (Tilman et al. 2002; Schulze 2016). While the expansion of these competitive demands are important to agriculture they are not study variables in the current research.

In this section, IPCM stages are outlined and defined to present the irrigation sector from the perspective of multilateral funding and donor agencies e.g. the World Bank, USAID and GTZ who invariably are the major investors in irrigation development. The IPCM approach which informs on the justification of the current study will be elaborated on and the data requirements for specific stages outlined. This will be followed by an exposition of the utility of GIS and RS in data provisioning in IPC. The IPCM stages and concepts are presented next.

Baum (1978) identified the cyclic pattern of investment projects and proposed six stages for a complete cycle. The natural sequence in the way projects are planned and carried out was further elaborated on by Gittinger (1984) in a book entitled "Economic Analysis of Agricultural projects". The circular nature of the IPCM stages are depicted in Figure 2.1. For readers requiring more detailed information on the respective data requirements per IPCM stage, the FAO Irrigation manuals series by Savva & Frenken (2001) and the SABI (2017) among others can be consulted.

Although researchers indicated differing project cycle number of stages they all accept the concept of the cyclic nature of investment projects as depicted in Figure 2.1, which were adopted for use in the current research on projects cycle management (IPCM) (Youker 1989) as applied in irrigation appraisal studies.

The initial stage is project conception where initial/ preliminary investigations of project feasibility are effected. The pre-feasibility stage is followed by the feasibility stages where the detailed project plans are made, and appraisals carried out, then the implementation phase, monitoring and finally evaluation. The evaluation phase is carried throughout the project cycles whereby experience generated in the previous cycle is inputted in the subsequent cycles. Figure 2.1 clearly demonstrates that project failure to meet the required criteria per given stage leads to elimination, leaving the suitable projects to pass to subsequent stages. The elimination process is inculcated in PCM to forestall the implementation of projects which do not meet project criteria. The data requirements at each specific stage are described below but not all are a subject of this research.
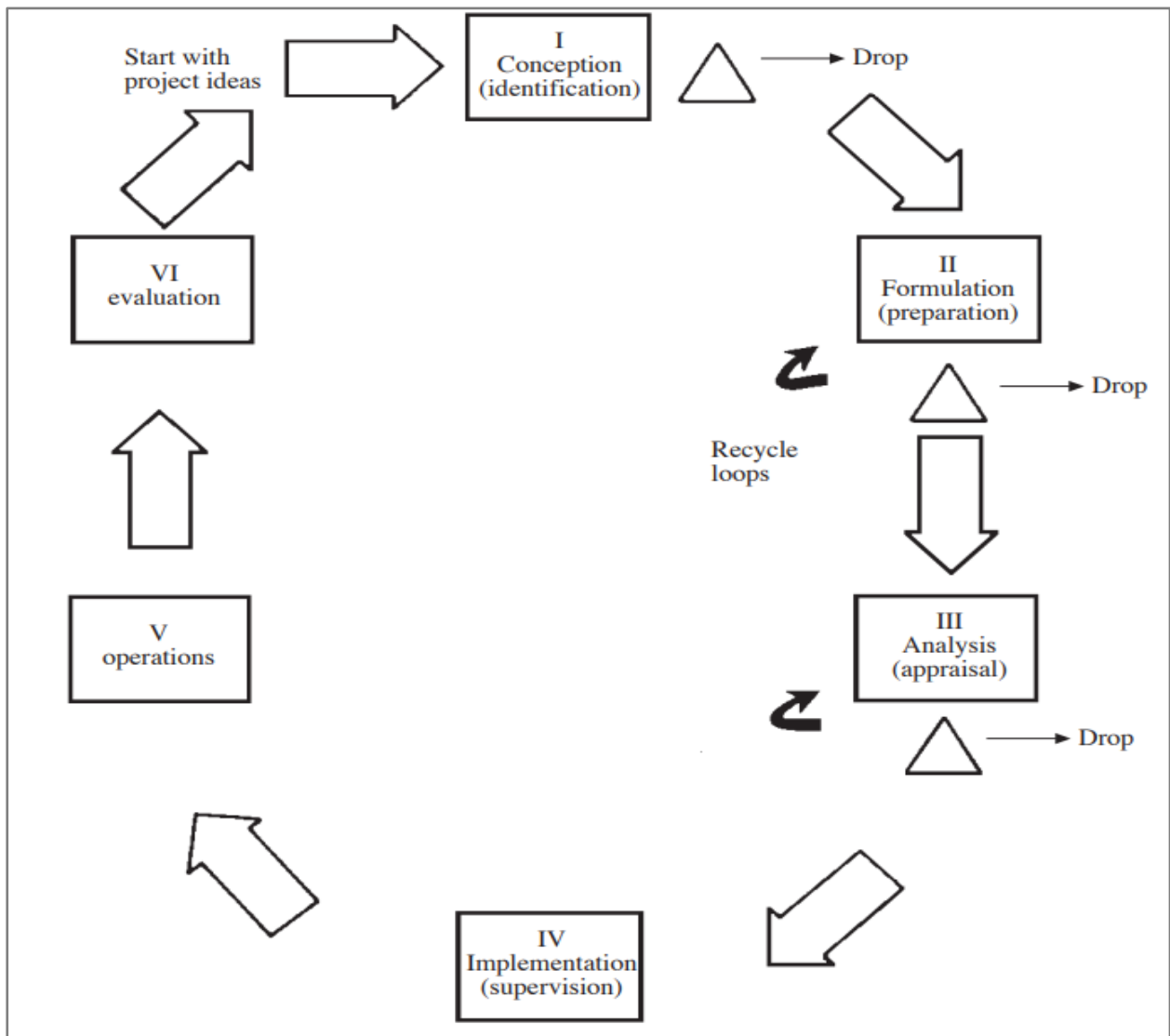
Source: Youker (1989)

Figure 2.1 The six stages of project cycle

The pre-feasibility stages data requirements aim to establish if irrigation is a plausible option within the study area. Technical and economic feasibility studies are tentatively attempted at pre-feasibility stage based on project area available resources, crop and water productivities and intended cropping patterns (Savva & Frenken 2001; 2002). The South African Irrigation Institute manuals (SABI 2017) details the steps involved in irrigation engineering designs for the pressurized irrigation systems. The irrigation resources typically include water, soils and climate. Data on current crop performance indicators with respect to yields, water productivities and value are critical for objective decision formulation. Low yield levels associated with high variability in crop yield indicate crop production potential in a given study area (Lobell 2013). On the contrary high yields coupled with low yield variability, suggests decreasing benefits to irrigation use. Furthermore, viability in irrigation use is the magnitude of the difference in value between the current project areas crops versus value of production under the proposed irrigation project. The

viability inferences required above can be arrived at based on variables investigated in the current research study.

The physical and chemical properties of water and soil available in the study areas have a bearing on the technical feasibility of proposed irrigation projects. As indicated earlier, concerning Iraq and in contemporary SA, salinity poses a real risk to irrigated agriculture (Jacobsen & Adams 1958; de Villiers et al. 2003, Van Niekerk et al. 2019). Salinity is defined as a build-up of toxic salts in the root zone due to a multiplicity of factors that affect crop productivity (Grattan 2002). Water table rise causes salinity, as water table water is typically saline and this is exacerbated by deep percolation losses, or irrigating soils with restricted profile drainage capacities. Irrigating with saline water without the incorporation of a leaching fraction leads to soil profile salinization. Salinity is therefore a significant threat to irrigation use and potential for its development has to be ascertained in the project cycle, preferably at the pre-feasibility stage such that corrective measures are inculcated.

Economics affect project viability in equal measure as physical considerations and therefore have to be considered in project appraisal (Gittinger 1984). Market considerations are critical in determining the volumes of produce that can be disposed of and the prices offered. Project success depends on the effective demand of irrigation produce at economic prices (Gittinger 1984). According to Gittinger (1984), projects that inherently have high operational costs are considered risky, especially in the context of agricultural produce which might have limited shelf lives and highly fluctuating market prices. If based on the factors presented the project could pass the pre-feasibility stage, then it will be subjected to a full-scale feasibility study, otherwise it will not be considered. Pre-feasibility and feasibility stage data requirements are essentially the same except in detail with the latter being more rigorous (Baum 1978). The feasibility stage involves the formulations of the detailed project plans, the irrigation system designs accompanied by the costed bill of quantities. The project physical inputs and outputs quantities must be identified including the respective price schedules. The project inputs and outputs are the irrigation infrastructure and operating annual costs to the irrigation project crop production volumes and values, respectively. The irrigation infrastructural and operating costs are based on the designs and pumping requirements, repairs and maintenance, and equipment and materials replacement schedule (Savva & Frenken 2001). For a semi-portable irrigation system the designs are based on the farm data as outlined in Figure 2.2.
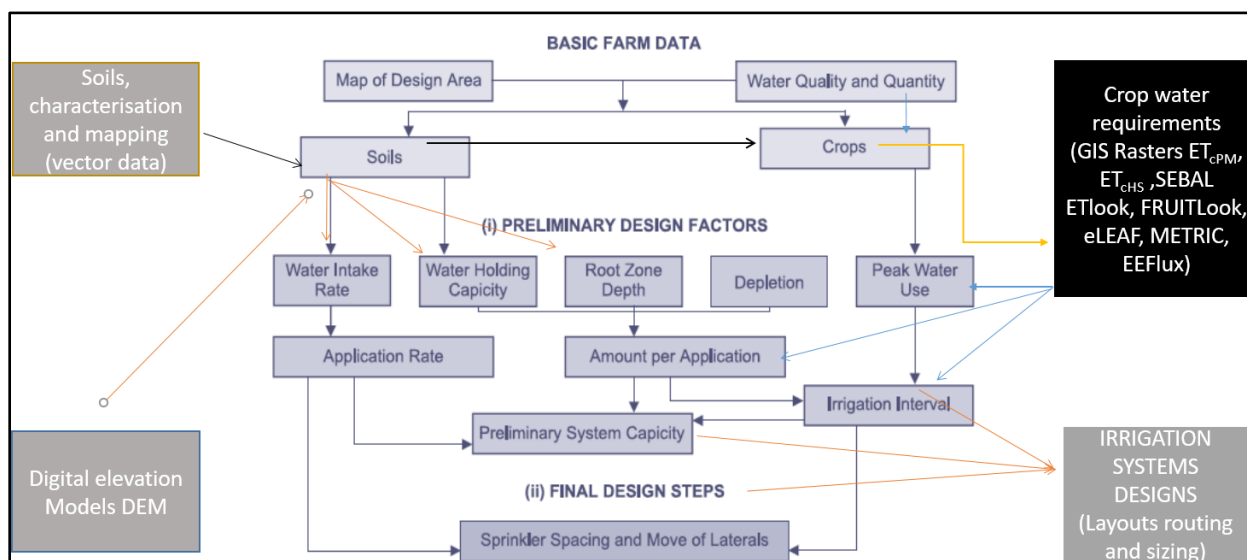
Figure 2.2 Irrigation System, adapted from Savva & Frenken (2001)

At feasibility stage two or more irrigation system options are usually designed and the technically efficient alternative adopted for implementation (Savva & Frenken 2001). Within the design parameters depicted in Figure 2.2, it is important to ascertain the impacts of soils and crop water requirements on irrigation systems water application rates, depth of irrigation and irrigation intervals. The irrigation system water application rates and irrigation depth are based on soil characteristics i.e. soil infiltration rates and soil water holding capacities (SABI 2017). The field water application equipment to be selected depend on the irrigation intervals, project area and project crop water requirements. Water applied at each irrigation event is calculated based on the dynamic interplay of crop water use based on climate evaporative demand in the irrigation interval and changes in soil moisture content also termed management allowable depletion (MAD) (SABI 2017). Furthermore and more importantly, scheme water application rates and irrigation duration times that exceed the soil water intake rates and soil water holding capacities, respectively leads to surface runoff and deep percolation losses, which are the biggest negative environmental impacts in irrigated agriculture associated with water table rise, root zone soil profile salinification and low water application efficiencies (de Villiers et al. 2003; Mouton 2019). According to Mouton (2019), 18% of irrigated agricultural land in SA is waterlogged or salinized. Van Niekerk et al. (2019) identified waterlogged and salinized agricultural landscapes in SA based on RS imagery, using object-oriented image classification methodologies. They highlighted the efficiencies associated with the use of RS in comparison to field monitoring campaigns in establishing salinity affected areas. Chemical and drainage-based methodologies can be implemented to reclaim the identified salt affected areas (Grattan 2002; de Villiers et al. 2003). This section gave a brief background to the importance of soils in irrigation designs and the need for its characterisation in feasibility studies. The landform modelled from a topographic map is a

major input in irrigation designs and is discussed next. This is intended to provide a concise background to readers interested in a comprehensive irrigation system appraisal that involves designs, and a fully-fledged feasibility analysis.

Irrigation engineering designs are typically carried out using a map populated with spot heights and contour lines as indicated in Figure 2.1. Irrigation designs involve routing irrigation water conveyance and distribution networks from water source to the irrigated fields, including infield application equipment layouts. After the layouts have been established, the irrigation infrastructure is sized based on the peak crop water requirements, soil characteristics and the MAD percentages (Walker 1989, Savva & Frenken 2001, 2002; Phocaides 2007, SABI 2017) among others. Surface irrigation schemes and micro irrigation systems are sensitive to topographic variation in the order of cm to mm and hence require detailed maps that adequately depict the terrain to facilitate irrigation systems design. Historically topographic maps were developed from manual surveys using Theodolites, Levelling machines and lately Total stations (e.g. Zeiske 2004). In addition, topographic maps can now be obtained by implementing a variety of methodologies on GIS platforms that include, geographic positioning systems (GPS) based surveys, photogrammetry based digital elevation models (DEM) derived from very high spatial resolution aerial, light detection and ranging (LIDAR), radio detection and ranging (RADAR) surveys (Nelson et al. 2009; Maune 2011). Utilisation of RADAR does not yield DEM of acceptable qualities for engineering purposes (Nelson et al. 2009). DEMs at varying spatial resolutions can be modelled in a cost-effective manner using GIS software interpolation schemes using surveys data from the indicated methodologies above (Childs 2004; Mitas & Mitasova 2005). The topographic map accuracies in the vertical and spatial domains has a bearing on the irrigation systems design qualities. Irrigation efficiencies are specified at three levels, conveyance, and distribution and application efficiencies. Irrigation designs aims to establish the most economic layouts which also minimises water losses (SABI 2017). The design procedure given the project terrain, soils and water characteristics, should establish the most technically efficient irrigation system. The background highlighted above serves to illustrate the potential technical pitfalls that can emanate from inaccurate representation of study area terrain. This is followed by a discussion that demonstrates the importance of the economic and or financial appraisal of irrigated agriculture in the IPCM.

The current study estimates the yield and yield gap which are required in carrying out the appraisal. Here the appraisal stage is taken as a post design stage where the detailed project documents and costings have already been made. Some authors include the appraisal stage in the feasibility stage e.g. (Gittinger 1984). The incremental benefit to irrigation is ascertained by considering the "with"

and the "without" project production scenarios values (Gittinger 1984). Establishing the "without" project production was historically accomplished by field campaigns to collect crop yield data from farmers, which is considered a costly exercise that does not necessarily yield objective data (Lobell et al. 2020). In a study in Uganda, Lobell et al. (2020) observed that RS based maize yield estimation was more accurate than farmer reported yields. The "with" project scenarios are based on estimating the annual value of the proposed crop production pattern. The magnitude of the difference between the "with" and the "without" project production values is the incremental benefit from irrigation development. This is then compared to the overall irrigation infrastructural costs and all annual overheads to determine the project net annual income. The feasibility stage is concluded with the determination of the economic and or financial appraisal viability indicators which are the net present value (NPV) (also called net present worth), the internal rate of return (IRR) and the benefit costs ratio (B/C) (Gittinger 1984; Youker 1989). Financial viability appraisal uses market prices within an economy as opposed to economic appraisal that uses the shadow pricing paradigm in costing project variable inputs and outputs. The appraisal template is similar for both the financial and economic approaches and spans a period of 15 to 25 years based on the longevity or replacement cycles of the major capital equipment. When appraisal is completed the project is implemented and becomes operational (Youker 1989).

Operational irrigation projects are assessed for water application adequacy and productivity, crop growth vigour and yields levels. Irrigation scheduling is the major water management input in irrigation systems management that mitigates negative environmental impacts of irrigation. Water application must be restricted to within the soil infiltration and water holding capacities to avoid run off and deep percolation losses which reduce water application efficiencies. A critical phase in irrigation project cycle management systems is irrigation scheduling which determines the amount of water to apply and the frequency of application. According to researchers (Reinders 2010; Lamm & Rogers 2014; Schulze 2016) water savings can be realised if scientific based crop water requirement estimation techniques are implemented and used in irrigation scheduling. This section has highlighted the importance of science-based crop water estimation at both feasibility and operational phases of the IPC to cope with irrigation scheduling and minimisation of negative environmental impacts of irrigation.

GIS and RS technology have potential to monitor a range of crop performance indicators at increasing temporal and spatial scales (Lobell et al. 2003). The potential use of GIS and RS technologies in estimating crop water requirements, crop yields and irrigation engineering designs layouts are discussed next.

The value of economic activities in the "without" irrigation project scenario is best characterized by GIS and RS outputs of land use /land cover (LU/LC) map of the study area. This map can be utilised to identify and quantify the current project area economic activities (Reis 2008). In addition, a novel output of GIS and RS is in determining current crop yield and water use at the pre-feasibility stage. A subsequent analysis of the characterised crop yields provide critical crop yield potential data pertinent in irrigation potential determination. Low crop water productivities are indicative of the physical potential for crop production intensification based on augmented water application. In contrast and based on the world wheat production statistics, Germany (van Wart et al. 2013) and France (Schauberger et al. 2018) are among the highest wheat producing nations with recorded national average yields of 7.6 and 7.0 t.ha^{-1}, respectively. These benchmark yield levels can be used as regional benchmarks in the computation of wheat yields gaps that are used in the estimation of the "with" irrigation project crop yields (Gittinger 1984). According to Grassini et al. (2013) study regions with very variable crop yields i.e. high yield gaps are indicative of potential of crop production intensification as opposed to regions where the yield variability is low, and the average yields are high. RS based crop yields and subsequently yield gap can be determined on GIS platforms using production models. For example, soil and water assessment tool (SWAT) (Schierhorn et al. 2014) and world food studies (WOFOST) (Boogaard et al. 2013) or single satellite image-based yield modelling (Mashaba et al. 2017). The current study area average yields are required in valuing current crop production which is an opportunity costs when embarking on an irrigation project and which can be determined from RS image VIs. According to Lobell et al. (2020), researchers have varying opinions on effectiveness of RS and GIS in yield monitoring it is generally agreed that physical survey methods are tedious and costly and are impractical to use for regional yields estimation studies and given the human input, lack consistence and objectivity achieved with RS and GIS based derived estimates. The perceived inaccuracies are more than offset by the objectiveness and consistence achieved with GIS and RS. VIs such as NDVI, enhanced vegetation index (EVI) and soil adjusted vegetation index (SAVI) can identify regions of impaired crop growth vigour and crop yields in either operational irrigation projects or rainfed agricultural production systems (Wiegand et al. 1991; Basso et al. 2004).

At pre-feasibility studies coarse DEMs can be used followed by high resolution DEMs at design stages. Crop production problem areas can be monitored from satellite images (Atzberger 2013). Salinity which is defined as toxic salts accumulation in the crop root zone (Schulze 2016) can be monitored from space or inferred from diminished crop growth vigour observable from VI variations (van Niekerk et al. 2019). Canal seepage is not easily identifiable from the ground, but synoptic satellite images based VI can point to lush vegetation along canal distributions networks. Crop coefficients modelled from vegetation indices have been found to improve on water

scheduling resulting in substantial water saving when compared to using the theoretical approach which results in excess water application (Reyes-González et al. 2018). The theoretical crop coefficient approach requires known planting dates and optimal water management, this was not applicable in the current study where wheat production was under dryland conditions with undefined planting dates, hence justifying satellite based K_c.

The current study intends to demonstrate the potential of GIS and RS in the determination of water/irrigation crop performance indicators for efficient and sustainable utilisation of irrigation technology in crop production in the current millennia. These indicators are crop water use, crop yields and water productivities. Technological advances which if exploited at farm field levels could mitigate the contemporary challenges of feeding the growing world population are discussed in the next section.

2.2   TECHNOLOGICAL ADVANCES IN RS AND GIS

The world is currently facing increasing challenges related to escalating agricultural production requirements to meet growing demand due to population growth, higher incomes, biofuel and feedstock demand (Hoogeveen et al. 2009; Schulze 2016). The above challenges are exacerbated by declining global agricultural resources of fresh water supply and land, and the recent negative impacts of climate change that threaten to render traditional dryland agricultural production unfeasible over large swath of the earth's surface (Du Plessis & Schloms 2017; Archer et al. 2019) among others. But there is a glimmer of hope which is premised on the potential exploitation of technological advances that has accrued in the digital age to develop crop production intensification strategies that can mitigate the negative impacts of global warming for sustainable development (Rowland et al. 2007). This section intends to outline briefly the observational capacities and growth registered in RS and GIS technologies respectively, that generates data which, when analysed could provide information critical for sustainable escalation of agricultural productivity. The aspects covered serves to illustrate with examples the utility of RS capabilities in monitoring plant growth, water consumption and yields which are a necessary background to the current study. The mention of GPS and Global navigation satellite system (GNSS) technologies, although not part of the current study is meant to indicates how the RS and GPS are used in precision agriculture (PA) (Basso et al. 2004; Walter et al. 2017). According to Walter et al. (2017), PA a form of conservation agriculture, is the technology expected to contribute to the sustainable intensification of agricultural production to meet the escalating global demand for food, feed and biofuel production feedstock, without incurring further negative environmental impacts. This is expected based on ascertaining the geo-spatial causes of yield gaps and addressing identified factors using PA aided by GPS (Basso et al. 2004). The next step in envisaged research

progression after the current study. Non-satellite based technological advances are discussed in Section 2.3 of the literature review in Chapter 2. Detailed and comprehensives reviews have been published and it's not intended to replicate them here but to highlight the major developments. Readers are referred to the following authors for detailed expositions on the matter, Light (1990); Toth & Józ´ków (2016) and Zhu et al. (2018) among others.

According to Toth & Józ´ków (2016) remote sensing is a rapidly advancing technology, mainly driven by imaging sensor development and endlessly increasing performance of the information infrastructure, including processing, storage and communication. Due to these rapid advances classical categorization is becoming increasingly difficult due to expanded integration. The discussion below follows the framework of Toth & Józ´ków (2016) which gives a comprehensive review of the RS and GIS innovations. Remote sensing has a long history commencing by the launch of Sputnik 1 satellite in 1957 by the Russians and as of 1990 the international community had launched more than 3000 satellites in space (Light 1990). The current active satellite population in space as at March 31st, 2019 was 2062, with 901 satellites operated by the USA, China operating 299 and Russia with the minimum number of 153 satellites (Mazareanu 2019). The expanding numbers of active satellites and satellite debris is viewed positively and negatively by scientists. Concerns have been registered since 2010 and possibly well before, about the satellites debris in space which totalled more than 15 000 objects (Wright 2010). The figures by Wright (2010) will be exceeded in the near future as more satellites are projected to be launched to replace decommissioned satellites and expected increases in new satellite constellations.

The reusability of rockets and the launching of multiple satellites from single missions is bound to lower the costs of deploying satellites in space (Zhu et al. 2018) and contribute to the availability of earth observation data at declining costs. The RS infrastructure is expanding phenomenally in tandem with the sensor characteristics enhancing satellite imaging capabilities. RS is defined as the noncontact technique whereby the image space can be observed. According to Lillesand & Keifer (1994) it is a science and art of obtaining information about the image space through analysis of remotely acquired data by a device that is not in contact with the object. This definition covers, satellite or airborne platforms acquiring optical and radar sensed data including airborne surveying and photogrammetry operations (Light 1990; Toth & Józ´ków 2016). RS technologies can be categorised by platforms on which the sensors are carried and orbital planes. Satellite sensors operate in different regions of the electromagnetic spectrum depending on the sensor design and envisaged data to collect. According to Zhu et al. (2018) RS platforms include airborne, terrestrial and space borne with the latter being the most stable. Satellites are categorised based on orbital geometry, of which there are three namely, geostationary, equatorial and sun synchronous.

The geostationary satellite stays over the same location over the earth and are used especially for telecommunication and weather purposes. The equatorial plane has a low inclination at 57^0 e.g. the Space shuttle orbiting the earth at an altitude of 300 km as opposed to the sun synchronous satellites that orbit the earth nearly over the poles at higher altitude and angles of inclination (also termed polar orbits) (Zhu et al. 2018). The sensors on board the satellites can be passive, depending on the sun for object illumination and they record the emitted or reflected electromagnetic (EM) radiation in the visible and near infrared regions. Active sensors on the other hand provide their own source of energy to illuminate objects and then record the return pulses (Anderson et al. 2006). The major disadvantages of passive sensors is atmospheric attenuation and intermittent coverage experienced due to clouds cover. The active and passive capabilities can be merged (Toth & Józ´ków 2016). The imaging capacities of typical active sensors systems depend on the use of single or multiple frequencies of either the C, L or X bands, using single or multiple polarisations i.e. HH, HV, VH & VV (Zhu et al. 2018). The active sensors bands are weatherproof having day and night time imaging capabilities as the sensors utilise the longwave region of the EM spectrum. The sensor imaging capabilities are typically characterised and evaluated, on a range of criteria that includes, the radiometric, spatial, spectral and temporal resolutions. Higher spatial resolution (SR) satellites are now available down from 1km to sub centimetre spatial resolutions. MODIS has an SR of 250 m in the visible as opposed to the Landsat 8 at 30 m SR and the Sentinel 2 constellation at 10 m spatial resolution and a five-day return period for the visible spectrum. Earth observation (EO) for crop phenology monitoring requires frequent images of high SR for monitoring crop growth status and management of timeous input application e.g. using Sentinel 2 at 10 m SR. Commercial satellites have RS products of high spatial and temporal resolution critical in PA (Basso et al. 2004).

The utility of RS has been enhanced by civilian access to the GNSS GPS system of satellites which were the preserve of the military from 1st of May, 2000 (https://www.cnet.com/news/celebrating-10-years-of-gps-for-the-masses /). Agricultural machinery currently under production includes GPS receivers for yield harvest mapping and facilitation of PA based interventions to target areas with restricted crop yields (Sing et al. 2013). In addition the European space agency (ESA) is building up another civilian based GPS called Galileo expected to be operational by 2020 (http://www.esa.int/Applications/Navigation/Galileo/What_is_Galileo). This facilitation was further augmented by the major satellite data archivers. USGS and ESA s' decisions for free data access policies of the entire Landsat series data (http://landsat.usgv/products) and Sentinel data (https://sentinel.esa.int/web/sentinel-data-access), respectively. In addition to data availability, the web based cloud computing platforms such as Google Earth Engine are set to expand the use of remote sensed data in EO for crop phenology and surface energy balance monitoring, for

determining crop water use e.g. using the L_8 thermal data (Shelestov et al. 2017). Other regions of the EM spectrum, the shortwave infrared (SWIR), C, L & X bands are utilised to monitor soil moisture which is a critical input in determination of crop water use. For example in ETLook soil moisture derived from passive microwave sensors is used in the determination of soil evaporation based on surface energy balances (Pelgrum et al. 2010; Bastiaanssen et al. 2012). Table 2.1 outlines a sample of satellites in space including their characteristics to give an indication of active satellites in space and capabilities.

Table 2.1 indicates that commercial satellite systems have higher spatial resolution and high return frequencies e.g. World View at 1.43 m SR and 4 days repeat cycles, respectively, which permit detailed imaging of crop phenological progression. Light detection and ranging (LIDAR) technologies generate highly resolved DEM for use in engineering services e.g. irrigation designs or farm infrastructure planning at sub centimetre accuracies from unmanned aerial vehicles (UAV) surveys data. Davidson et al. (2019) conducted research on airborne Lidar in precision mapping of the earth's surface and concluded that given the continued reduction in size, weight and power requirements UAVs can be engaged to perform the above tasks more cost effectively if ground control points (GCP) management is optimised.

The satellite sensor technical characteristics used in yield and crop coefficient modelling are reproduced in Table 2.1, to enable an informed analysis of the research findings. Also included is the MODIS sensor details, based on which the wheat yield model was formulated.

Table 2.1 Study satellite sensor characteristic

Satellite	Spatial Resolution (m)	Wavelength Red & Red band width (nm)	Wavelength NIR & NIR band width (nm)	Quantization	Where satellite data was used in the study?
MODIS	250	B_{1MODIS}, 620 -670,50	B_{2MODIS},841-876,35	12-bit	Mashaba et al. (2017) wheat yield formula
Landsat8	30	B_{4L8} ,636-673,37	B_{5L8},851-879,28	12-bit	NDVI, K_c, ET_c & Yield
Sentinel2	10	B_{4S2}, 665, 30	B_{8S2}, 842,115	16-bit	NDVI , K_c, ET_c &Yield
	20		B8A,865,20	16-bit	Not used

Bands have been abbreviated to B in Table 2.1. Please take note of the S_2, B_8 and B_{8A} bandwidths values. The S_2 B_{8A} has a bandwidth of 20 nm which is in the same range as the MODIS, B_1 at 35 nm and Landsat8 B_5 at 28 nm. Whereas the S_2B_8 (NIR) which was used in the study has a wide bandwith of 115 nm but with the same SR of 10 m as the S_2 R band.

Crops in addition to water requirements require nutrients from the soils. Remote sensing can monitor a range of variables related to soil fertility including soil salinity and water logging (Van

Niekerk et al. 2019) soil carbon content (Yang et al. 2015),crop yields (van Ittersum et al. 2013;
Mashaba et al. 2017) and crop growth vigour based on vegetation indices NDVI, EVI and SAVI

Table 2.2 Active satellites examples compiled from internet sources

Satellite constellation	Date launched	Characteristics	Data site	Source
MODIS Offers continuity to NOAAs Advanced very high-resolution radiometer	Terra platform 1999 Aqua platform 2002	Bands 1 & 2 at 250 m SR Bands 3 -7 at 500 m SR Bands 8 -17 at 1000 m SR 12 bits pixels Repeat cycle 16 days	https://earth.esa.int/web/guest/home http://ladsweb.nascom.nasa.gov/ https://lpdaac.usgs.gov/ http://nsidc.org/daac/modis/index.html http://oceancolor.gsfc.nasa.gov/	https://modis.gsfc.nasa.gov/about/specifications.php
TerraSAR X Active sensors German	June 15th ,2007	Sun synchronous orbit Inclined at 97.440 Centre frequency 9.65 GHz (X Band) Single or dual including quadruple polarisation modes. Repeat cycle 11 days Altitude 514km	https://spacedata.copernicus.eu/web/cscda/missions/terrasar-x	https://earth.esa.int/web/eoportal/satellite-missions/content/-/article/terrasar-x
RADARSAT Active sensors Canada	June 12th, 2019	Sun synchronous orbit inclined at 98.60 Swath 45 to 500km Centre Frequency 5.405 GHz (C Band) Orbit duration ~ 100 minutes Repeat cycle Altitude 798 km	https://www.asc-csa.gc.ca/eng/satellites/radarsat/default.asp	https://www.asc-csa.gc.ca/eng/satellites/radarsat/default.asp
Landsat8 16 Bit USA	February 11th ,2013	Pan:15m, OLI MSS:30m, TIRS 100 m and RS to 30 m GeoTIFF, Altitude 705km Swath width 16-bit pixels Repeat cycle 16 days Datum WGS 84	Earth Explorer, http://earthexplorer.usgs.gov. GloVis http://glovis.usgs.gov LandsatLook Viewer, http://landsatlook.usgs.gov.	https://landsat.gsfc.nasa.gov/landsat-data-continuity-mission/
Sentienl2 two polar orbiting constellation S2A & S2B ESA European Union	June 15th, 2015 & March 7th, 2017	MSI: 10 m SR, 12 Bit	https://earth.esa.int/web/guest/home	https://www.satimagingcorp.com/satellite-sensors/other-satellite-sensors/sentinel-2a/
World view 4 (Previously known as Geoeye)	November 11th, 2016	Laser altimeter and MSS Pan 0.31cm, MS 1.24m SR Altitude: 681 km 1.1 days	January 7th, 2019 satellite failure reported	https://directory.eoportal.org/web/eoportal/satellite-missions/v-w-x-y-z/worldview-4
SPOT 6 & 7 two polar orbiting constellation - stereo capabilities Continuity for SPOT 4 & 5 France	June 30th, 2014	Pan;1.5m MSS :6m, 12 bit per pixel Altitude 694 km, Period 98.79 minutes Location Accuracy :10m, Image swath width 60 km	https://spacedata.copernicus.eu/web/cscda/missions/spot-6-7	https://earth.esa.int/web/eoportal/satellite-missions/s/spot-6-7

(Basso et al. 2004; Hatfield & Prueger 2010). The RADAR satellites active C, L and X bands and passive microwave data can indicate soil moisture content which is used in some crop water use estimation methodologies/procedures e.g. ETLook (Pelgrum et al. 2010). Short wave infra-red wavelengths are used in the estimation of crop residues quantities in conservation agriculture-based research as imaged by the World View-3 sensors, as well as soil moisture content (Hively et al. 2018). The latter is used in surface energy balance-based crop water estimation algorithms such as Mapping for evapotranspiration with internalized calibration (METRIC) (Allen et al. 2007) surface energy balance systems SEBS (Su 2002), surface energy balance algorithm for land SEBAL (Bastiaanssen et al. 1998) and ETLook among others which require soil moisture data. Web based technologies have evolved and regional ET_c can be accessed on the web e.g. FruitLook in SA (Letsebe 2018), eLEAF in the Netherlands and EEFlux in the US. In the North American region EEFlux (Allen et al. 2015) offers METRIC ET_c data to the public. The increasing availability of ET_c data products on WEB platforms will lead to the expansion in use of these products and reduce water wastage thus mitigating global climate change challenges. Direct observational technologies such as the eddy covariance (EC), optical microwave scintillometers, Time domain reflectometry (TDR) and sap flow approaches are presented in Section 2.3.3. This section has outlined the technological advances in remote sensing and the enhancement of RS data acquisition for estimating crop use computations. The limitations of certain regions of the EM spectrum in acquiring required earth observation data were presented. Cloud based computing platforms e.g. Google Earth Engine (GEE) are set to expand the utilisation of GIS and RS data sets in meeting the global agricultural production challenges facing the world at reduced costs (Kumar & Mutanga 2018).

2.3   CROP WATER USE COMPUTATION

Irrigation leads to higher crop yields of better quality to meet dietary requirements of growing populations and has been associated with early civilizations in arid, semi-arid and hyper xeric areas (Jacobsen & Adams 1958; Stanhill et al. 1986). However, a range of negative impacts are typically attributed to irrigation use notably, soil profile salinization due to deep percolation losses and consequent rise in water table, diseases i.e. malaria and bilharzia from ponded irrigation water and downstream pollution from irrigation water runoff (Jacobsen & Adams 1958; Boelee & Madse 2006; Schulze &Taylor 2016). Researchers have advocated the use of science-based crop water requirements determination procedures to minimise the negative impacts of irrigation (Gowda et al. 2008; Jensen 2010). Since 1900 objective and science-based procedures to estimate crop water requirements have been practised in the USA. Evapotranspiration (ET) or crop evapotranspiration (ET_c) is an important yet complex part of the water cycle as it cannot be measured directly but is

inferred through energy budget methods (Westerhof 2015). A generalized classification of the different methodological approaches to estimate or measure ET_c, reference crop evapotranspiration (ET_0) and the crop coefficient (K_c) are presented in Figure 2.3 .
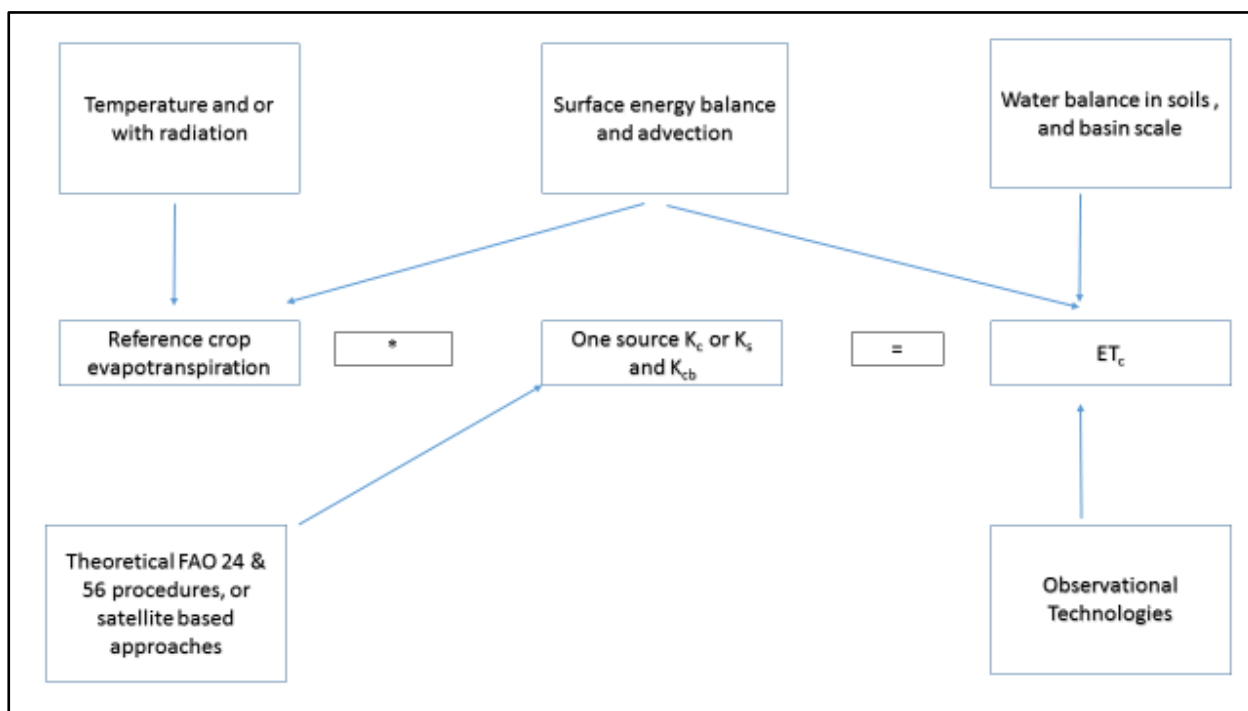
Figure 2.3 Crop water use (ET_c) estimation

The overview of presents the optional methodical approaches which have been used in the determination of crop water requirements research. The three options are, temperature and or with radiation, surface energy balance and advection, and finally water balance in soils and at basin scale. The traditional agricultural engineering approach uses the one or dual source, crop coefficient and reference crop evapotranspiration determine crop water use or requirements. The literature review covered the three options and was intended to critically assess the suitability of the methodologies used in the research. The crop coefficient concept, its theoretical basis and historical evolution and usage in crop water requirements research is presented first followed by the reference crop and actual crop water requirements quantification methodologies.

2.3.1 Crop coefficient concept (K_c)

Crop coefficient facilitates the utilisation of climatic data-based reference evapotranspiration to compute actual crop water consumptive use. However, the physical determination of K_c is cumbersome and complex, as it is a theoretical concept not directly measurable but its use is set to escalate in GIS based crop water use research (Pocas et al. 2015, Tasumi et al. 2014). This sections recaps on the K_c literature detailing the progression of the K_c determination methodologies to the current approaches that involve vegetation indices. It is concluded by justifying the choice

of the K_c estimation methodology utilised in the current study. The K_c role in wheat water use computation is illustrated in the flow diagram in Figure 1.1.

The crop coefficient (K_c) (Jensen 1968) is formally defined as the ratio of actual evapotranspiration to reference crop water requirements (Doorenbos et al. 1977; Glenn et al. 2011). The details of K_c determination are as outlined in the Food and Agricultural Organization (FAO) of the United Nations (UN) document (FAO 24) (Doorenbos et al. 1977) and updated in FAO 56 (Allen et al. 1998) or from soil-based observation e.g. gravimetric or lysimetric methodologies (Reynold 1970; Davies et al. 2019). The crop coefficient approach has become the acceptable practice or standard in irrigation engineering given its continued use with the FAO of the UN since the 1970s. The current worldwide irrigation engineering and water management procedures utilise the crop coefficient approach as this estimate water deliveries required in irrigation scheduling and designs within acceptable levels of accuracy (Farahani et al. 2007; Irmak 2008; Cahn & Johnson 2017). The crop water requirements ET_c at each growth stage is the product of the K_c and ET_0 for the period under consideration. The typical seasonal K_c pattern is depicted in Figure 2.4 for the four crop development stages.
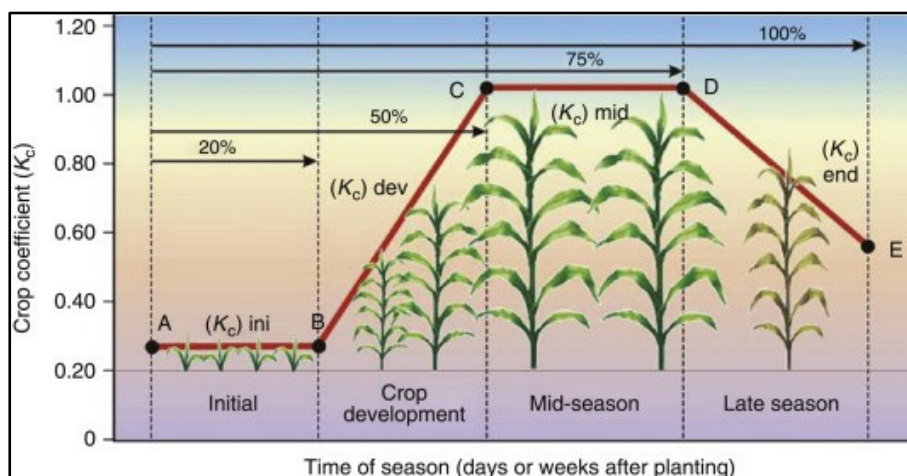
Source: Irmak (2008)

Figure 2.4 Generic crop K_c seasonal curve

At crop establishment stage, the K_c factor depends more on relative soil wetness as soil evaporation will dominate ET_c hence the low value of 0.26. As the crop develops vegetal ground shading increases and crop transpiration predominates ET_c and the K_c rises to above 1.00. During the mid-season stage the K_c factor stabilizes and starts to decrease with crop senescence (Allen et al. 1998). The above described crop coefficient approach or "the big leaf" determines ET_c based on a single coefficient , as opposed to the dual approach indicated in Figure 1.1. Evapotranspiration processes include water loss from the soil and vegetation surfaces and through transpiration via leaf stomata. As the soil loses moisture, water loss to available evaporative heat decreases. This has led researchers to introduce the K_s coefficient, which is the soil response variable to

evaporation at different soil moisture content. The K_s is used in conjunction with a crop basal coefficient, K_{cb} representing transpiration from the vegetated surface area. The procedures to estimate the K_{cb}, K_c and K_s are detailed in the FAO 56 (Allen et al. 1998) and is implemented in the SAPWAT4 model. It is important to note that the contribution of soil evaporation to total evapotranspiration increases with the frequency of either rainfall or irrigation events. Under dryland conditions and reduced rainfall events the soil evaporation can be catered for by the single leaf approach as was carried out in the current research.

Since the advent of satellite technology in the 1970s vegetation indices (VI)s have been modelled based on satellite optical spectra, giving objective measures of crop growing conditions and actual rates of water use at field to regional scales for single or mixed biomes on a pixel by pixel basis (Lobell 2013). Red light is strongly absorbed by chlorophyll **a** and **b** in leaves, interacting mostly with the top layers of a dense canopy, but nearly all the near infrared (NIR) is transmitted, reflected or scattered by the mesophyll structure in leaves, penetrating deep into the canopy and interacting with multiple leaf layers (Glenn et al. 2011). VIs are correlated to leaf area index (LAI), fractional canopy cover (fc), absorbed photosynthetically active radiation (APAR) which in turn are related to transpiration and carbon uptake rates and therefore more appropriate in modelling K_c and actual ET_c of field crops where conditions vary from the standard conditions. The VIs include the normalised difference vegetation index (NDVI), soil adjusted vegetation index (SAVI) and the enhanced vegetation index (EVI) (Huete et al. 2002; Glenn et al. 2011; Nagler et al. 2013). The indices commonly used in a variety of plant related research activities is the NDVI, see Equation 2.1 showing NDVI computation using S_2 spectral data.

$NDVI_{S2}$ = (NIR $_{B8S2}$ - Red $_{B4S2}$) / (NIR $_{B8S2}$ + Red $_{B4S2}$)   Equation 2.1

Where   NIR $_{B8S2}$ S_2 Band 8, central wavelength 835.1 nm, 145 nm bandwidth and

                    R $_{B4S2}$ S_2 Band 4, central wavelength 664.5 nm, 38 nm bandwidth.

 Although NDVI saturates at LAI greater than 3 it is linearly correlated to plant physiological processes as opposed to SAVI and EVI which are curvilinearly correlated. In wheat research NDVI based K_c outperformed FAO 56 time based computed K_c leading to the conclusion that modelled K_c from satellite data gives realistic crop water use values (Hunsaker et al. 2007a; 2007b). Hunsaker et al. 2007 , further concluded that using NDVI to model crop basal coefficient is a robust approach in wheat studies which can estimates water use more effectively than the FAO time based K_c. These researchers concluded that the NDVI methodology amply predicted actual ET_c under both typical and abnormal conditions. It has been observed that using satellite-based

VIs, crop growth conditions can be monitored at increasing temporal and spatial scales enabling timely and accurate irrigation water use determination at regional scales, thus curbing negative impacts of over irrigation in large regions of the earth's surface (Glenn et al. 2011).

Modelling of crop K_c from vegetation indices has been carried out over a number of crops and a number of formulations have evolved. Johnson & Trout 2012, used satellite NDVI to determine fractional vegetation cover which was used to model the basal crop coefficients in vegetable crops in the San Joaquin Valley. They obtained highly accurate relationships between NDVI and F_c with a coefficient of determination of r^2 at 0.96 and a RMSE of 0.062. The researchers used the developed model to estimate water consumption for broccoli, bellpeper, head lettuce and garlic. Research results indicated that the general form of the NDVI curve was similar to the Lysimetry based K_c curve leading some authors to speculate on the possibility of modelling K_c from satellite based NDVI. Tasumi et al. 2006 carried out studies to calibrate the NDVI - K_c functional relationship. They investigated alfalfa, beans, sugar beet, corn, potatoes, and small grain crops, the major crops grown in southern Idaho. They determined a single mean regional K_c modelled from satellite NDVI and mapped seasonal crop water use. Seasonal ET_c errors were below +/-10%. This gives confidence on the operational use of NDVI based K_c in seasonal crop water use studies. However, Tasumi et al. 2006's NDVI-K_c functional relationship did not include wheat and therefore was deemed unsuitable for modelling wheat K_c from satellite data.

Studies by Calera et al. 2017 led to the development of a predictive model that determined wheat crop coefficient development over a growing season based on NDVI. The specified model is presented in Equation 2.2, where K_{cS2} was modelled according to a functional relationship proposed by Calera et al. 2017 for wheat.

$$K_{cs2} = 1.46*NDVI_{S2} - 0.26 \hspace{4cm} \text{Equation 2.2}$$

Where: $NDVI_{S2}$ S_2(Sentinel 2) normalised difference vegetation index (NDVI),

                    1.46   regression coefficient (slope) and

                    0.26   y intercept.

The K_c is directly related to NDVI by a factor of 1.46 and has a value of -0.26 when NDVI is zero.

Besides the wheat NDVI-Kc model they studied other crops i.e. corn, cotton, Row vineyards, vegetables and fruits trees, and the functional relationships determined (Calera et al. 2017). The current study used the above formulation as presented in Equation 2.2, for its simplicity in GIS implementation for crop water use computation.

2.3.2   Temperature and or radiation methodologies in ET_0 & ET_c estimation

The temperature-based methods where developed in the US in the twentieth century to estimate water consumption in the areas under irrigation to estimate duty of water requirements. The notable temperature-based methods identified included the Thornwaite (1948) equation and the Blaney & Criddle (1945) equation (Jensen 2010). The Thornwaite method was based only on mean monthly temperature and failed to give accurate results when used in varying environmental conditions as it did not consider all climatic variables that impact evapotranspiration. The Blaney & Criddle (BC) (1949) method included temperature in Fahrenheit (^{0}F) and mean monthly percent of annual daytime hours. Though it's   a coarse method it has historical importance given that in some US states water is still allocated according to the BC equation (Blaney & Criddle 1964). The inclusion of monthly mean percent of annual daylight hours was based on the realisation of the importance of radiation energy to drive evapotranspiration (ET_c), however this formulation did not capture the radiant energy variable adequately. The BC method was found to produce unreliable crop water use estimates during the peak irrigation demand period (Hargreaves & Allen 2003). In what Jensen (2010) termed "the transitions methodologies" radiation variables were added in the emerging ET_c estimation methodologies in the 1960s, which included the Hargreaves & Samani (HS) (1985) among others. The HS methodology has been widely used at global scale and has been shown to have comparable accuracies with the Penman Monteith equation (Hargreaves & Samani 1985; Hargreaves & Allen 2003; Moeletsi et al. 2013). According to Hargreaves & Allen (2003) about 80 percent of ET_0 can be explained by temperature and solar radiation which are the HS parameters. Due to the HS's relative and historically validated accuracies with respect to PM and widespread usage it has been used in the current study.

Analysis of eight years of evapotranspiration data from a precision lysimeter planted to Alta fescue grass at Davis California found that 94% of the variance in ET_c was explained through average temperature and global solar radiation (Hargreaves & Samani 1985). This led to the Hargreaves (1975) equation with a coefficient of 0.0135 using mean temperature in degrees Centigrade (^{0}C) and solar radiation in units of equivalent water depth evaporated (mm). The HS equation has shown ET_0 estimation capabilities of the same order of accuracy as the PM in different environments, (Hargreaves & Samani 1985; Vincente-Serrano 2007; Moeletsi et al. 2013). Terrestrial R_a can be estimated from latitude (Allen et al. 1998) and the only extra climate data variables required are the minimum and maximum temperature seen in Equation 2.3:

$$ET_{0HS} = 0.0023Ra(T_{mean} + 17.8) * (T_{max} - T_{min})^{0.5} \qquad \text{Equation 2.3}$$

Where ET_{0HS} Reference evapotranspiration according to the HS methodology;

                 R_a Incident solar radiation; $MJm^{-2}\ day^{-1}$

                 T_{mean} Mean temperature;

                 T_{max} Maximum temperature and

                 T_{min} Minimum temperature.

The solar incident radiation term (R_a) is estimated based on extra-terrestrial radiation according to Equation 2.4.

$$R_a = \frac{24(60)}{\pi} G_{SC} d_r \left[\omega_s \sin(\varphi) \sin(\partial) + \cos(\varphi) \cos(\partial) \sin(\omega_s) \right] \qquad \text{Equation 2.4}$$

Where R_a extra-terrestrial radiation $MJm^{-2}\ day^{-1}$;

                 G_{SC} solar constant = $0.082\ MJm^{-2}\ min^{-1}$;

                 d_r Inverse relative distance Earth Sun;

                 ωs   sun set hour angle in radians;

                 Δ   solar declination and

                 φ   climate station latitude in radians,

Please note that Equation 2.4 does not consider altitude and aspect in computing R_a. Several attempts to modify Equation 2.3 based on humidity and wind speed have yielded non-significant improvements hence it's recommended that it be used in its current form (Allen 1993). It has accurately estimated ET_0 based on climate data for periods exceeding five days, in comparison to the PM methods (Hargreaves & Allen 2003). Due to its parsimonious attributes many researchers have evaluated the HS equation in many regions of the world, and results indicate conflicting reports on its levels of accuracy and reliability. In Brazil the HS equation was compared to the PM approach on an experimental station based on two years of data covering 2011 and 2012 (Lima et al. 2013). The un-calibrated HS had a RMSE of 1.43 $mm.d^{-1}$ which was reduced to 0.52 $mm.d^{-1}$ after calibration. The over estimation mainly occurred in the months of lowest evaporative demand from May to June. In SA the HS was evaluated together with the Thornwaite approach in the Free State Province (Moeletsi et al. 2013). Using 1999-2008 data set the researchers discovered that the uncalibrated HS closely correlated with the PM method more than the Thornwaite equation, even after both were locally re-calibrated. They concluded that using the HS either in its original or calibrated form, is recommended for the Free State Province of SA.

Implementing the HS on GIS platforms has been carried out and suggestions made on how to better model solar radiation. According to Vincent-Serrano et al. (2006), the planar approach can result in inaccurate R_a computation. They recommended the use of a digital elevation model (DEM) in the estimation of solar radiation in conjunction with latitude rather than assuming a planar surface. In a case study carried in the Ebro valley Northern Spain, Vincent-Serrano et al. (2006) demonstrated that calculations of R_a using a digital terrain model (DEM) and GIS solar radiation modelling provided a realistic characterisation of ET_0 than the conventional planar approach which is solely based on latitude as proposed by Allen et al. (1998). The planar surface approach might be the major cause of the conflicting results in ET_0 when R_a is estimated using latitude only, in heterogeneous terrain. In addition, climate station data quality is subject to errors due to instrument malfunctioning (Vincente-Serrano 2007).

Physically based methodologies that include the surface energy balance (SEB) approaches, advection and the MOST theories including satellite-based data retrievals methodologies are reviewed next. The PM methodology is reviewed first in this subsection.

2.3.3 Surface energy balance and advection based ET_0 & ET_c

The Penman Monteith (PM) is a robust physically based ET_0 estimation method applicable worldwide under variable conditions of aridity and advection. It has been adopted by the United Nations Food and Agriculture Organization (UN FAO) as the standard method to calculate ET_0 (Allen et al. 1998; Glecer et al. 2010). It combines surface energy balance with mass transfer, (Penman 1948; Allen 1998) (Equation 2.5). The FAO 56 Allen et al. (1998) and Zotarelli et al. (2010) publications among others, give more details of the terms used in the PM equation and their estimation in the case of incomplete data sets.

$$ET_0 = \frac{0.408\Delta(R_n - G) + \gamma\frac{900}{T + 273}u_2(e_s - e_a)}{\Delta + \gamma(1 + 0.34u_2)}$$

Equation 2.5

where:

Rn	Net radiation at the crop surface, MJ m^{-2} d^{-1}	
G	Soil heat flux density, MJ m^{-2} d^{-1}	
T	Temperature at 2m height in Kelvin	
u_2	Wind speed at 2 m above ground level	
γ	Psychometric constant, kPA ^{0}C^{-1}	
Δ	Slope of the saturation vapour pressure curve	
e_s	Saturation vapour pressure, kPA	
e_a	Actual vapour pressure kPA	

The R_n net solar radiation term is defined in Equation 2.6.

$$R_n = (1-\alpha) \cdot R_{swd} + \varepsilon \cdot R_{lwd} - \varepsilon \cdot \sigma \cdot (T_o)^4 \qquad \text{Equation 2.6}$$

where	A	Albedo
	R_{swd}	down dwelling short wave radiation
	R_{lwd}	down dwelling long wave radiation
	ε	Emissivity
	σ	Stefan Boltzmann constant, and
	T_0	surface temperature in ^{0}Kelvin

The PM equation incorporates two terms, the aerodynamic and energy terms and the associated bulk surface resistances for heat and vapour movement respectively attributed to several researchers including Monteith (1985). In the determination of the PM reference evapotranspiration the resistances variables are held constant as proposed by Allen et al. (1998). The FAO 56 PM methodologies has been implemented worldwide in models that estimate crop water requirements e.g. SAPWAT 4. It is a free online program developed in SA and is described on the internet at https://sapwat.org.za/sapwat-description/. It uses the FAO 56 procedures to compute ET_0 based on climate station databases for SA. This was preceded by earlier SAPWAT version based on CROPWAT routines that implemented the FAO24 crop water requirements procedures based on the American class "A "pan (Crosby &Crosby 1999), and using SA climate databases. South African researchers have over the years developed   a large number of computer programs that have been implemented countrywide and are of international renown and these were presented by Singels et al. (2013) and Annandale et al. (2010), among others. These models compute reference crop evapotranspiration based on SA climate station databases. The SAPWAT model was used to determine crop water requirements at the Orange-Vaal and Orange_Riet WUA (Van Heerden et al. 2001). Results indicated that the SAPWAT model accurately estimated crop water requirements in the study area. Crop factors determined by direct methods are tedious to carry out. As was suggested by several authors e.g. Annandale et al. (2010), the developed SA models could be improved further, by the complimentary use of satellites technologies. Time based crop coefficients assume ideal conditions of adequate moisture and nutrients which do not occur under practical field conditions leading to over watering and waste of water. Incorrect crop water use computation are due to inaccuracies in K_c determination (Allen et al., 1998; Lazarra & Rana, 2012). Some models include crop yields routines for specific crops in addition to crop water

requirements determination. The SA crop water determination history started with the use of the "Green Book "(Van Heerden et al. 2001) and was succeeded with the computer programs that implementing FAO24 methodologies SAPWAT3 and subsequently the FAO56 based SAPWAT4.

In modern implementations of PM for example in ETLook the actual soil and canopy resistances are inferred from earth surface satellite observations (Pelgrum et al. 2010; Bastiaanssen et al. 2012). The aerodynamic term is the basis "in which evaporation is regarded as due to turbulent transport of vapour by a process of eddy diffusion", the energy term is composed of the net energy remaining after reflection of incident radiation that provides latent heat of vaporisation (Penman 1947). The PM requires four climate variables of air temperature, air humidity, wind speed and radiation data. The ET_{0PM} is the equivalent evapotranspiration of an actively growing reference grass crop of "12 cm height, a fixed surface resistance of 70 sm^{-1} and an albedo of 0.23" (Allen et al. 1998). Because the PM methodology considers both the net radiation and aero dynamic aspects of evaporation, and canopy resistances it has consistently outperformed methods which are based on statistical and empirical formulations which require less climate data such as the Priestley & Taylor (P-T)(1972) and Hargreaves & Samani (1985), respectively.

The high climatological data demand and specific standard conditions regimen has led researchers to utilise other approaches to determine crop evapotranspiration for regions without the complete climatological data sets as required in PM (Priestley & Taylor 1972; Hargreaves & Samani 1985) among others. The accuracy of the PM depends on input data quality and utilisation of estimated inputs as suggested in FAO 56 or using coarse general circulation models (GCM) derived data, its performance is further degraded (Allen et al. 1998). The main drawback to using the PM approach for regional ET_0 studies is the limited climate stations coverage where all the required range of variables for its computation are available, this situation is prevalent even in developed countries (Vincent-Serrano et al. 2007). Given adequate data the PM methodology gives the most reliable estimates for reference crop evapotranspiration and is the standard against which other methodologies are rated (Allen et al. 1998, Shahidian et al. 2012) among others. Other energy ET_0 formulations include approaches that use the PM radiation term only plus a P-T coefficient (Priestly & Taylor 1972; DeBruin 1983). Priestley and Taylor (1972) proposed using the energy term of the PM equation only and replaced the aerodynamic term of the PM equation with α P-T coefficient which varies with soil water status, decreasing with reduced moisture content (Wang et al. 2012). The biggest shortfall in the P-T equation is that it is not robust and requires continuous recalibration. This is because the α P-T coefficient fails to capture the full impact of vapour pressure deficits and canopy resistances on evapotranspiration (Wang et al. 2012). Originally the P-T approach was developed for saturated conditions, its use has extended to non-saturated areas

which entails modification of the α P-T. World-wide environmental conditions vary from the saturated conditions rendering its use in non -saturated conditions ineffectual. The impetus to use the P-T approach emanates from its simplicity and availability of energy data from satellite thermal bands. The draw back to using P-T is that in non-saturated soil conditions α P-T has to be modified to reduce errors in determining reference evapotranspiration (Venturini et al. 2011). It remains a popular methodology given its simplicity and reduced climate data requirements.

The Makkink equation, an energy-based reference evapotranspiration methodology, was developed in Holland by Doorenbos et al. (1975) which uses the FAO radiation methodologies and is based on Makkink (1975). It gives accurate results when used under stable and humid conditions and becomes inaccurate under highly adjective conditions. It requires less climatological parameters. The Makkink approach, as proposed by De Bruin (1987), in an assay on unstressed maize crop water requirements, outperformed estimates made using the PM equation fitted with soil and canopy resistances in the Netherlands (Jacobs & De Bruin 1998). It has not been widely tested in ET research on a global scale. The current study area has highly advective conditions in winter rendering the use of the Makkink methodology inappropriate. The potential utility of P-T and Makkink approaches in regional ET_0 studies is complicated given the re-calibration requirements that are imperative to suite different environmental conditions. These are not robust methodologies and therefore not recommended in long term and regional estimation of ET_0.

Surface energy balance methodologies incorporate the Monin Obukhov Stability Theories (MOST) which are implemented using satellite-based retrievals at over pass times and with enabling assumptions determines ET_c for daily to longer time periods (Bastiaanssen et al. 2005; Pelgrum et al. 2010; Wang & Dickinson 2012). The methodologies proposed by micro meteorologists, considers interplanetary boundary layer physics to determine available energy for evapotranspiration (Su 2002). Their methodological frameworks form the basis of the current approaches that determine ET_c from remotely sensed thermal radiation.

The SEB are implemented by partitioning the incident down dwelling net radiation flux on the earth's surface into ground flux and sensible heat flux components and equating the residual energy term to a latent evaporation flux on a pixel by pixel basis (Allen et al. 1998; Bastiaanssen et al. 1998a, 2005; Su 2002; Wang & Dickson 2012) (Equation 2.7).

$$R_n = G0 + H + \lambda E \hspace{4cm} \text{Equation 2.7}$$

Where: R_n The net radiation,

G_0 soil heat flux (W.m^{-2}),

H sensible heat flux (W.m^{-2}) and

λE latent heat flux associated with evapotranspiration.

Equation 2.7 stipulates the surface energy balance concept, where the available latent heat flux is the residual energy from net incident radiation R_n (Equation 2.6) after deduction of sensible and soil heat fluxes respectively. Measurements of the soil heat and sensible heat fluxes are accomplished differently in the surface energy balance methodologies. The λE estimate depends on the accuracy of the defining variables, G_0 and H (Allen et al. 2007).

A critical assessment of the most recent and widely used SEB methodologies based on Equation 2.7 i.e. SEBS (Su 2002), (SEBAL) (Bastiaanssen et al. 1998) and the METRIC (Allen et al. 2007; 2011) are undertaken in this section. According to Tasumi (2019) the above methodologies are the most popular, currently used surface energy balance approaches. The detailed methodologies are not replicated here however their subtle differences are highlighted and advantages and disadvantages presented. Bastiaanssen et al. (1998); Su (2002) and Allen et al. (2007; 2011) among others provide details on the SEB methodologies, The SEBS requires the net radiation energy as described in Equation 2.6. After estimating the R_n SEBS evaluates the soil heat flux based on R_n and the ratios of soil heat flux for bare and for full vegetation canopy cover. The intermediary G_0 values are determined by interpolation. The SEBS procedure determines the evaporative fraction on the basis of the limiting cases as detailed by Su (2002). Each image pixel ET_c is evaluated based on the established relationship at the wet and dry limits. At the dry limit sensible heat is at its maximum given that the evaporative flux is nearly zero due to moisture limitations whereas at the wet limit the sensible heat has its minimum value and λE has its maximum value. The individual image pixel λE value is based on its estimated relative moisture content with respect to the image moisture range between the dry and wet pixels thus establishing the per pixel latent heat fluxes. The λE is useful when considered on a daily basis than just at satellite overpass times. The scaling up to daily values from instantaneous values is achieved by using the evaporative fraction concept which is kept constant throughout the day (Su et al. 2002). Some researchers however have recorded diurnal variations in the evaporative fraction and on that basis concluded that this introduces uncertainties in evaporation flux estimation (Mkhwanazi & José 2013). The existence of dry and wet pixel in an image is not guaranteed to occur every time unless wet areas occurs in

the scene. All surface balance models assume that energy use during photosynthesis and that stored in vegetation is negligible. The evapotranspiration (ET_c), is then calculated by dividing the latent heat flux by the latent heat of vaporization. Gibson et al. (2013) after observing accuracy discrepancies and model sensitivities recommended that the SEBS methodologies use, be restricted to homogenous agricultural landscapes than in heterogeneous environments. SEBS has been evaluated widely in SA for academic purposes as it is based on open source software freely downloadable from internet. It is implemented in ILWIS (Su & Wang 2013) and permits researchers unhindered access to its use. The above authors have an online practical guide (https://earth.esa.int/documents/10174/643007/ D5P1c-1_SEBS_LTC2013.pdf) that shows step by step procedures in implementing the SEBS equations and subroutines in ILWIS based on MODIS data. All SEB methodologies require estimates of soil, and canopy resistances to momentum and heat transfer which can be estimated from vegetation height, LAI or NDVI. Landsat and MODIS thermal bands reflectance are used to estimate surface reflected radiation and deduce the sensible heat fluxes which are required inputs in Equation 2.7.

The SEBAL method, is a SEB based methodology that converts RS emitted and reflected radiance's to surface energy balance and soil moisture indicators (Bastiaanssen et al. 1998a). The image pixel evapotranspiration fluxes (λE) rates are determined by a scaling scheme that incorporates the difference between the λE fluxes at the dry(hot) and wet (cold) pixel identified by experts based on temperature and NDVI (Bastiaanssen et al. 1998a). It has been validated in many countries including SA. As it uses both the MOST and BR theories it's subject to the usual criticisms of use under non-ideal unstable conditions that violate the basic assumptions of MOST resulting in energy closure balance discrepancies. The assigning of the wet and dry pixels introduces human subjectiveness limiting its use to qualified personnel. It has given accurate estimates of evapotranspiration when compared to SEBS and can be applied under heterogeneous environments (Gibson et al. 2013). The SEBAL evapotranspiration fraction assumes ET does not exceed ET_0 which is not always the case. The SEBAL methodology has been evaluated globally and results indicate that it's a robust approach whose levels of accuracy are comparable to Lysimeter based ET values in the western US (Tasumi et al. 2003). However, it is protected by intellectual property law and is not available for unaffiliated researchers to use (Gibson et al. 2013). Several commercial and ET_c algorithms were developed from SEBAL (Bastiaanssen et al. 1998: Waters et al. 2002)

Mapping Evapotranspiration with Internalised Calibration (METRIC) was developed from SEBAL by Allen et al. (2007; 2011). METRIC uses a DEM to incorporate effects of aspect and slope functions, including temperature lapsing with altitude in mountainous terrain. In both

SEBAL and METRIC procedures short wave and long wave (thermal) images from satellites images are required for computing the net radiation in Equation 2.6 and sensible heat fluxes in Equation 2.5. The set back to the use of METRIC has been the requirement of skilled operators in choosing the cold and hot pixel based on temperature and NDVI. According to Dhungel & Barber (2018) the above limitation is a challenge that remains unresolved. Although the establishment of candidate pixels has been automated the final selection still introduces human subjectivity resulting in ET variability of 5 to 20 % by different users. In addition, METRIC uses the ET fraction which is essentially the same as the crop coefficient defined as the ratio of satellite image evapotranspiration to ET_r representing the crop type and the development stage of the crop (Spiliotopoulos et al. 2017). METRIC is now implemented on Google Earth Engine Evaporation Flux (EEflux) using Landsat 8 imagery to map ET in the US (Allen et al. 2019). The ground meteorological data to estimate the evapotranspiration from the cold pixel with high NDVI value is based on the North American Land Data Assimilation Systems hourly gridded weather data. The standardised American society of civil engineers (ASCE) (2005) PM is used in the computation of the anchor cold pixel evapotranspiration flux METRIC.

The SEBAL methodology variants have been developed into commercial products in the Netherlands and currently used to map and quantify a range of crop performance indicators in South Africa. The eLEAF is a Dutch company with local partners in SA, i.e. GrapeLook a predecessor to FruitLook who offer satellite monitoring of water use in wine and table grapes production, and currently include monitoring for all fruit trees and grain crops production (Letsebe 2018). According to the author above water savings from 10 to 30 % have been achieved by farmers in the WC who are scheduling irrigation according to the eLEAF ET_c products. SA eLEAF crop water estimates service are paid for by DA. In a water accounting study that covered the whole of SA the eLEAF procedures were used that involved synthesis of satellite and climate data (Van Niekerk et al. 2018). The availability of satellite-based ET products in SA is expected to assist farmers in the practice of science based crop water scheduling thus curtailing over irrigation and mitigate water shortages currently experienced in the region.

The ETLook methodology was developed by the eLEAF and uses the PM two source equation to estimate crop water use. It requires soil moisture data in addition to determine soil evaporation (Pelgrum et al. 2010).The ETLook remote sensing model infers information on actual evaporation and transpiration from combined optical and passive microwave sensors which can observe the land-surface even under persistent overcast conditions (Bastiaanssen et al. 2012).The model implements the two PM equation with satellite derived deliverables from the optical and passive microwave sensors. Its advantage over other estimation methodologies is the utilisation of passive

microwave radiation which observes the land surface even under overcast conditions. The other SEB algorithms rely on thermal bands for estimating the surface energy balance which cannot monitor the ground under overcast conditions (Pelgrum et al. 2010).The use of the two source PM methodology is premised on, the determination and incorporation of the soil and canopy resistances to evaporation and the aero dynamic resistance for soil and canopy respectively. The evapotranspiration is based on the PM equation (Allen et al. 1998) under nonstandard conditions with variable soil and canopy resistances. The soil evaporation and transpiration fluxes are converted to actual evapotranspiration using a temperature dependent function of the latent heat of vaporisation. A study carried out by Bastiaanssen et al. (2012), ETLook was validated in the Indus Basin over a 116.2 million hectare area. The results indicated $R^2 = 0.76$ and RMSE of 0.29 mm.day^{-1} when compared to previous studies. ETlook validation in Australia and China indicated the accuracy of the procedure in estimating ET_c and a R^2 of 0.92 obtained for the latter site (Pelgrum et al. 2012.

The energy balance Bowen ratio (β) is the ratio of sensible heat (H) to evaporation flux (λE). The fluxes are estimated from temperature and humidity gradients under the usual assumptions of the equality of the resistances to heat and water vapour transfer in the constant flux layer (MOST) (Fritschen 1965; Angus & Watts 1984; Wang & Dickinson 2012). Knowing the β ratio and using the energy balance equation depicted in Equation 2.7 one can compute the ET_c ( ). It's a cheap method and requires less maintenance as compared to the EC technique. The BR energy balance method is widely used at a number of agricultural research stations and its data is readily available e.g. at the BR systems of U.S. Atmosphere Radiation Measurement (ARM) (http://www.arm.gov) with continuous measurement of H and λE (Wang & Dickinson 2012). In addition to energy closure problems it has issues of being a point-based method that cannot be easily upscaled to represent ET_c over heterogeneous landscapes (Wang & Dickinson 2012). In SA, the BR method determined from   13 measurement points of temperature and humidity gradients , was compared to the eddy covariance surface layer scintillometer and the surface renewal methods with the following coefficients of determination (R^2), 0.91, 0.81 and 0.86 respectively (Euser et al. 2014). These results were generated at Ukulinga Research station of the University of KwaZulu-Natal.

2.3.4   Water balance paradigm

This section intends to discuss the use of soil water balance determined at soil level to catchment scale including observational methodologies used to estimate crop water use at catchment level. The water balance approach is depended on scale which can be point based as in a defined soil volume, catchment area, continent or in the atmosphere. Hydrologist and climatologists have used the catchment to continental scales water balance in monitoring ET, while agriculturalist have used

at the soil or plant   water content or flow respectively, in evapotranspiration research. Wang & Dickinson (2012) defines a catchment scale ET as the balance from precipitation after considering river outflow and storage depletion. The discrepancy between the deduced evapotranspiration, after considering precipitation, and change in storage and river outflow is an error term that emanates from the input variable data errors (Glenn et al. 2011). The change in storage for periods covering one or more years is considered negligible.

The accuracy of the basin scale water balance approach to estimate evapotranspiration depends on the quality of the input data i.e. incident rainfall and river discharge data (Senay et al. 2011). It has been observed that large errors exceeding ten percent for precipitation and river discharge rates are typical. In addition, the value obtained of ET_c is a lumped sum and does not give the temporal and spatial variation in ET_c necessary in geospatial analysis of evapotranspiration (Glenn et al. 2011). The basin scale ET_c approach was not a considered option in the current study given that the enquiry intended to determine per pixel ET_c. However, the basin scale methodology can be used in validating seasonal estimates of ETc as carried out in the current if river discharge and rainfall data are available. Annandale et al. (2010) gave a comprehensive outline of crop water requirement research in SA. They attribute the progress made in water research to sustained funding by the DWAF (Annandale et al, 2010, Singles et al, 2013).

In South Africa basin scale cropwater requirements was implemented in the ACRU model (Singels et al. 2013). The ACRU model was developed in the early 1970s as a hydrological model but its agricultural component gained importance during research on agro climatological and agrometeorological atlas for Natal (Schulze 1975; Schulze 1983). It is a multiplatform model which can be used in hydrological studies that includes calculation of basin scale evapotranspiration. Point or area wide values of crop water requirements can be calculated using the ACRU model. Singles et al. (2013) reported the utility of the ACRU model as a teaching and research tool in SA and at the international stage. The current study was at a basin scale but restricted to a wheat crop in defined field polygons. If the current study were to be upscaled to include water basin scale water use and availability, the ACRU platform would be appropriate.

Sustained WRC funding culminated in the development of irrigation scheduling models based on soil moisture balance. Annandale et al. (2010) cites these as   BEWAB, PUTU, SWAMP and MyCanesim. The PUTU model was used for wheat irrigation water scheduling and was later developed into a generic model that determined crop water use for many crops. According to Annandale al. (2010) it used concepts developed by De Jager et al. (1987) in computing crop water requirements and to schedule weekly wheat irrigations. For the sugar industry the Mycanesim simulated cane growth and water consumption. The BEWAB developed at University of the Free

State (UFS) assists farmers to schedule irrigation in the Vaalharts, Sandvet and Riet River irrigation (Singels et al. 2013).The cited model developments although not part of the methodologies used in the study serves to indicate how water use research has been prioritised in SA. The funding initiatives by the DWA in itself an indication of water scarcity in the region and the need for its efficient usage to minimise loses.

Other soil water balance point based crop water requirements estimation methodologies are presented below but please note that these cannot be upscaled to regional scales. Point based methodologies that include gravimetric based soil moisture content monitoring (Reynold 1970), soil tension based, soil water content monitoring (Richards and Neal, 1936; Walhan 1939). These include lysimetry, time domain reflectometry (TDR) (Jones et al. 2002) and neutron probes (Chanasyk & Naeth 1996). These methods are in use at field level.

The gravimetric method is the most accurate soil moisture content measuring methodologies and is in intensive use in water use research. It involves soil sample extraction, oven drying the sample and based on the difference in mass before and after the drying gives the water content in the soil. This can be expressed as mass of water in a given mass of soil or on a volumetric basis based on soil bulk density. According to Reynolds (1970), gravimetry gives very accurate results and consequently is used in calibrating instrument that indirectly measure soil moisture content. The major disadvantage is great physical effort and time to collect and oven dry the samples, weigh and compute moisture content changes over time. Tension meters indirectly measure soil moisture content through the measurement of soil matric potential. Neutron probe have been used in SA to monitor soil moisture content and crop water requirements. According to Annandale et al. 2010, water savings of 24 % were realised using the neutron probe based irrigation scheduling. However its continued use is being superseded by logged capacitance type sensors. In addition to radioactivity risks upscaling of neutron probe measurements to regional scales is difficult.

Lysimeters (Davies et al. 2019) are the most precise method for monitoring soil moisture over time and thus ET_c. They are very expensive to install and given that these are a point based measurements of ET_0 , cannot be upscaled, but are useful for determining several parameters at point scale that include K_c, ET_0 and ET_c . Upscaling of soil moisture content (SMC) made at specific points using ground-based measurements poses an impractical solution for continuous spatial and temporal coverage of this parameter at regional to global scales (Rahimzadeh-Bajgiran et al. 2013). Eddy covariance towers have been used worldwide in determining canopy evapotranspiration fluxes. In SA, several researches have been carried out eddy covariance based evapotranspiration enquiries. Ramoelo et al. (2014) validated the MODIS evapotranspiration product at Skukuza and Malopeni sites in the Kruger national parks. The results were inconclusive

due to parameterization of the PM model, eddy covariance foot print to the MODIS pixel sizes. In dual approach ET studies on apple orchards in the WC, Dzikiti et al. (2018) quantified soil and plant evapotranspiration using sap flow and eddy covariance towers with 150 -180 m footprints. The use of these point based methods however poses challenges at upscaling to regional level.

This has led some researchers to consider the potential of remote sensing technology. Soil moisture content from satellites can be established based on passive microwave. The soil water content methodologies such as e.g. lysimetry ,TDR neutron probes among others although being point specific are very accurate in general, but difficult to upscale to field or regional levels and are best used for calibration of regional methodologies (Gowda et al. 2008).

2.3.5 Geographic surfaces generation (ET$_0$).

There is a need to generate geographic phenomena surfaces for use in analysis that include processed RS data. This is achieved by implementing interpolation methodologies in GIS. The choice of a given interpolation scheme depends on the complexity of the phenomena and sampled data available and the phenomena being investigated. Determining the most appropriate interpolation methods for use in a GIS study poses several challenges (Mitas & Mitasova 2005). This section will briefly describe interpolation techniques used to generate geographic phenomena surfaces in general and thereafter those used to generate surfaces from climate station based data such as ET$_0$. The following methods are typically used in GIS to interpolate geographic phenomena, Inverse Distance Weighted (https://www.gisresources.com/types-interpolation-methods_3/), Natural Neighbour Interpolation, Triangulated irregular network (TIN) or Rectangle-based, Geostatistics and the variational approaches described in detail by Mitas & Mitasova (2005). Inverse distance weighted determines the value at the unsampled point based on the value at sampled points weighted by distance since sampled points near to the unsampled points have greater influence than those further away. The nearest neighbour interpolation computes values at unsampled points based on coordinates of Thiessen polygon or Thiessen polyhedra. These have been used in topographic, bathymetry and soil data (Mitas & Mitasova 2005).

The spline interpolator estimates the unsampled values using a mathematical function that minimises overall surface curvature and passing through the sampled points (Franke 1982, Mitas & Mitasova 1988). It is suitable for mapping continuous smooth geographic surfaces by ensuring that the modelled surfaces passes through the known inputs points. ArcGIS implements two flavours of the spline interpolator. These are spline with tension and the regularized spline surface interpolator (https://pro.arcgis.com/en/pro-app/tool-reference/3d-analyst/how-spline-works.htm). The spline with tension option was used in the current study. The reference evapotranspiration are

smooth surfaces which are expected to pass through the climate station based on which the estimated K_c were determined. The general spline equation is presented Equation 2.8.

$$S(x,y) = T(x,y) + \sum_{j=1}^{N} \lambda_j R(r_j) \qquad \text{Equation 2.8}$$

Where: J is 1,2………N,

       N is number of points ,

       λ coefficients based on solution of a system of linear equations, and

       r_i is the distance from the point (x,y) to the jth point.

The T(x, y) and R(r) for the tension spline are defined in Equation 2.9 and Equation 2.10 respectively,

$$T(x, y) = a \qquad \text{Equation 2.9}$$

Where: a_1 is a coefficient determined by the solution of system of linear equations.

and

$$R(r) = -\frac{1}{2\pi\varphi^2}\left[\ln\left(\frac{r\varphi}{2}\right) + c + K_c(r\varphi)\right] \qquad \text{Equation 2.10}$$

Where: r distance between the unknown and known points

       φ^2 the Weight parameter ,

       K_0 the modified Bessel function, and

       c a constant equal to 0.577215.

The tension spline methodology was used in the current study to generate the ET_{0HS} & ET_{0PM} distributed reference evapotranspiration surfaces. The advantage of this methodology is restricting error introduction to the generated surfaces by forcing the modelled surface to pass through the known sample points. Other interpolators implemented in ArcGIS have not been considered in the current study because of interpolator structural deficiencies in generating smooth geographic surfaces that passes through sampled points (Childs 2004).

2.4 YIELD, YIELD GAP AND CLOSURE

Crop yield is a benchmark variable to compare crop production across different spatial and temporal scales. Its utility however is not complemented by difficulties in its quantification and over the years, manual and satellite-based methodologies have evolved. The yield gap is a product

of crop yields statistical analysis that aims to ascertain the yield growth required to reach attainable yields for a given crop in a geographical setting (Lobell 2013). The analysis involves three steps, acquiring or estimating crop yields and statistical determination of the yield gaps, and finally identifying the causes of yield gaps (Label 2013, van Ittersum et al. 2013). In this section a review of yield determination methodologies are presented first, followed by yield gap estimation methodologies. And this is concluded by yield gap closure recommendations for the WC province.

2.4.1   Crop yield

Crop yield is a highly sought after variable, its temporal and spatial variation is critical in the dynamics of regional/national crop supply and demand and hence trade and production studies Crop yields are generally established at specific places and times e.g. at research stations agronomic trials or farmer fields where inputs are varied, and crop production functions estimated. However, the results obtained would be for specific sites and times and not necessarily representative of the whole range of conditions that farmers' face in other years or places (Lobell 2013).

A robust yield estimation methodology developed by Monteith (1977) stated that total biomass production is proportional to total photo synthetically active radiation absorbed (APAR) by the crop during the growing period coupled with the plant radiation use efficiency. The basic and enduring paradigm for yield estimation using remote sensing was formulated by Monteith (1972, 1977). This is a physically based method based on photo synthetically active radiation (PAR), radiation use efficiency (RUE) and the harvest index (HI) data to compute   crop yield. The HI varies with crop types, depending on crop type whether it's C_4 or C_3. Crop model simulation or plant process models can be used to generate yields from defined climatic conditions and production inputs (Gleason 1982) values and to match the VI that gives the minimum RMSE in yield estimation. Lobell et al. (2003) implemented the Monteith approach to determine wheat yields in the Yaqui Valley Mexico under irrigated conditions. He determined yield using the product of the seasonal sum of plant absorbed photosynthetic active radiation (APAR) by the radiation use efficiency (RUE) and the harvest index (HI).Simulation however have yielded inconsistent results given that crop models do not cater for water stressed conditions or pests and weed infestations. Satellite based vegetation indices based yield estimation procedures are gaining popularity.

Plants are reflective in the near infra-red wavelengths (NIR) and absorptive in the red wavelengths (R) (Tucker 1979; Sellers 1987), hence any indices combining these wavelengths reflect plant growth vigour. Gitelson et al. 2003 demonstrated the utility of using all wavelengths in more sophisticated approaches. About 80% of yield variation has been explained by VIs based on the R

and NIR wavelengths. Regression based studies have related actual yields observed in a study area to vegetation indices. However, extrapolating of empirical models to other regions and years has proven problematic requiring extensive local calibration (Lobell 2013). With the development of highly responsive VI such as the wide dynamic range vegetation index (WDRVI) (Gitelson 2004), coupled with high resolution sensors such as the S_2 (10 m), the feasibility of accurately estimating yields is now greater than was ever possible before. Satellite-based yield estimations have received a major promotion by the free online availability of Landsat archive data, following the decision by the USGS in 2008 to make the entire archive data set of Landsat available at no charge (http://landsat.usgv/products). A similar policy has been adopted by the European Space Agency (ESA) for Sentinel data access. Furthermore, improvements in pre-processing algorithms for image co-registration and the increasing availability of high temporal and fine spatial resolution imagery at decreasing costs all leads to the precise determination and monitoring of VIs' over longer periods of time (Lobell 2013). Single satellite image NDVI based yield modelling can now be routinely carried out to monitor crop yields at scales ranging from fields to regions and national levels to complement other yield estimation methodologies (Mashaba et al. 2017).

Following a case study carried out in the Orange Free State, Mashaba et al. (2017), a wheat yield model based on a single MODIS image was developed. They regressed MODIS based NDVI against observed wheat yields to calibrate the model. The single image was timed in the wheat flowering (blossoming) stage. NDVI in the mid season stages has a plateaued region as exhibited by the generic crop K_c as indicated in Figure 2.4. Based on extensive studies it has been established that NDVI and the K_c are directly related as reviewed by Calera et al. (2017). The MODIS sensors have a pixel resolution of 250 m. The developed equation is presented below for the Landsat8 NDVI.

$$Y_{L8} = 12.1136 \, NDVI_{L8} - 2.7307 \qquad\qquad\qquad \text{Equation 2.11}$$

Where $NDVI_{L8}$ NDVI,

                12.1136   regression line gradient and

                - 2.7307   y intercept.

The use of a single image is less complicated than aggregating multiple images which might not be available due to intermittent cloud cover. The major setback for using the Mashaba et al. 2017 is that it's based on a large footprint and as mentioned below might lead to model inaccuracies. In addition the MODIS sensors if used for small plots i.e. those at Langgewens one pixel footage

would straddle several plots. The model has moderate accuracies. The NDVI and wheat yield equation was significant with a coefficient of determination (R^2-value) of 0.73, a p-value of 0.00161 and an RMSE of 0.41t.ha^{-1}. The use of coarse spatial resolution data such as the moderate resolution imaging spectro radiometer (MODIS) sensors at 250 m pixel in yield modelling have been shown to be poorly correlated to the VIs (Sibley et al. 2014). The above methodology was recommended in the study given that it was developed in a similar setting as the study region i.e. a dryland wheat crop in South Africa. The use of the equation was to facilitate the carrying out of the study with available models in the literature and in comparable environments as proof of concept than an exercise in accuracy assessment per se. In advanced studies model formulation with robust data sets is envisaged.

2.4.2 Yield gap

The yield gap approach intends to establish the production potential in an area based on statistical analyses of farmers current yields. It also includes the identification of the causes in yield variations to enable focussed extension efforts and policy formulation to address and reduce the yield gaps. The current study was limited to the determination of the yield gap and not the causes were not specified nor quantified. The appraisal of crop productivity in a given area involves the crop yields comparison to local and regional benchmarks. The yield gaps ascertained constitutes the crop production intensification opportunities. Yield gaps have been defined as the difference between potential yields and average yields obtained by farmers (Lobell 2013). Statistical methods are used to estimate yield gaps by setting the yield potential Y_p equal to the 95th or 90th percentiles in a statistical distribution. The yield gap will be the Y_p less the average farmers yield. This assumes that some farmers are already attaining potential yields within the study area. Alternatively, mean yield in the study area can be compared to average yields obtained in highly developed countries at a global level. Farmer competitions can serve to generate and expose the within study area crop yields data based on which yield gaps can established.

2.4.3 Yield gap closure

As stated by Snyder et al. (2017) any attempts to close yield gaps requires the analysis of wider scope of factors that impact crop yields, including those that affect farmers decisions . Effective rainfall management implies the implementation of cultivation practices that increases rather than reduces water intake rates, including raising the soil water holding capacities. It has been observed that conventional tillage systems lead to surface sealing and high runoff volumes as compared to reduced tillage practices carried out under conservation agriculture (CA) (Thierfelder & Wall 2009). They arrived at the above conclusion based on field trials carried out in Zambia and

Zimbabwe which had identical results. Many authors attribute increases in infiltration rates and retained moisture to CA practices. Bodner et al. (2015) gives a detailed account of the benefits of CA under drought conditions. In a literature review they concluded that efficient green water management to reduce effects of drought is accomplished under CA practices. However, research results vary, depending on the conservation practices. Small scale farmers 'attempts on CA use in Zambia had opposite soil effects, to those observed by (Thierfelder & Wall 2009) where minimum tillage had lower infiltration rates, lower moisture retention than with CA (Esser 2017). Esser 2017 admits however that crop residue cover had disappeared by the time of the assay implying that it became solely a tillage effect without CA. Sustainable drastic soil fertility augmentation is achievable if conservation agricultural practices are carried out. There is a triple synergy effect envisaged under conservation agriculture. Increasing soil carbon content ameliorates the soil microbial environment raising ecological productivity in crop production (Harman & Uphoff 2018). Overall organic farming has enhanced total microbial abundance and activity in agricultural soils on a global scale (Lori et al. 2017). Note that organic farming is taken as CA. In addition, Liang et al. (2006) recorded increases in cation exchange capacity in soils with carbon accumulation soil. The soil water holding capacities vary with soil carbon content. Higher soil carbon content results in high soil water holding capacities which leads to the efficient rainfall use by reducing surface run off thus availing more water to the soil plant system (Bodner et al. 2015). Lastly increasing the soil organic carbon reduces the levels of carbon dioxide in the atmosphere by carbon sequestration which mitigates negative impacts of global warming in the long term (Harman & Uphoff 2018). Strategic irrigation use for wheat crop establishment coupled with supplementary irrigation during drought episodes ameliorates the seasonal soil hydric content increasing yields. The increased water holding capacities from high levels of organic matter would reduce the number of irrigation events by extending irrigation duration leading to reduced irrigation machinery movement (Mueller et al. 2012). Institutional incentives that positively impact the farmers' socio economic conditions and encourages CA adoption are suggested as viable drivers of sustainable yield gap closure (Snyder et al. 2017).

2.5   CROP WATER PRODUCTIVITY

Agricultural factor productivities have been investigated over the past decades, and divergences and variations in definitions have been registered. Water productivity, similarly has been defined in various ways including the physical and economic terms (Molden et al. 2010). In the economic approach water productivity is defined as the value of production per unit of water used by the crop. The mass of crop output to unit volume of water used by the crop is the characteristic physical crop water productivity. The increased researches on water and nutrient crop yield productivities

are indicative of the scarcity of these factors in crop production and the need for augmenting these to meet world food, fibre and energy requirements (Mueller et al. 2012). The contemporary challenges facing agricultural based crop production is multifaceted given the escalating food , fibre and energy requirements and the reduced availability of land and water resources caused by rapid urban population growth , industries and ecosystems reserves. The required thrust consists of food fibre and energy crop production augmentation without incurring environmental costs by engaging in sustainable crop production intensification (Mueller et al. 2012).

Forecasted future growth in agricultural production is expected from increases in land and water productivity without negatively impacting the environment (Edreira et al. 2018). Contemporary crop productivity focus has shifted from crop yield per Ha, to crop yield per Ha per mm of water used ($kgs.ha^{-1}.mm^{-1}$) which can also be expressed as crop yield to water depleted ratio ($kgs.m^{-3}$) (Zwart & Bastiaanssen 2004).The availability of water world-wide for agricultural production is forecast to decline given the increases in non-agricultural demand for fresh water resources (Zwart & Leclert 2009; Schulze 2016).

Computed water productivity values are important benchmarks which indicate water use efficiencies based on which improvement strategies can be formulated. Researchers have developed global maps on water productivities for wheat production (Zwart et al. in 2010). The mappings indicated wheat water productivity ranging from 0.2 to 1.8 $kgs.m^{-3}$. Computed water productivity values depend on crop yields and water use quantities. A decrease or increase in any of the input parameter variables affects the resulting water productivity values. High yield levels correspond to increasing water productivity levels. Similarly, reduction in water consumption by better water scheduling augment water productivities. Since crop water productivity studies invariably utilise RS and GIS, technologies and methodologies, standards need to be developed and maintained to ensure the accuracy and precision of values computed. Blatchford et al. (2019) pioneered work in this regard and have compared RS approaches to in situ methodologies taken as the actual productivity values. Error propagation were quantified, and this indicated the need for users to define accuracy levels that suit specific investigations than reliance on general recommendations.

Mueller et al. (2012) investigated global fertiliser and water use in yield gap reduction investigations and concluded that the limitations of these factors to yields and by extension to productivity varied by region. Africa has the least fertiliser use levels thus limiting water productivity in the region. Other researchers proposed alternatives to the crop water productivity approach as outlined above. These are presented in the section below as background information that indicates the diversity of views concerning water productivity in the literature. Renault &

Wallender (2000) suggested that dietary changes have a potential to result in water savings. A 25% reduction in animal products use in the developed world diets could generate approximately a 22 % of the additional crop water requirements expected for the year 2025. The effect of the above computation is countenanced by a significant population in the developing world who are transiting to animal-based diets due to increasing affluence, thus escalating water intensive food production (Alexandratos & Bruinsma 2012).

According to Renault & Wallender (1999) nutritional water productivity and diets are more appropriate benchmarks than the general crop water productivity ratio. They argued that in the face of worldwide escalating food requirements its best to consider the nutritional output per m^3 water depleted than the gross food weight per se. On the other hand, irrigation specialists have maintained the water use application efficiency which is not related to crop water uptake but to the technical efficiency of the irrigation system to supply water to the plant root zone. They based their computation on canal flow measurements data as the only source of water in determining irrigation performance indicators disregarding the inputs from other water sources such as rainfall or ground water recharge (Bastiaanssen & Bos 1999). Use of RS data sets for agricultural water productivities computations are justified on the basis objectivity, accuracy and repetitive and ability to cover large area. Agricultural water use performances indicators as defined by agronomists include water yield that has as components crop yields and crop water use or net return for a unit of water used (Molden et al. 2010). Crop physiologists defined crop water productivity as assimilated carbon and yield per unit of transpiration (Molden et al. 2010).

Mueller et al. (2012) investigated raising of yield to close yield gaps which could result in escalating water productivity. They asserted that water management is critical to raising yields and water productivity. Increased water productivity can augment food production without increasing cropped area or water use which fits well with the current challenges of increasing food production requirements under conditions of decreasing water and land resources (Molden et al. 2010; Mueller et al. 2012; Blatchford et al. 2019). In this research study water productivity, calculated as the ratio of crop yield to the water used or depleted in units of kg.m^{-3} was used as defined by Zwart & Bastiaanssen (2004). Based on the above definition seasonal water productivity is determined according to Equation 2.12 (Edreira et al. 2018). EOS and SOS in Equation 2.12 are, end of season and start of season in JD respectively with 10 as a conversion factor from t.mm^{-1}.ha^{-1} to kg.m^{-3}. According to Blatchford et al. (2019), Equation 2.12 can equally be applied to irrigation and rainfed crop production systems.

$$CWP = Y/10 * \sum_{i=SOS}^{EOS} ETa$$ Equation 2.12

where $\quad CWP \quad$ Crop water productivity (kg.m^{-3});

$\quad\quad\quad\quad Y \quad\quad\quad\quad$ harvested crop yield (t.ha^{-1}) and

$$\sum_{i=SOS}^{EOS} ETa$$ the season crop water use (mm).

Some researchers evaluated the spatial variation in water limited and actual on farm water productivities across regions for maize in sub-Saharan Africa and Asia, high yielding maize in North America and wheat in Western Europe and concluded that results are region specific and not transferrable to other regions or years (Edreira et al. 2018). The current study was limited to establishing wheat water productivity based on a snapshot analysis of the 2016 winter season in the Berg river catchment of the WC province.

2.6 LITERATURE SUMMARY

The literature review outlined the range of methodologies that have been encountered in the literature has covered the data requirements critical in rainfed and irrigation project appraisal.

Assessment of irrigation development using the IPCM framework was discussed and the usefulness of RS and GIS in data provisioning in carrying out the appraisal highlighted. The IPCM data requirements include crop water requirements and wheat yield, and how these are used in the appraisal process was described. Technological advances used to quantify NDVI, and thereafter crop K_c were described including the band characteristics of sensors used in the study. The advantages of using remotely sensed data in comparison to the traditional methods was highlighted. The central role of the crop coefficient approach was indicated firstly in the research design and in the literature. Although there exists a range of K_c estimation methodologies that includes the dual approach, the NDVI based single leaf approach is gaining popularity given that it has been reported to give realistic crop coefficients values when compared to the FAO 56 methodologies. The review justified the use of NDVI based crop coefficient given reported research results e.g. Hunsacker et al. (2007) among others, which indicate the robustness of this approach. In their findings NDVI based Kc outperfomed the time based FAO 56 under rainfed and irrigated agriculture. Furthermore the effects of different nitrogen levels on K_c was only detectable using the NDVI approach. Using satellite-based energy balance approaches crop water use can be determined without the use of the crop coefficient approach as shown in Figure 1.1.

Since the current study did not include on site validation of estimated ET_c and was regionally based the BR, eddy-covariance (Butterworth & Else 2018) or scintillometers were not used. Since the study was regionally based, the above methodologies are site specific with limited coverage, these were deemed not appropriate as they cannot be upscaled. Similarly, Lysimetry, EC, sap flow and TDR point measurements were not recommended for use in the study due to operational upscaling difficulties to regional scales.

The literature reviewed surface energy balance based crop water use methodologies. There are methodological shifts backwards towards the combined use of climate station data and SEB methodologies e.g. "cold" anchor pixel ET_c in METRIC (Gowda et al. 2008). The PM equation two-source crop water determination approach using on soil and canopy resistances is implemented in ETLook in mapping regional ET_c (Bastiaanssen et al. 2012). The ETLook is a commercial product, although it can be used for research it's not a free online software and therefore was not used.

There are more climate stations which have temperature data than the full set of climatic variables as required for the PM rendering the HS methodology an attractive alternative to the PM in regions with sparse climate stations or where data are of questionable quality (Allen et al. 1998; Vincente-Serrano 2007). The Priestley-Taylor (P-T) methodology although it requires less climate data, it was developed under saturated conditions and requires re calibration under non-saturated conditions. As result the P-T equation was not recommended for use in the current study. Given its relative attributes as outlined in the literature review, the HS methodology has been used in the current study. The PM methodology was used in the current study as the standard against which the Hargreaves Samani (HS) empirical equation was evaluated. The PM has been adopted by the United Nations Food and Agriculture Organization (UN FAO) as the standard method to calculate ET_0 (Allen et al. 1998; Glecer et al. 2010).

The surface energy balance approaches based satellites where discussed. These require thermal satellite imagery and have dedicated algorithms some of which are not free online. They are important inputs in scientifically based irrigation scheduling and are being used in SA e.g. Fruitlook (Letsebe 2018) and in the US (METRIC). METRIC is now implemented on Google Earth Engine Evaporation Flux (EEflux) using Landsat 8 imagery to map ET_c in the US (Allen et al. 2019).

There are a number of interpolators used in generating geographic surfaces. The methodology that was recommended the Spline with Tension, minimises errors by passing through the known data points.

The Irrigation appraisal strategies as adopted by the major multi-lateral institutions, the PCM framework was fully presented. The technical data requirements and data sources for the IPCM were outlined. The feasibility to determine the regional distributed crop water use and yields surfaces based on manual methods is a challenge. Researchers have concluded that ground based generation of appraisal data such as crop yields and crop water requirements are laborious and do not necessarily give accurate estimates when compared to satellite-based approaches which are consistent and cover large geographic regions. Crop wheat yields estimation can be carried out based on a single image or multiple images as reported by Monteith (1972, 1977). Although the latter is physically based and hence very robust its routine /operational use is limited by the extensive range of inputs required to implement it. The simplest approach that uses a single image was recommend in the study. Parsimonious approaches are useful in research since they generate the required output without undue complications that can lead to erroneous results. Water productivity calculated as wheat yield to seasonal water use as proposed by Molden et al. (2010) was adopted. The carbon assimilated per water transpired approaches which are difficult to implement were not recommended in the current enquiry. The methodologies recommended for use in the current study were interpolated ET_{0PM}, ET_{0HS} based crop water use and modelled yield, that can be implemented in a GIS thus permitting further calculations to determine water productivity and yield gap analysis , the critical inputs in IPCM.

CHAPTER 3:   MATERIALS AND METHODS

Data used in the study included L_8 and S_2 satellite imagery and tabular climate data from 17 weather stations. The weather station data was provided by the Agricultural Research Council (ARC) Stellenbosch offices, while the L_8 and S_2 satellite imagery were downloaded from the USGS archives and the Copernicus Open access Hub respectively. This chapter describes the study area and thereafter outlines the steps followed, and procedures undertaken in the execution of the research.

3.1   STUDY AREA LOCATION AND CHARACTERISTICS

The study area is located within the Berg river catchment of the WC province of SA. The area is situated in the Berg river catchment seen in Figure 3.1 , in blue colour with a faint red boundary. It is bounded within the rectangle whose vertices coordinates are 18°25'36.678" and 19°20'48.894" E and 32°40'39.414" and 33°45'56.686" S, shown in brown colour. The study area climate stations network has been included. The three insert maps serve to indicate the location of SA in Africa, the WC Province in SA and finally the Berg river catchment area in the WC province. The wheat fields' polygon is shown in dark brown colour.
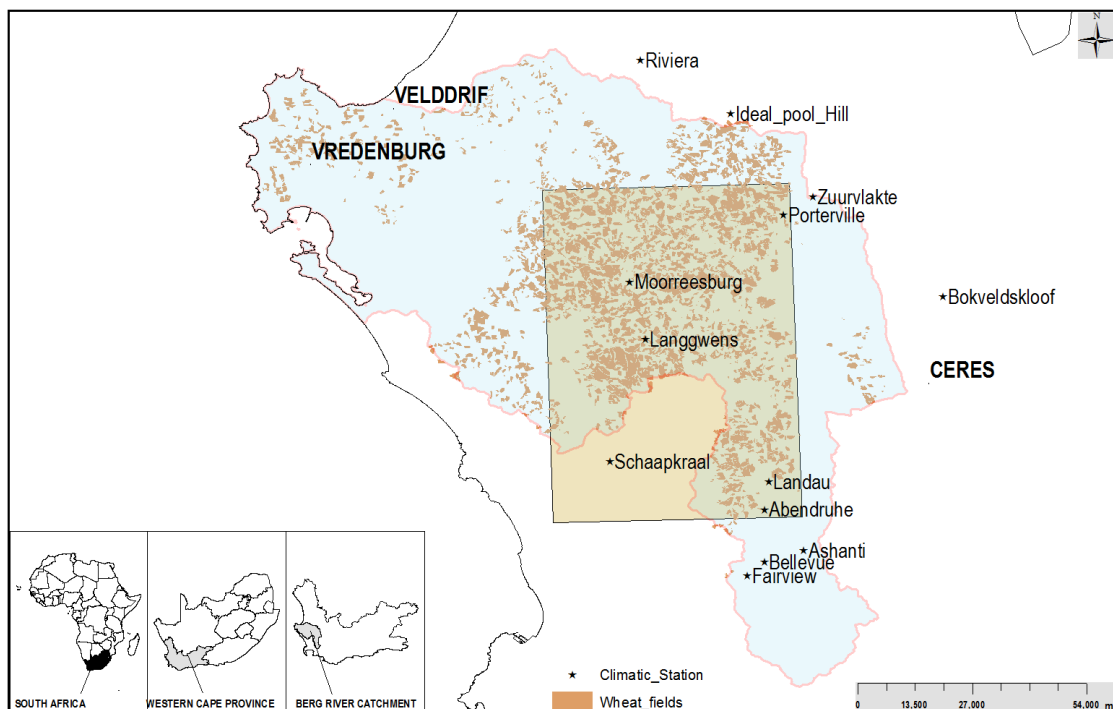
Figure 3.1 Study area

The WC has a Mediterranean climate with cold and wet winters between April and September, followed by hot and dry summers from October to February. According to the Agricultural research council (ARC) climate station data provided June and July were the coldest months. The daily minimum temperatures ranged from 2.97 ^{0}C at Moorreesburg (199 m.a.s.l) to -3.38 ^{0}C at Zuurvalkate (1000 m.a.s.l). The maximum daily temperature occurs during the summer months peaking in December. The temperature varied according to the climate stations' height above sea level. Pools Ideal hill and Riviera at 161and 90 m.a.s.l had maximum temperatures of 40.2 and 45.04 ^{0}C in December 2016, respectively. Boksveldskloof (1038 m.a.s.l) and Zuurvalkate (1000 m.a.s.l) had maximum temperatures of 33.05 and 32.67 ^{0}C respectively. From a climatic perspective the study area had a wide variation in terms of maximum and minimum temperatures which had an impact on the results obtained in the research study.

The Berg River, which   originates in the Drakensberg Mountains near the town of Franschhoek is the principal source of fresh water in the study area. The upper Berg River supplies the Cape Town metropolitan area and its suburbs with freshwater, in addition to providing water for irrigation along the middle and lower reaches of the river (de Villiers 2007). The water quality decreases as one descends downstream due to inflows of untreated sewerage from informal settlements, towns, industrial and agricultural effluent e.g. wineries and piggeries' including non-point pollution originating from agro chemicals used in the Swartland farming area (Görgens & de Clercq 2005; DWAF 2007, Rensburg et al. 2011).

The reduction in water flow in the Berg River due to upstream damming and decreases in rainfall in the current decade exacerbate its water trophic levels with phosphorus and nitrates being the major pollutants (de Villiers 2007). Ground water quality declines from the upper to the lower Berg river sections due to geological changes from the Table mountain group quartzite in mountainous areas, to the Malmesbury shale and the Cape granite suite (Seyler 2015).

The decline in rainfall in the WC in the past decade highlights has had a negative impact of dryland wheat production. Given the above, there is a need to consider supplementary wheat irrigation in the WC. It is important to note that in the WC region in addition to droughts, water availability is constrained by an increase in competitive demand for fresh water from non-agricultural water users.

3.2   SATELLITE IMAGERY DATA PROCESSING

The satellite data sets acquired were processed to ground reflectance using PCI GEOMATICA (PCIGM) software followed by the computation of the normalized difference vegetation index

(NDVI). The pre-processing of the satellite imagery was carried out as outlined in Sections 3.1.1 and 3.1.2 for L_8 and S_2, respectively.

3.2.1   Landsat 8

The L_8 imagery spanning the period April to October were downloaded from the USGS data archive centre's (https://lpdaac.usgs.gov/tools/usgs-earthexplorer/). Out of these only six L_8 images acquired on the following dates 30/4, 16/5, 1/6, 3/7, 4/8 & 21/9 , which span the 2016 winter wheat growing season were cloud free. The L_8 level 1 product contains georeferenced scenes in reflectance values recorded in digital numbers (DN). The DN values are processed to ground reflectance values referred as to as level 2 products using the Focus module of the PCIG software. The Focus module uses the calibration coefficients stored in the image Landsat metadata file (MTL) to compute ground reflectance values, atmospheric correction level 2 (ATCOR2) from image DN values . The MTL file c contains data on the sensor type, solar zenith and azimuth angles, and acquisition dates. Cloud and water masking were checked, and a constant default elevation used. The aerosol type was set to rural for mid altitude winter conditions, and visibility at a default of 30 km. A kernel size of 7 cells and 3 iterations were set for adjacency effects in the reflectance correction step and maintained throughout the processing of all images for consistency. The L_8 image inventory are tabulated (Table 3.1), based on which the crop coefficient (K_c) were subsequently modelled.

Table 3.1 L_8 satellite images inventory

Image acquisition date (day /month) in 2016	L_8 image denoted as JD from which was modelled K_c.	ET_0 (HS & PM) (mm/day) surfaces at 30 m SR denoted in JD to be multiplied by K_c surface in calculating the interval ET_c	Number of (HS & PM) ET_0 surfaces in the interval per given K_c surface in days
30/4	121	89..129	30
16/5	137	130..145	15
1/6	153	146..161	15
3/7	185	169..209	32
4/8	217	210..241	32
21/9	265	241..289	48

Table 3.1depicts the date L_8 image acquisition date in day/month, seen in the first column followed by the same date expressed as JD in column two. Column three shows the interpolated reference (either PM or HS) ET_0 surfaces denoted as JD, which were multiplied by L_8 NDVI based K_c of the

L_8 image acquired on date in column 2 (JD). The last column in Table 3.1 gives the total number of daily distributed references surfaces ET_0 depicted in JD per row, and indicates the variability in intervals between the usable satellite imagery acquired in the study.

3.2.2   Sentinel 2

Of the S_2 downloaded images, only ten cloud free 9-day composite S_2 images were of acceptable quality. Out of the ten deemed usable images only seven acquired on the following dates, 26/4, 17/5, 6/6, 26/7, 5/8, 26/8 and 13/9 /2016 which span the 2016 winter wheat growing season and are presented in Table 3.2 were eventually used.

The same processing steps as undertaken in the L_8 images processing were replicated for the S_2 images to determine the ground reflectance values from S_2 image DN values in order to maintain computational consistency. Table 3.2 details the seven S_2 imagery used to compute the season wheat crop water use in Section 3.3.

Table 3.2 S_2 Satellite image inventory

Image acquisition date (day /month) in 2016	S_2 image denoted as JD from which was modelled K_c	ET_0 (HS & PM) (mm/day) surfaces at 10m SR denoted in JD to be multiplied by K_c surface in calculating the interval ET_c	Number of (HS & PM) ET_0 surfaces in the interval per given K_c surface in days
04/07	98	89…107	18
26/4	117	108..149	20
6/6	158	150..212	63
5/8	218	213..227	14
26/8	239	228..247	19
13/9	257	248..261	14
23/9	267	262..272	10

Table 3.2 above indicates the interval between usable S_2 satellite images.

3.3   CLIMATE DATA PROCESSING & INTERPLATION

Climate data from 17 stations comprising of eight weather elements recorded on a daily basis i.e. maximum temperature (T_{maxi}), minimum temperature (T_{mean}), maximum humidity (Rh_x), minimum humidity (Rh_n), solar radiation (R_s), wind speed (U_2) and Rainfall (R) and Penman Monteith reference crop evapotranspiration (ET_{0PM}) were acquired from the ARC. Python scripts to compute daily ET_0 using the HS procedure (Hargreaves & Samani 1985) were developed and

presented in Appendix A. The detailed implementation of establishing the daily distributed ET_{0HS} and ET_{0PM} surfaces are carried out in Sections 3.2.1 and 3.2.2 respectively.

3.3.1 Hargreaves Samani reference (ET_{0HS})

The study area climate station geo references and altitude data are presented Table 3.3.

Table 3.3 Climate station geo-references

Climate station	Latitude	Longitude	m.a.s.l
LANGGEWENS	-33.27635	18.70623	191
POTERVILLE	-33.01247	18.99947	149
MOORREESBURG	-33.15406	18.67307	199
SCHAAPKRAAL	-33.53479	18.63126	111
KOPERFONTEIN	-33.10000	18.41796	61
LANDAU	-33.57783	18.96795	126
HLS BOLAND	-33.65424	18.88279	151
ABENDRUHE	-33.63701	18.95926	131
NEDERBURG	-33.71349	19.01295	144
BELLEVUE	-33.74809	18.95857	158
ASHANTI	-33.72356	19.04239	249
DE POORT	-33.70132	19.08466	892
RIVIERA	-32.68475	18.69635	90
ZUURVLAKTE	-32.97386	19.06136	1000
PIKETBERG: POOLS-IDEAL_HILL	-32.79748	18.88785	161
BOKSVELDSKLOOF	-33.18551	19.33753	1038
FAIRVIEW	-33.77729	18.92297	153

The ARC availed climate station data included, altitude in m, latitude in degrees, JD, minimum and maximum temperature in ^{0}C. To ensure enhanced clarity the first term of the Hargreaves Samani (HS) Equation 2.3 is reproduced below.

$$\text{ET}_{0HS} = 0.0023\text{Ra}(T_{mean} + 17.8) * (T_{max} - T_{min})^{0.5}$$

The equation terms were presented in Section 2.3.1. The station latitude in radians were calculated from the decimal degrees' latitude data in Table 3.3. The python script developed requires input

of latitude in radians and not in degrees, the JD, sunset hour angle, inverse relative earth sun distance, to compute the R_a term, which is the incident radiation as required in Equation 2.3 and implemented in Script A.1.1. The computed daily ET_{0HS} for all climate stations for the period 1st of January 2016 to the 31st of December 2016 were saved as an ET_{0HS} csv database indexed by JD. The set of equations used in computing ET_{0HS} using Script A.1.1 are as defined in FAO 56 (Allen et al. 1998) and were presented in Section 2.3.1. To enable the generation of study area interpolated daily ET_{0HS} surfaces, an ET_{0HS} csv database indexed by JD comprising all stations was joined to the climate station shapefile in ArcMap based on the climate station name field. In Section 3.4.1 the daily ET_{0HS} surfaces were multiplied by the appropriate crop coefficient (K_c) presented Table 3.1 the L_8 imagery inventory .The Spline with Tension interpolator (Mitasova et al, 1993) is a set of polynomial equations that generates a smooth surface passing through the sample points that minimising first derivative errors as described in Section 2.3.5.

The study area daily distributed ET_{0HS} mappings at 10 m and 30 m spatial resolution for 2016 were subsequently generated in ArcMap using the Spline with Tension interpolator based ArcPy scripts A.1.3 and A.1.4 respectively.

3.3.2   Penman Monteith reference ET_0

The study area daily reference ET_{0PM} data for the 17 stations was provided in an Excel workbook for the year 2016. An ET_{0PM} Excel csv data base was compiled from the above data, to include all climate stations ET_{0PM} arrays indexed by JD .The ET_{0PM} values are based on Equation 2.5 presented in Section 2.3.2. Using jupyter notebook release 5.0.0 in the Python ANACONDA Navigator
(https://www.google.com/search?q=anaconda+navigot&rlz=1C1GCEC_enZA865ZA865&oq=a naconda+navigot&aqs=chrome..69i57j0l7.38494j0j15&sourceid=chrome&ie=UTF-8), the climate station daily ET_{0PM} arrays where v-stacked to generate a Pandas data frame indexed by JD and climate station name, and saved as a csv database file in Excel using Script A.2.1. To enable spatial interpolation the ET_{0PM} csv data base file was joined to the climate station shapefile in ArcMap using the climate station name field. A Python script based on the spline with tension interpolator were implemented in ArcMap iterating on the daily PM values joined to the climate station shapefile. The study area daily distributed ET_{0PM} surfaces at 10 and 30 m SR were generated according to Scripts A.2.2 & A.2.3 respectively. The generated ET_{0PM} surfaces denoted in JD were multiplied by corresponding reference K_c presented in Table 3.1 and Table 3.2 at 30 and 10 m SR respectively, in Section 3.3 to compute crop water consumption on a pixel by pixel basis.

3.3.3 ET_{0HS} Validation.

ET_{0PM} data were taken as the actual study area reference crop evapotranspiration to which the computed ET_{0HS} values were validated. The ET_{0HS} validation was carried out based at   climate station level data. An ET_0 difference table was generated to indicate the level of errors when one uses ET_{0HS} in comparison to ET_{0PM}. The ET_{0HS} validation was important in ascertaining the accuracy of the HS methodology in determining study area ET_0. The absolute difference was generated by subtracting the ET_{0HS} values from the corresponding values of ET_{0PM} from which ET_{0HS} overestimation and underestimation of study area ET_0 could be discovered.

3.4   WHEAT CROP WATER USE

The wheat crop water use presented in this section was based on reference crop evapotranspiration (ET_0) computed using the Penman Monteith (PM) and the Hargreaves Samani (HS) methodologies.

3.4.1   Penman Monteith

The study area distributed daily Penman Monteith reference crop evapotranspiration (ET_{0PM}) surfaces were interpolated at 10 and 30 m SR in Section 3.2.2. In Section 3.4.1.1 the steps followed in computing the ET_{cPM10} are outlined followed by the ET_{cPM30} products in Section 3.4.1.2.

3.4.1.1   The PM_{10} crop water use product (ET_{cPM10})

The seasonal wheat crop water use (mm) was determined from modelled K_{cS2} and ET_{0PM} surfaces. The wheat crop coefficients (K_{cS2}) were modelled based on NDVI of Sentinel2 (S_2) imagery presented in Table 3.2 . The ET_{0PM} surfaces interpolated at 10 m SR were computed using the spline with tension interpolator in ArcMap. The interval ET_{cPM10} corresponded to the product of modelled K_{cS2} and sum of ET_{0PM} distributed daily surfaces presented per given data row in Table 3.2, 3rd column. These interval ET_{cPM} calculated above were subsequently summed up to give the seasonal ET_{cPMS2} drawn at 10 m SR, which is the S_2 image pixel size. The above computation were implemented in ArcMap using Script A.2.2.

Image NDVI values includes both positive and negative values, and for the purposes of this study all values below zero were all set to zero. The K_{cS2} was computed from NDVI using Script A.2.4.2. In the single big leaf approach crop water use was defined as the product of ET_0 by K_c (Allen et al. 1998). The ET_c computation from the daily distributed surfaces of ET_0 and K_c based on Equation 3.1. NB that the above referred to ET_0 and K_c values were calculated at pixel level and covering the whole study area. An aggregation scheme was implemented, where the interval ET_{cPMS2} were accumulated to give the seasonal crop water use, according to Equation 3.2. The

implementation of Equation 3.2 was carried out using Script A.2.4 in ArcMap based on S_2 image inventory seen in Table 3.2 . The summed up reference surfaces depicted as $\sum ET_{0pm10j}$ refer to the JD denominated ET_{0PM} surfaces in the 3rd column of Table 3.2 which were multiplied by the interval K_{cS2}. For example the 1st row and 3rd column in Table 3.2, has daily ET_{0PM} surfaces for JD, 89th to 107th 2016, i.e 18 ET_{0PM} study area surfaces, whose corresponding K_c value is modelled from the S_2 image of 98th day in 2016 given in 2nd column.

Equation 3.1

Interval $ET_{cPMS2} = K_{cS2} * \sum ET_{0PM10}$

Where: ET_{cPMS2} Crop water use based on the PM at 10 m SR and S_2 modelled K_c;

K_{cS2} S_2 modelled crop coefficient (); and

$ET_{0\ PM10}$ PM ET_0 interpolated at 10 m SR.

Equation 3.2

Seasonal $ET_{cPM10S2} = \sum ET_{cPMS2}$

Where ET_{cPMS2} Seasonal crop water use using S_2 and ET_{0PM}.

$\sum ET_{0pm10}j$ Sum of Interval crop water use determined (per satellite pass) in Equation 3.1 based on S_2 inventory in Table 3.2.

The generated daily $ET_{0PM10S2}$ and $ET_{cPM10S2}$ surfaces are in mm and the seasonal $ET_{cPM10S2}$ are in mm for the whole season on a pixel by pixel basis.

3.4.1.2   The PM 30 crop water use product (ET_{cPM30})

The ET_{cPM30} was estimated as indicated above for the ET_{cPM10} but this time using the K_{cL8} calculated as indicated in Equation 3.6. The procedure is repeated below for the computation of the distributed seasonal crop water requirements ET_{cPM30} in the study area. The L_8 image inventory presented in Table 3.1 indicates the image acquisition dates and JD , the interval between satellites overpass times in days, the sets of daily distributed ET_0 study area surfaces denoted by JD that were used with the corresponding satellite K_c map, to compute the crop water use as proposed in Section 3.3. For example using the 3rd row in Table 3.1 to illustrate the computation shown below the Landsat8 (L_8) image of the 1st of June 2016 was 153 JD and the NDVI of that scene was calculated according to Equation 3.3 .The K_{cL8} were modelled from Landsat8 NDVI. The crop water use ET_c was estimated as the product of modelled K_{cL8} multiplied by the sum of the associated sets of daily distributed ET_0 surfaces 146 to 161 JD of 2016, in 3rd column and 3rd row of Table 3.1. The third row has 15 ET_0 surfaces whose common K_c surface is of the 153 JD L_8, image. The K_{cL8} was held constant in each interval between successive satellites overpass dates. The $ET_{c\ PM30}$ crop water use was determined using daily distributed $ET_{0\ PM30}$ surfaces and the

modelled K_{cL8} values. The $NDVI_{L8}$ was calculated as shown in Equation 3.3 below using map algebra in ArcMap.

<div align="right">Equation 3.3</div>

$$NDVI_{L8} = (NIR_{B5L8} - Red_{B4L8})/(NIR_{B5L8} + Red_{B4L8})$$

Where: NIR_{B5L8} Band 5, 845 - 885 nm and

                  Red_{B4L8} Band 4, 630 – 680 nm.

The K_{cL8} was modelled using Equation 2.2 but in this instance using the NDVI from Equation 3.3 for the L_8 sensor ($NDVI_{L8}$) and implemented based on Script A.2.4.1 in ArcMap. The interval ET_c for L_8 datasets was determined based on Equation 3.4 using K_{cL8} and daily distributed ET_{0PM30} surfaces (mm.day^{-1}) at 30 m SR for the specific interval.

<div align="right">Equation 3.4</div>

$$\text{Interval } ET_{cPM30} = K_{cL8} * \sum ET_{0PM30m}$$

Where ET_{cPM30} the crop water use/consumption,

                K_{cL8} L_{8NDVI} modelled K_c and

                ET_{0PM30} PM Reference crop water requirements at 30 m SR per satellite interval.

The seasonal water use was based on summing up the interval crop water use surfaces generated from the L_8 images shown in Table 3.1 using Equation 3.5 implemented in ArcMap (Script A.2.5) .

Seasonal $ET_{cPML8} = \sum ET_{cPML8}$ <div align="right">Equation 3.5</div>

Where ET_{cPML8} Seasonal PML8 based crop water use (mm);

                $\sum ET_{cPM30}$ interval ETc associated with each usable L8 image

The $\sum ET_{0PMj}$ distributed daily study area surfaces denoted by JD used in Equation 3.5 are given in the 3rd column of Table 3.1 and are in mm.day^{-1}.

3.4.2 Hargreaves Samani

3.4.2.1 **The HS$_{10}$ crop water use product (ET$_{cHS10}$)**

The HS_{10} crop water use product (ET_{cHS10}) was computed using K_{cs2} modelled from $NDVI_{S2}$ derived from the S_2 images, presented in Section 3.1.2, Table 3.2 and the distributed ET_{0HS10} surfaces Equation 3.6.

Interval $ET_{cHS\,10} = K_{c\,S2} * \sum ET_{0HS10}$ Equation 3.6

Where ET_{cHS10} HS based crop water use;

                  K_c S_2 Modelled crop coefficient ; and

                  ET_{0HS} HS reference ET_0 at 10 m resolution.

The distributed cumulative seasonal crop water requirements were computed according to Equation 3.7 by summing up the interval ET_{cHS10} determined in Equation 3.6.

Seasonal $ET_{cHS10} = \sum ET_{cHS10}$ Equation 3.7

Where $ET_{c\,HS10}$ Seasonal HS crop water use, and

                  ET_{cHS10} interval $ET_{cHS\,10}$.

The seasonal ET_{cHSS2} was calculated based on Table 3.2 data and Script A.2.7 which implements Equation 3.6 and Equation 3.7 in ArcMap. The set of distributed daily ET_{0HS} (mm) denoted in JD associated with each K_c data set are given in the 3rd column of Table 3.2. Please remember that the $ET_{0\,HS10}$ and ET_{cHS10} are based on the 10 m SR interpolated ET_{0HS} surfaces and the K_{cS2} at 10 m SR using Sentinel2 scenes.

3.4.2.2   The HS_{30} crop water use product (ET_{cHS30})

The L_8 based NDVI was calculated as shown in Equation 3.3 using L_8 band 4 (R_{L8}) and L_8 band 5 (NIR_{L8}) in ArcMap. The used Landsat 8 image data inventory were shown in Section 3.1.1, Table 3.1.From the above dataset the study area distributed seasonal $NDVI_{L8}$ were calculated. The K_{cL8} crop coefficients were modelled from the $NDVI_{L\,8}$ according to (Script A.2.4.1) to give the distributed study area K_{cL8}. The distributed study area crop water use based on the HS methodology and at 30 m SR was determined according to Equation 3.8. Note that the L_8 satellite has a 30 m SR compatible with the HS_{30} interpolated ET_0 surfaces.

Interval $ET_{cHS30} = K_{cL8} * \sum ET_{0HS30}$ Equation 3.8

Where ET_{cHS30} HS based ET_c at 30 m SR,

                  K_{cL8} K_c modelled from $NDVI_{L8}$ based and

                  $\sum ET_{0HS\,30}$ Sum of interval ET_0 surfaces calculated at 30 m SR for   HS computed ET0.

The interval ET_{cHS30} were summed up to give the cumulative seasonal crop water use as outlined in Equation 3.9.

Seasonal $ET_{cHS30} = \sum ET_{cHSL8j}$ (mm)   Equation 3.9

Where: ET_{cHS30} Seasonal HS crop water use at 30 m SR ,

                 $\sum ET_{cHSL8j}$ ET_0 sum of ET_0 based on JD_j between L8 passes.

Equation 3.9 shows the summation of the interval ET_{0HS30} determined per given L_8 scene modelled K_c and associated ET_0 surfaces as depicted in   Table 3.1. The implementation of Equation 3.8 and Equation 3.9 was carried using Script A.2 in ArcMap based on L_8 image data in Table 3.1. The interval ET_c is calculated using each row data i.e. the L_8 satellite K_c multiplied by sum of the ET_{0HS} surfaces in 3rd column Table 3.1. The interval ET_c are subsequently summed up to give the seasonal ET_{cHSL8}, a summation of the row based ET_{cHSL8} computations. The season ET_{cHSL8} data values were extracted from crop water use map seen in Figure 4.6 using the study area wheat field polygons.

3.5   WHEAT YIELD

Wheat yields were determined using the empirical model based on NDVI (Mashaba et al. 2017) and developed scripts in ArcMap as indicated in the literature review. The flowering period was estimated to coincide with relatively   high NDVI values that occur at the end of the vegetative growth period. In addition, to facilitate comparability of the modelled yields the $NDVI_{L8}$ and $NDVI_{S2}$ based images were supposed to be imaged approximately at the same time, to have near identical values NDVI values. To satisfy both the criteria above, the L_8 and S_2 scenes imaged on the 4th and 5th of August respectively, were chosen. NDVI values are highly dynamic and change as the season progresses. The seasonal K_c curves which have been used as proxy for monitoring seasonal NDVI evolution are shown in Figure 4.6. Remember the K_c were modelled directly from NDVI using a linear relationship.

3.5.1   Landsat 8 based wheat yield

Wheat yields were modelled using Equation 2.11 based on NDVI of the L_8 image of 5th of August 2016 and Script A.3.2 implemented in ArcMap. To recap, the yield equation is reproduced below.

$Y_{L8} = 12.1136$ NDVI $_{L8} - 2.7307$ Equation 3.10

The wheat yields are in t.ha^{-1} based on dry grain and mapped at 30 m pixels. The yield data was extracted using the zonal statistics as table tool in ArcMap. The statistics generated were saved as a dbase and converted to Excel spreadsheets.   The modelled yields were presented in Section 4.2.

3.5.2   Sentinel 2 based yield

The distributed winter wheat yields were estimated as outlined in Section 3.5.1. The Equation 3.11 shown below was implemented in ArcMap using Script A.3.3 and S$_2$ image NDVI of the 4th August.

$Y_{s2} = 12.1136$ NDVI$_{S2}$ - 2.7307   Equation 3.11

Where Y_{s2} wheat yield (in t.ha^{-1}),

                     $NDVI_{S2}$ NDVI based on S$_2$ image of 4/8/2016,

The computed wheat yields surfaces are in t.ha^{-1} of dry wheat grains and mapped at 10 m spatial resolution. The yield results were extracted using the zonal statistics tool and are presented in Section 4.2. These were validated using Langgewens yields and those in the literature.

3.5.3   Yield gap

Yield potential is the yield that best farmers utilising the latest technologies and applying requisite inputs including water can attain in a given area, approximated by yields achieved in irrigated fields with good management (Van Ittersum et al. 2012). Yield gaps on the other hand is the difference between average farmers, yields and the 90th or 95th percentiles level, for a given area yields data. In addition to percentile statistical analyses methodology, the mean difference statistic comparison was used to determine yield gaps considering the study area mean yields and yield averages attained in other areas in SA and in in Europe, i.e. France, Netherland and the United Kingdom. The latter difference between the means of the worst and best producers is commonly used in potential yield gap calculations (Sosibo et al, 2016).

The yield gap indicates a study area production potential. There are a number of approaches indicated below,

1.   Yield gap (t.ha^{-1}) = 95th Percentile crop yield - mean crop yield. Higher gap expected.

2.   Yield gap = 90th Percentile crop yield - mean crop yield. Conservative gap.

3.   Yield gap = productive country mean yield – study area mean yield (Sosibo et al, 2016).

In this study methods 1 and 3 were implemented. As indicated earlier the yield data were extracted using the zonal statistics tool and the study area wheat field polygons.

3.6   WATER PRODUCTIVITY

The amount of grain produced per unit of water consumed is a measure of water productivity. Water productivity is formally defined as the wheat yield to seasonal crop water use in units of $t.ha^{-1}.mm^{-1}$ or $kg.m^{-3}$ (Molden et al. 2010; Descheemaeker et al. 2013; Zwart & Leclert 2010). In the study water productivity was determined according to Equation 3.12.

$$WP_{wheat} = \ y \ / \ cwu$$ Equation 3.12

Where y wheat yield per study area pixel $t.ha^{-1}$,

                cwu season crop water use in mm.

Four WPs were generated as outlined in the table below

Table 3.4 The four water productivity outputs

WP	y [Based on]	cwu [Based on]
$WP_{YL8/ETcHSL8}$	$Yield_{L8}$ (y_{L8})	ET_{cHSL8}
$WP_{YL8/ETcPML8}$	$Yield_{L8}$ (y_{L8})	ET_{cPML8}
$WP_{YS2/ETcHSS2}$	$Yield_{S2}$ (y_{S2})	ET_{cHSS2}
$WP_{YS2/ETcPMS2}$	$Yield_{S2}$ (y_{S2})	ET_{cPMS2}

As indicated in Table 3.4 water use computation was based on PM and HS at 10 and 30 m SR giving rise to four water products denoted as ET_{cHSL8}, ET_{cPML8}, ET_{cHSS2} & ET_{cPMS2} respectively. The yield surfaces were modelled using two scenes from Landsat8 and Sentinel2 giving two yield surfaces denoted as Y_{L8} and Y_{S2} respectively. The yield surface generated from S_2 image was alternatively divided by the seasonal ET_c calculated from S_2 based K_c and the PM and HS reference crop water requirements at 10 m SR. The L_8 yields were alternatively divided by the PM and HS based ET_c generated using Landsat8 based crop coefficients at 30 m SR.

The above computations were carried out in ArcMap using map algebra. Since the yields were modelled in $t.ha^{-1}$, and the water use estimates in mm hence the water productivity were denoted in $t.ha^{-1}.mm^{-1}$, a multiplication factor of a hundred was applied to convert the water productivity

to kg.m^{-3} (NB, 1mm water depth per ha is equivalent to 10 m^3 and a tonne is equal to 1000 kg hence the 100 multiplication factor).

CHAPTER 4:   RESULTS AND DISCUSSION

In this Chapter study results are presented first, followed by the discussion section. The computed wheat crop water use, yield, water productivity and yield gaps are presented under Sections 4.1 to 4.4, respectively. Crop water use is presented in the following section.

4.1   CROP WATER USE

The reference crop evapotranspiration (ET_0) computation results are presented first including a sample of distributed study area daily ET_0, followed by satellite-based crop coefficient (K_c) and crop water use (ET_c).

4.1.1   Reference crop evapotranspiration (ET_0)

The overall study area climate stations' PM and HS reference crop evapotranspiration mean monthly values for the year 2016,   were presented Table B 4 . The climate station ET_{0PM} and ET_{0HS} are presented side by side on a monthly basis to facilitate comparison and identification of anomalous values. Based on these ET_{0HS} and ET_{0PM} data a bar plot shown in Figure 4.1 was drawn. Note the average monthly standard deviation of 8.78 and 28.06 mm for ET_{0PM} and ET_{0HS} respectively seen in Table B 4 last row. A closer scrutiny of Table B 4 shows that the ET_{0HS} and ET_{0PM} are in close range of each other, however the ET_{0HS} has consistently higher values in nearly all the months, except in January, March and December.
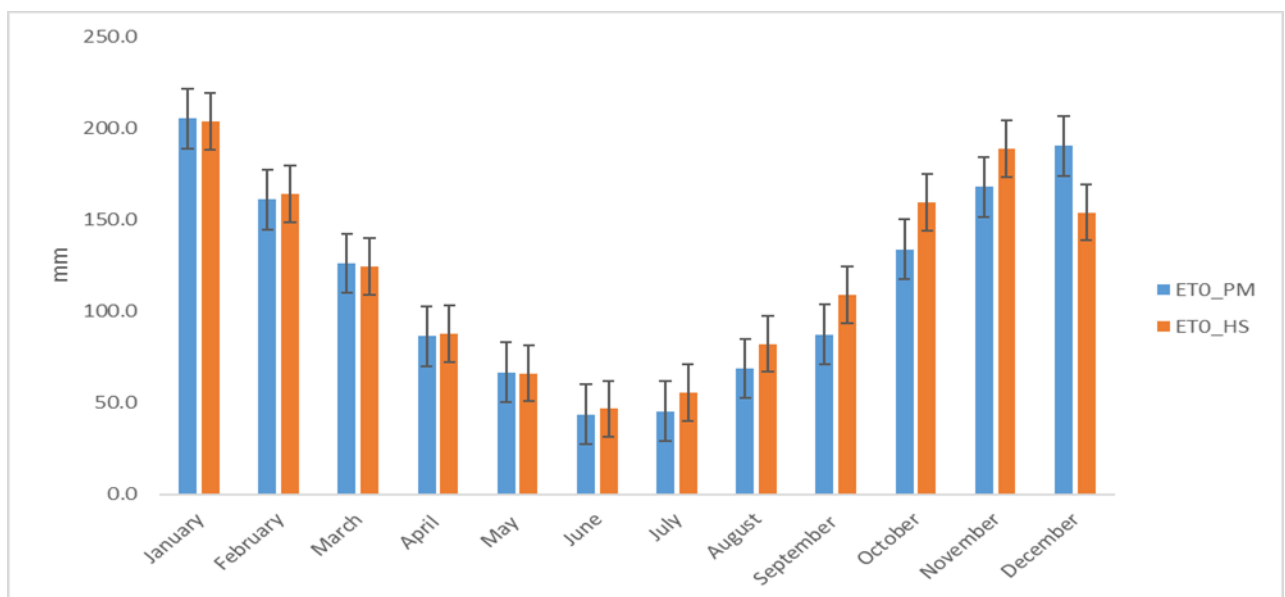

Figure 4.1 Berg catchment averaged climate station monthly ET_0 data in 2016

The study area climate station data ET_{0PM} and ET_{0HS} data were presented pairwise per month annotated with error bars in Figure 4.1. Both the ET_{0PM} and ET_{0HS} demonstrated the general tendency of reduced values in winter and higher values in summer given the high incident radiation in summer compared to winter. In addition, under low temperatures the vapour pressure deficit is lower leading to reduced evapotranspiration. The above is indicated by the short ET_0 bar heights during winter and   longer ET_0 bars during the summer periods. The detailed monthly summations of ET_{0HS} per climate station, are shown in Table B 1, while the monthly summed ET_{0PM} are given in Table B 2. Based on the values in Table B 1 and Table B 2, the highest ET_{0PM} values of 131.04 mm were recorded at Ideal_pool_Hill climate station and the lowest annual ET_{0PM}, of 104.60 mm recorded at De_Poort climate stations. The annual monthly average ET_{0PM} for Abendruhe was 108.50 mm compared to an ET_{0HS} of 125 mm, indicating a slight ET_0 overestimation at that station. The ET_0 results varied according to computational methodologies (Table B 1 and B 2).The monthly ET_{0HS} overestimation and underestimation of ET_0 using the ET_{0PM} as the standard are shown in Table B 3 . The annual based monthly climate station average ET_{0HS} and ET_{0PM} were used to depict the temporal and spatial variation of the ET_{0PM} less ET_{0HS}. In December, Porterville climate station had a monthly ET_{0HS} value of 121.48 mm compared to an ET_{0PM} of 212.65 indicating an ET_0 underestimation of 90 mm i.e. equivalent to an error of 3mm.day^{-1}. The results indicated that climate stations ET_{0HS} tended to deviate from the monthly ET_{0PM} values in the year 2016 with the magnitude of the differences higher in some stations and months for example, Zuurvlakte and Riviera and Porterville. Figure 1.1presentsa graphic depiction of ET_{0HS} overestimation and underestimation of study area ET_0 values per station and per month, using Table B 3 data. Positive values above the zero horizontal axis depicts the ET_{0HS} underestimation of study area ET_0, while negative values indicated over estimation of study area ET_0.

Climate stations with the lowest absolute monthly variation were identified as Abendruhe, Ashanti, Bellevue, Bokveldskloof, De_poort, Langgewens, Fairview and HLS_Boland, while the rest show high absolute difference values, especially for the months of December 2016. Zuurvlakte climate station had high absolute monthly values of over- and under- estimation of ET_{0HS} at 70 mm and 50 mm, respectively. To ascertain the level of errors in the HS methodology a RMSE computation was carried out. The climate stations ET_{0HS} root mean square error summary are presented in Table 4.1.
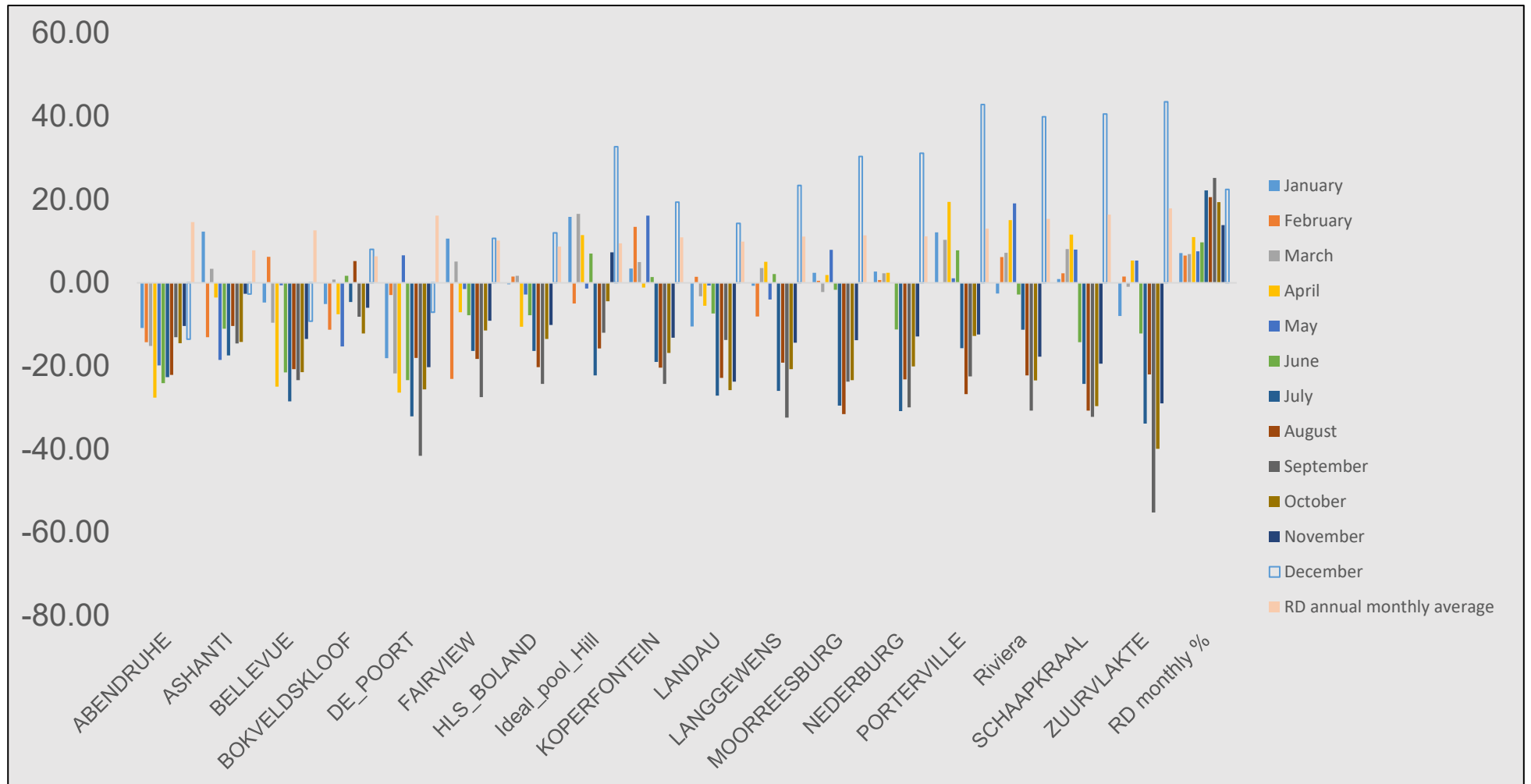
Figure 4.1 Relative difference % [$ET_{0PM} - ET_{0HS}$]/ET_{0PM}

Table 4.1 ET_0 RMSE Summary

Berg river catchment 2016	RMSE	RMSE
Annual station ET_0 values [ET_{0PM} vs ET_{0HS}]	24.51mm per year per station	2.0425 mm/month
Monthly average station ET_0 values [ET_{0PM} vs ET_{0HS}]	12.78 mm per month per station	0.426 mm / day

Note that the description in this section was based at climate station reference evapotranspiration values. Please note the low ET_{0HS} errors shown in Table 4.1 generated using ET_{0PM} as the benchmark. The study area ET_0 spatial variation was demonstrated on a GIS surface generated on 140th JD. The distributed ET_{0PM} and ET_{0HS} surfaces at 10 and 30 m SR for JD 140 generated in the study area was presented in

Figure 4.2, where JD referred to the number of days elapsed from January the 1st in 2016. The relative difference of the ET_{0HS} and ET_{0PM} using climate station data was generated based on ET_0 values in Table B 2 and Table B 3. The relative difference percent was determined as the ET_{0PM} less ET_{0HS} and divided by the respective ET_{0PM} in Table B 3 and Table B 2 respectively. The relative difference data in percent was presented in Table B 5 . The relative difference data in Table B 5 was depicted in Figure 4.1

The values within the table are the RD in percent and were calculated as follows (ET_{0PM} less ET_{0HS}) /ET_{0PM} value per month and station. The negative values indicated over estimation of ET_0 when using the ET_{0PM} as the standard. And the positive values were an under estimation of ET_0

The absolute values were added down each columns to give the station annual sum of relative absolute difference which were in turn averaged on a monthly basis .The resulting values were presented in the last row of Table B 5. The RD % did not exceed 20 percent which means that on average the ET_{0HS} was within 20% of ET_{0PM} values.

The Figure 4.2 shows the interaction of the methodology and spatial resolution effects on the generated ET_0 surfaces for the 140th JD in 2016. The surfaces are at the same scales and the towns have been included to put the spatial variation in a geographic context. The included common ET_0 legend (mm.day^{-1}) serves to indicate the respective values of ET_0 per given locality, allowing for one to compare the differences due the methodologies and spatial resolution.   Please note the ET_0 surface similarities per given methodology, irrespective of the spatial resolutions.
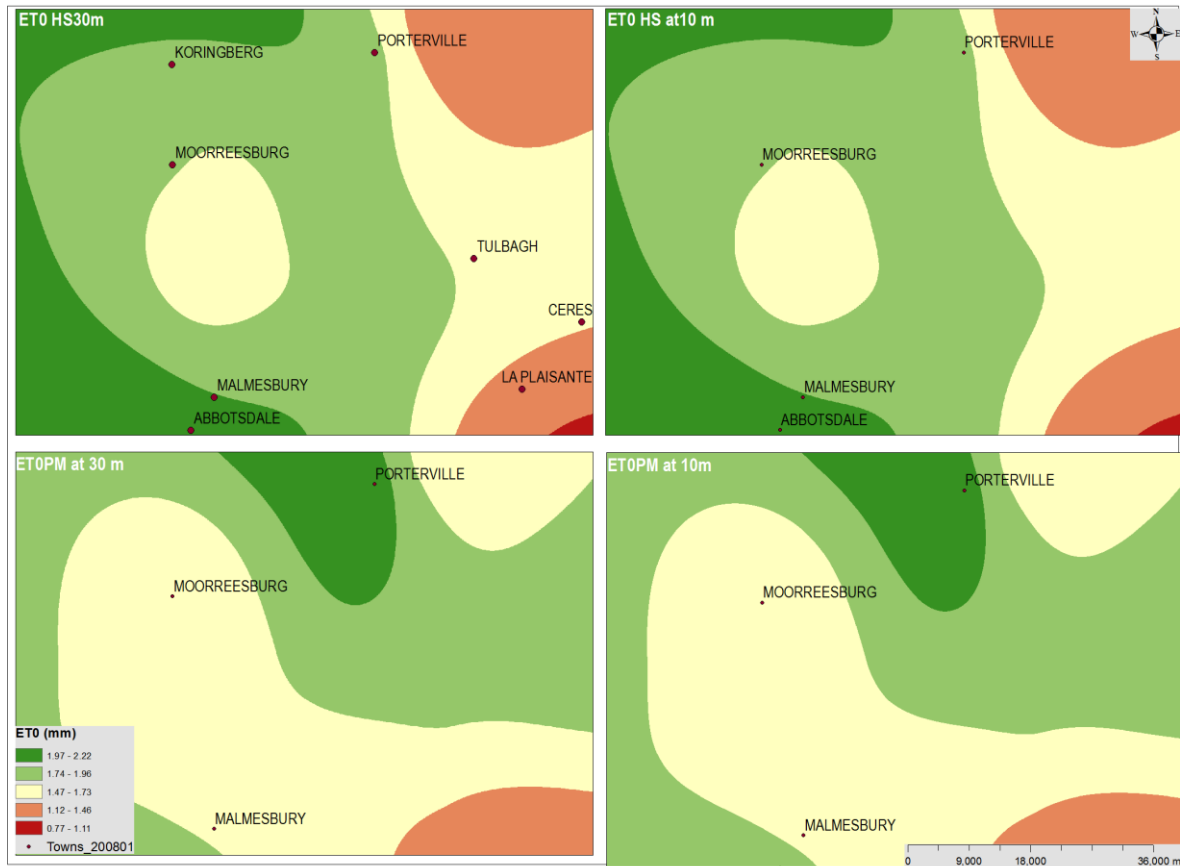
Figure 4.2 Study area 140 JD ET_0 surfaces 2016

The distributed ET_0 surfaces indicated that ET_{0HS} had higher values (green colour) when compared to ET_{0PM} values (brown colour) seen on the colour legend. The crop coefficients (K_c) results are presented next.

4.1.2   Crop coefficient (K_c)

A sample of S_2 and L_8 scenes captured in 2016 paired with modelled K_c are presented in Figure 4.3 .

Samples of K_{cL8} and L_8 images are presented in pairs in the first row, followed by K_{cS2} and S_2 images pairs in the 2nd row. To reduce data clutter the town names have been shown only on the L_8 image of the 5th of May. The S_2 images are crisp and lighter in colour than the L_8 images. The representation serves to illustrate how the research study was carried out. Subsequent to satellite image processing the pixel NDVI were computed.
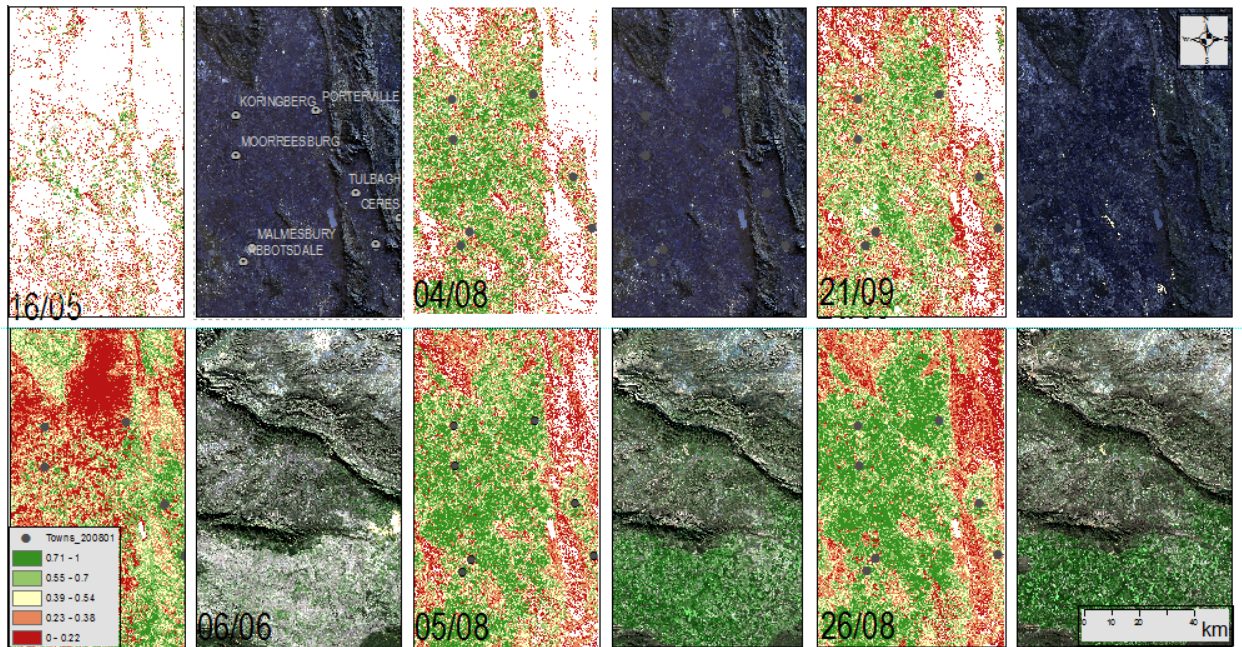
Figure 4.3 S_2 & L_8 Scenes and modelled K_c

The NDVI modelled K_c were used to compute study area ET_c. Frequent cloud cover in the 2016 season, reduced the number of usable L_8 and S_2 images for computing NDVI and modelling K_c. The sample used to illustrate the $NDVI_{L8}$ and $NDVI_{S2}$ evolution for the winter wheat season are presented in Figure 4.4.
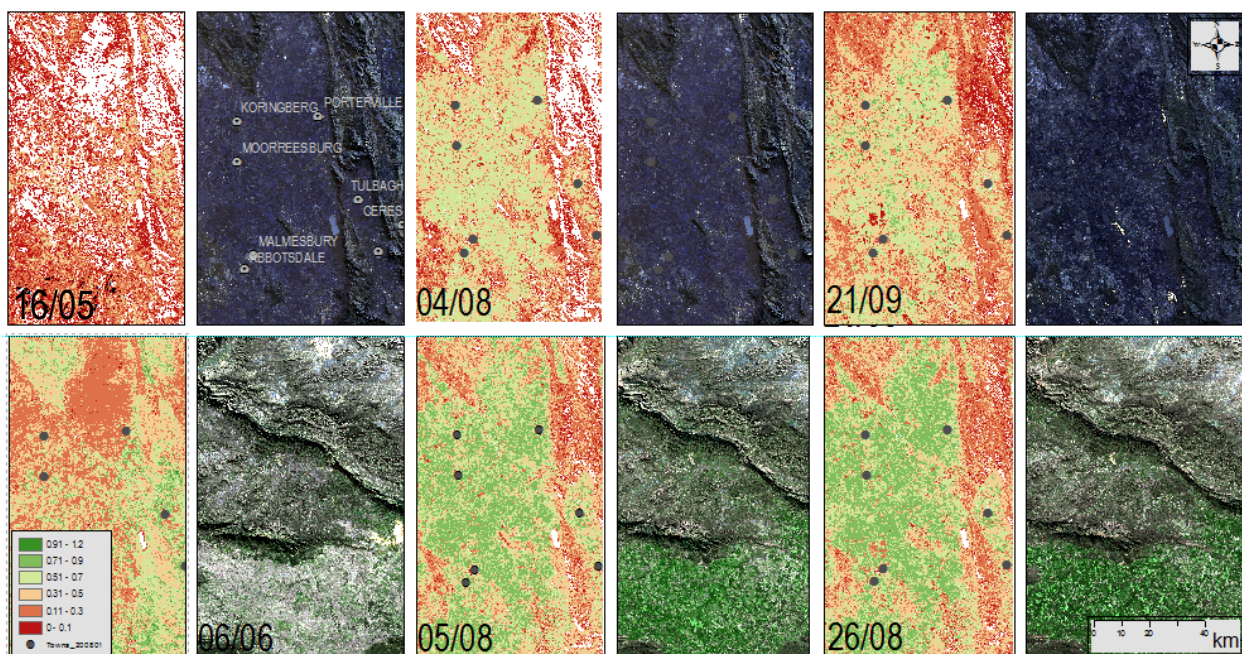
Figure 4.4 Sample of L_8 and S_2 NDVI surfaces

The satellite scene quality depended on prevailing atmospheric weather conditions since L_8 and S_2 are both passive sensors that depend on solar illumination. Image quality can be ascertained by colour variations with images being dark due to either sensor malfunctioning or obscured scene,

hence low ground level reflectivity. Bastiaanssen & Bos (1999) highlighted that technical shortcomings in the satellite imaging and receiving systems have negative impacts on image quality and subsequent retrievals. Seven S_2 images were finally used out of a possible thirty that were imaged, due to persistent cloud cover. The white patches in the modelled K_c surfaces are pixels with nodata values. The L_8 and S_2 images inventories are presented in Table 3.1 and Table 3.2 respectively.

According to the colour scheme in Figure 4.4 the high NDVI values were observed later in the season indicating crop growth vigour. The L_8 and S_2 of 16/04 and 06/06 respectively, had the lowest NDVI values typical of the crop establishment stages. According to the colour scheme adopted the NDVI $_{S2}$ were consistently higher than the NDVI $_{L8}$. This is expected because of the difference in S_2 and L_8 SR. When the S_2 satellite imagery, availed climatic data and corresponding NDVI are considered together, a discernible pattern is evident. The pattern indicated the prevalence of low NDVI values in the high altitude regions with low lying areas having high NDVI values. Crop coefficients, determined from L_8 and S_2 NDVI maps were presented in Figure 4.3. Given that K_c were modelled based on satellite sensor's NDVI, which are directly related, Figure 4.3 mirrors the seasonal NDVI trajectory.

Seven S_2 images were used in the computation of NDVI and modelling of K_{cS2}. The reduced number of satellite images and hence the sampled K_c maps were not expected to negatively impact the seasonal wheat crop water use values. A few K_c values if spread throughout the season coupled with daily ET_0 surfaces can be used in estimating seasonal ET_c. The quantitative crop coefficient data was extracted from the modelled K_c surfaces using the zonal statistics tool in ArcMap based on study area wheat fields polygons and are presented in Table 4.2 and Table 4.3.

Table 4.2 K_{cS2} (ratio unitless) inventory

Date	JD	Mean	Max
04/07	98	0.236	1.029
26/04	117	0.236	1.029
06/06	158	0.595	1.157
05/08	218	0.938	1.094
26/08	239	0.954	1.096
13/09	257	0.87	1.071
23/09	267	0.84	1.094

Table 4.2 and Table 4.3 outline the average and maximum of the K_{cS2} and K_{cL8} statistics respectively. Note the low values at the start and end of the season for the mean statistic but the maximum K_{cS2} statistic did not indicate a decline implying that some pixels included in the study had other vegetation and not wheat. However, the mean study area statistic captures the study area K_{cS2} seasonal trajectory.

Table 4.3 K_{cL8} inventory

Date	Image acquisition date in JD	Mean	Max
30/04	121	0.185	0.761
16/05	137	0.248	0.841
03/07	185	0.419	0.846
04/08	217	0.637	0.846
21/09	265	0.660	1.004
23/10	297	0.160	0.986

Take note of the K_c values shown in the 3rd column of Table 4.2 and Table 4.3, these represent the gross average study area K_{cS2} and K_{cL8} values respectively. The above K_{cS2} and K_{cL8} mean values versus time (JD) plots are depicted in Figure 4.5. The October mean and maximum statistics indicated lower K_{cL8} values late in the season.

Note the difference between the mean study area K_c values in Table 4.2 and Table 4.3 respectively. The graphic representation in Figure 4.5 showed similarities of the general form of K_c curves irrespective of the K_c estimation methodology. However, the L_8 based coefficients were consistently lower than the corresponding S_2 based coefficients. Based on Table 4.2 and Table 4.3, and Figure 4.5, crop coefficient increased in value from 0.23 and 0.185 to maximum values of 0.954 and 0.660 for the K_{cS2} and K_{cL8} respectively. Thereafter the coefficients started to decrease, as the crop reached maturation and senescence.
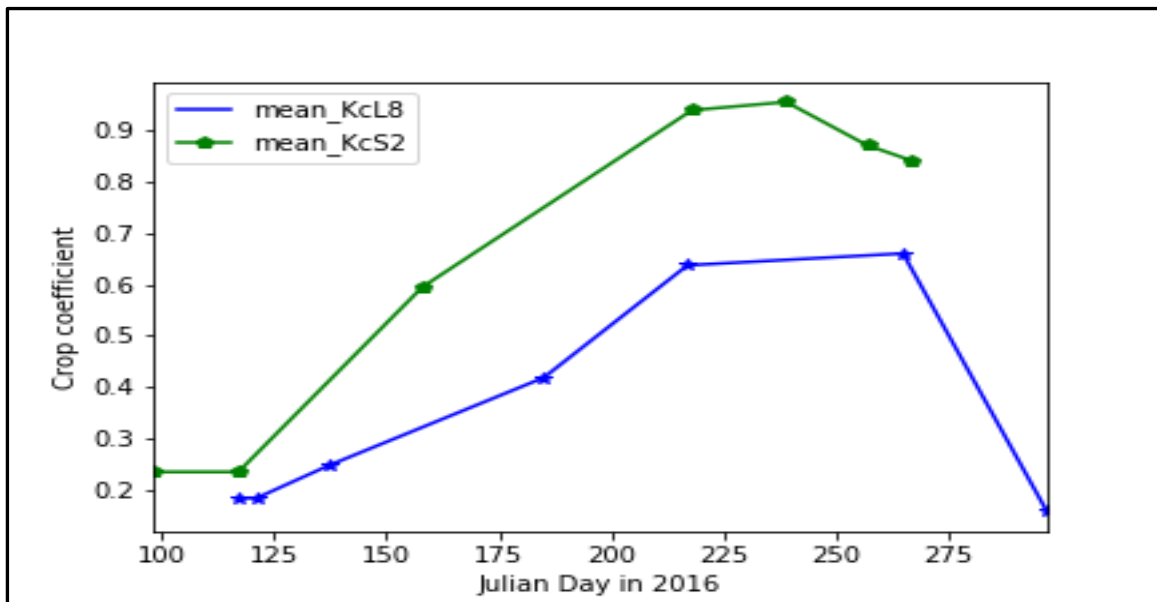
Figure 4.5 Wheat mean K_{cS2} and K_{cL8} curves, Berg river 2016

4.1.3 Crop water use

The seasonal crop water use distributed surfaces are presented in Figure 4.6. There are four seasonal wheat crop water requirements products computed in the study area for the 2016 winter wheat growing season .These were the Hargreaves Samani ($ET_{c\,HS}$) based crop water use at 10 and 30 m spatial resolution, using S_2 and L_8 based crop coefficients (K_c), respectively and the Penman Monteith (ET_{cPM}) at corresponding resolutions and are outlined in Table 4.4.

Table 4.4 Wheat crop water use products

Remote satellite sensor……. Crop water use Methodology	Hargreaves Samani (HS)	Penman Monteith (PM)
Landsat8 (L_8) at 30 m spatial resolution	ET_{cHSL8}	$ET_{c\,PML8}$
Sentinel2 (S2) at 10 m spatial resolution	ET_{cHSS2}	ET_{cPMS2}

In the second row of Table 4.4 is presented the   crop water use products based on the HS and PM methodologies, with crop coefficients (K_c) developed from L_8 satellite data , at 30 m spatial resolution ($ET_{c\,HS\,L8}$ and $ET_{c\,PML8}$). The distributed study area ET_0 surfaces were generated at 30 and 10 m spatial resolution for compatibility with the L_8 and S_2 sensor pixel, respectively (Section 3.2).In the third row, the ET_{cHSS2} and ET_{cPMS2} products which are at 10 m spatial resolution, determined from K_{cS2} and the study area distributed ET_0 surfaces are shown. The respective seasonal crop water use mappings are presented in Figure 4.6.
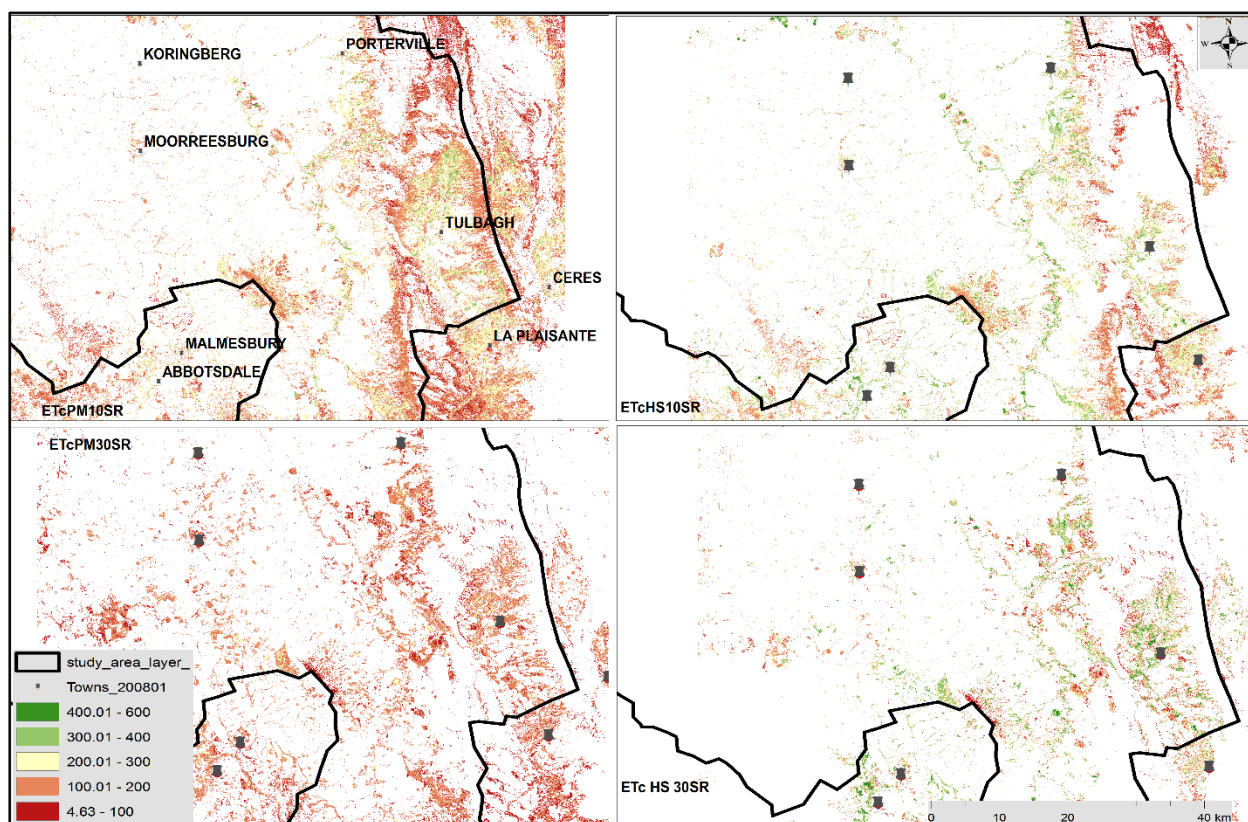
Figure 4.6 Seasonal wheat crop water use (mm) in Berg river catchment, 2016

Based on zonal statistics extracts of crop water computations presented in Figure 4.6 the crop water use tabulated summaries are presented in Table 4.5.

Table 4.5 Seasonal wheat water use (mm)

Zonal statistics	ET_{cPML8}	ET_{cPMS2}	ET_{cHSL8}	ET_{cHSS2}
minimum (median)	99.22	123.06	151.36	188.34
maximum(median)	149.20	221.99	207.02	330.93
minimum(average)	97.87	125.40	151.73	193.00
maximum(average)	151.14	222.96	204.93	321.09
maximum	290.90	414.07	316.47	463.83

The crop water use statistics were impacted by both ET_0 estimation methodologies and the spatial resolution. The HS based crop water use had higher values than the PM based values which can be ascribed to the overestimation of ET_0 by the HS (ET_{0HS}) methodology as noted earlier. The columns from the left to the right indicated increasing values in crop water use with the ET_{cHS} values being higher than the ET_{cPM} values per given spatial resolution. For example in the maximum statistics row of Table 4.5, the ET_{cPM} and ET_{cHS} values are 290.90 and 316.47 mm at 30 m spatial resolution, compared to 414.07 and 463.83 mm at 10 m spatial resolution, respectively. The S_2 based distributed wheat crop water use surfaces had higher values than the L_8 based values.

To appreciate the resultant crop water use values given the different methodologies, and spatial resolutions estimation dynamics the Table 4.5 data was graphed in Figure 4.7.

The graphic depiction in Figure 4.7 illustrated the HS methodology's consistency in overestimating crop water use at both the 10 and 30 spatial resolutions.
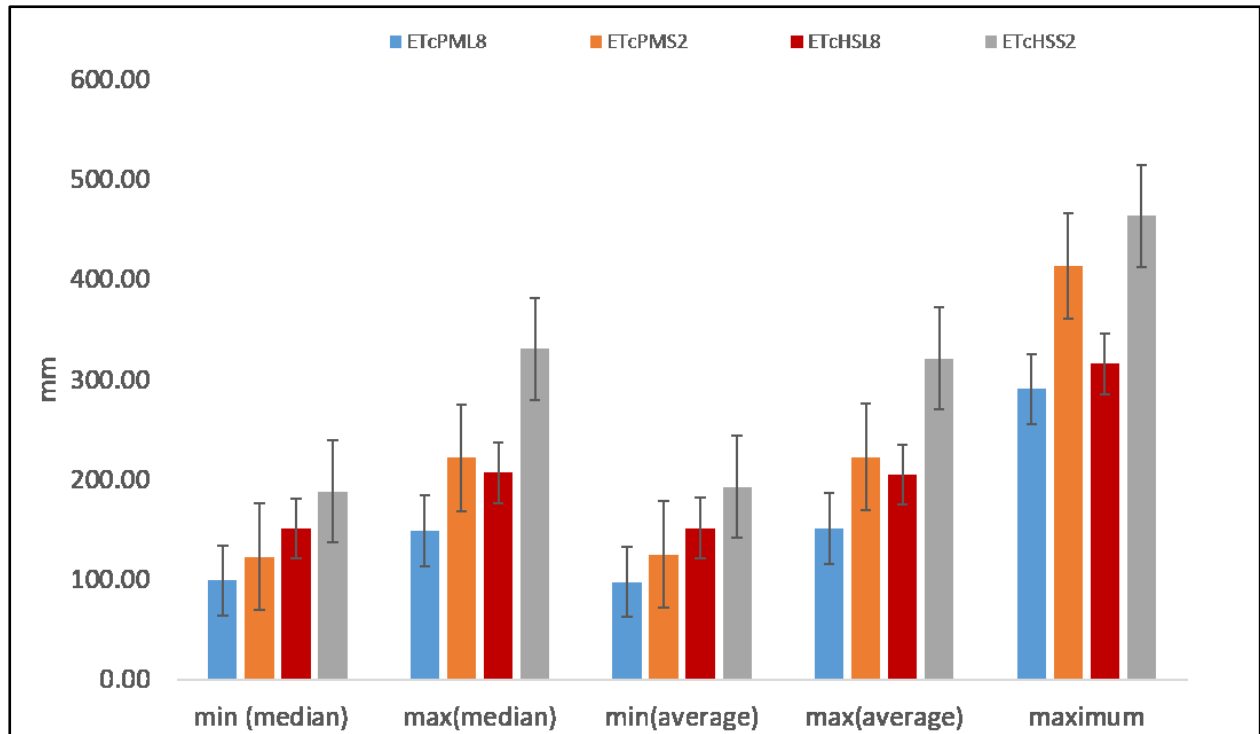
Figure 4.7 Seasonal wheat crop water use graph

The L_8 based ET_c crop water use values were lower than the S_2 based values due to lower $L_{8\ Kc}$ values.A discernible pattern of increasing water use values is indicated in Figure 4.7 from ET_c values based on L_8 based retrievals of $NDVI_{L8}$ & K_{cL8} generated ET_c to the S_2 based computed crop water use. The modelled wheat yields results were presented in the section below.

4.2   WHEAT YIELD

The wheat yield results indicated that the modelled yield values depended on the sensors which had different spatial resolutions and spectral characteristics Wheat yields were modelled according to Equation 3.11 using the study area distributed S_2 and L_8 scenes NDVI imaged on the 4th and 5th August, respectively. The images were chosen on the basis of the highest observed NDVI of S_2 & L_8 images and temporal proximity, to ensure identical crop phenology, and hence similar image identical vegetation indices. The scene L_8 & S_2 NDVI on which the yields were modelled, and the generated yields are presented in Figure 4.8.The qualitative presentation clearly indicates that the S_2 based yields had elevated values than the L_8 yields seen in Figure 4.8

The NDVI and yield maps were generated in ArcMap using a seven colour classification scheme, from red to green bright to expose the sensors' differences. The legend in Figure 4.9 shows that the $NDVI_{S2}$ modelled wheat yields had higher values than the corresponding estimates based on $NDVI_{L8}$. The yield variation in this instance indicated that modelled yield depended on sensor spatial resolution with the higher spatial resolution S_2 modelling higher yields than the lower resolution L_8 sensor. The L_8 and S_2 based wheat yields zonal statistics were extracted using the Langgewens experimental farm plots. Langgewens conservation trials plots are presented in Figure 4.9 anotated with plot numbers. Actual yields from Langgewens plots were used in modelled wheat yields seen in Table 4.6 and Table 4.7, 6th column, validation.
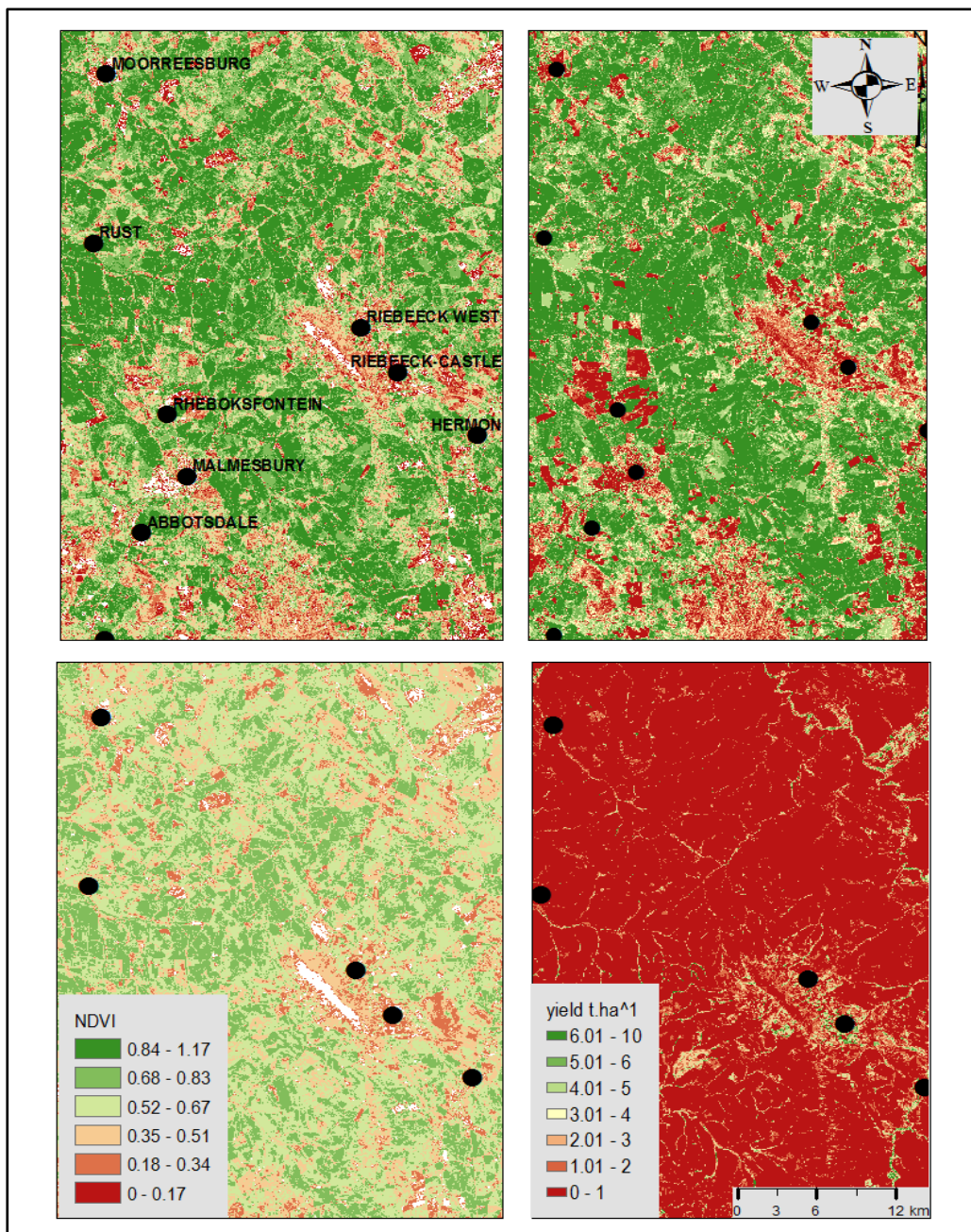
Figure 4.8 S_2 and L_8, NDVI and wheat yield surfaces, the Berg river catchment 2016

The study area wide L_8 and S_2 yields were extracted using the study area wheat field polygons.
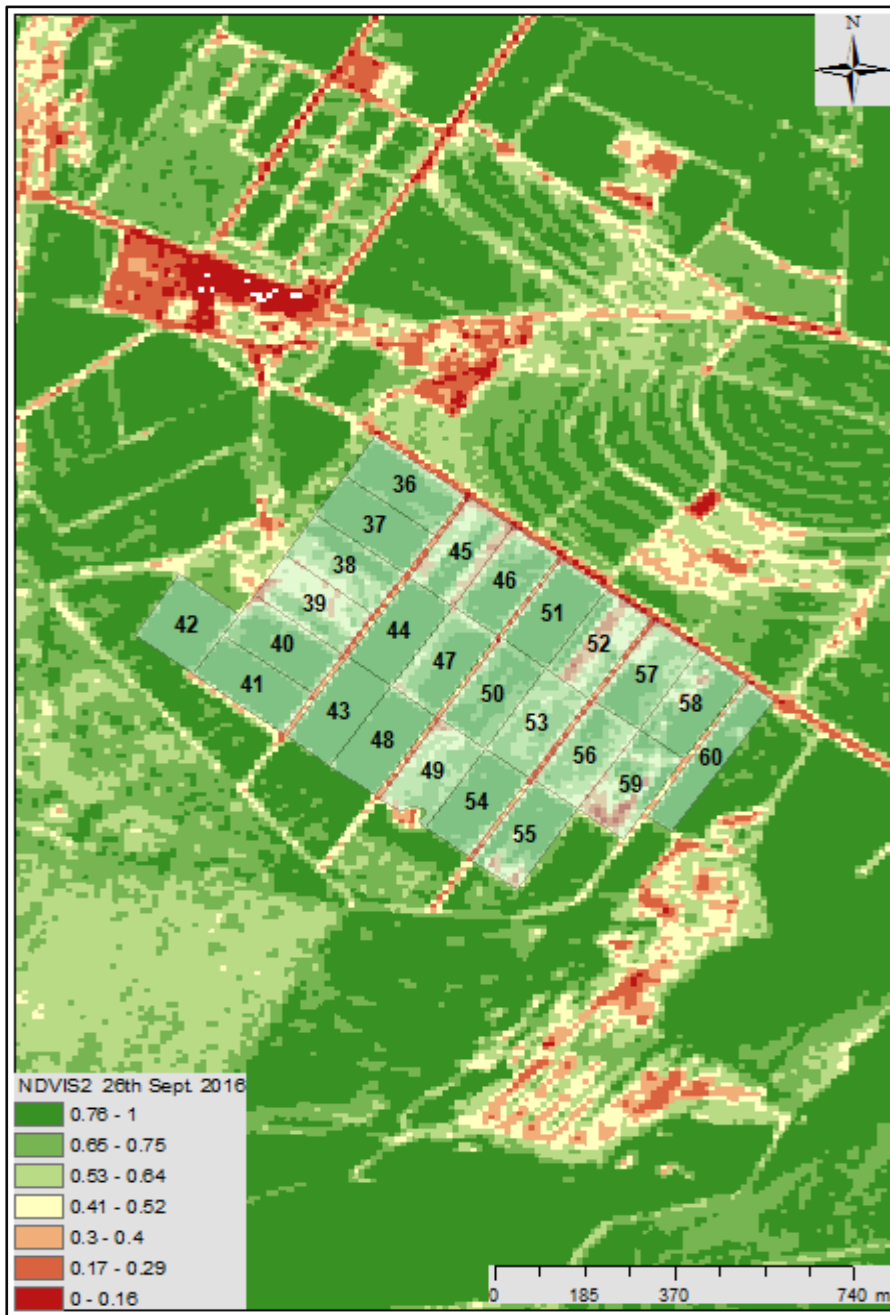
Figure 4.9 Langgewens plots

A scatter plot of the L_8 and S_2, based yields mean and maximum zonal statistics, seen in the 3rd and 4th columns of Table 4.6 and Table 4.7, respectively and the Langgewens yields are presented in Figure 4.10.
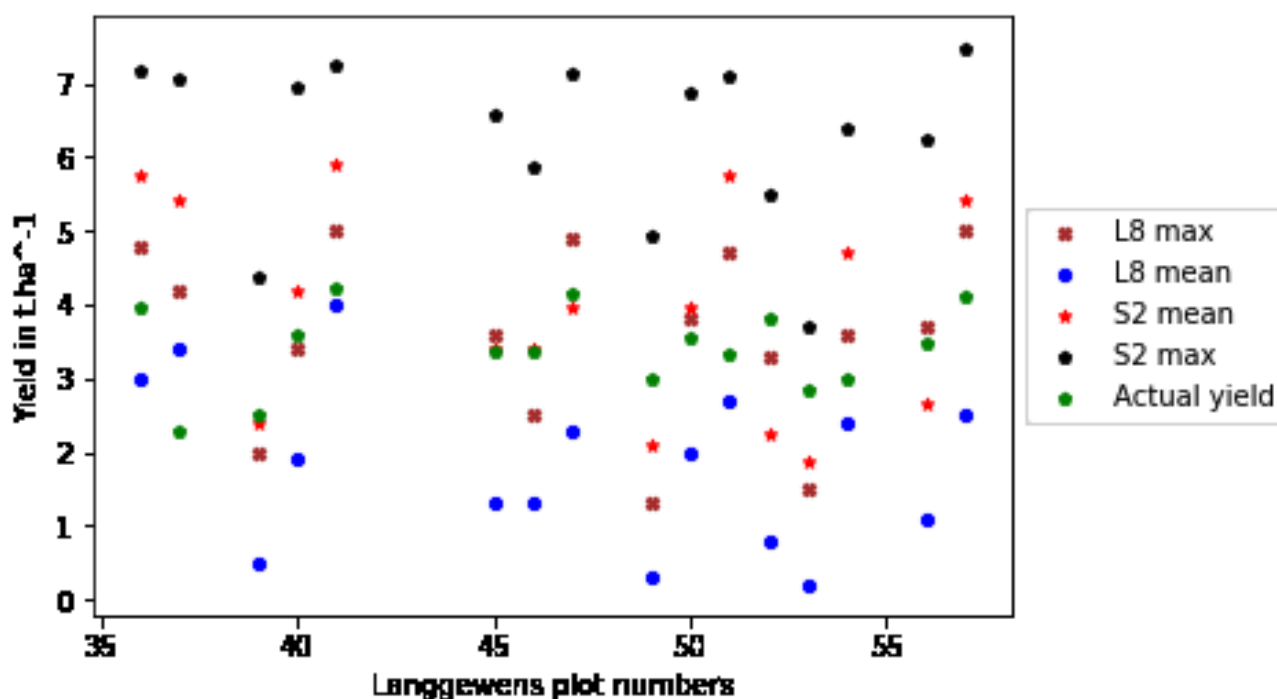
Figure 4.10 Modelled L_8, S_2 and Langgewens wheat yields scatter plot

The presented scatter plot shows the spread of modelled yields about the Langgewens observed yields in green colour. The yields denoted in blue and dark brown represent the L_8 mean and maximum zonal statistics respectively while the red and black denoted yields refer to the S_2 mean and maximum statistics respectively. In the absence of pixel level field data, the entire study yield validation and descriptions were based on zonal statistics.

The S_2 modelled yields are presented in Table 4.7, which included the actual yield data obtained in the experimental plots at Langgewens research station on conservation agriculture research trials. The crop rotation sequences were presented in the 5th columns of Table 4.6 and Table 4.7. Although this was not the subject of the current study it is interesting to note the differences in the plot yields due to the treatments. The yield range for the same crop rotation but at different plots, numbered 37 and 42 had yield differences of 1.93 t.ha^{-1}. Subsequent studies could investigate and map the benefits of conservation agriculture (CA) practices at field to regional scales. The crop rotation codes are presented in Table 4.8 (available from https://glten.org/experiments/11).

The Langgewens yields are presented in the 6th columns of Table 4.6 and Table 4.7. The rotation sequence with highest yields is the McWMcW rotation with a recorded yield of 4.2 t.ha^{-1}. The yield for plot 37 with a McWMcW crop sequence had the lowest yield of 2.28 t.ha^{-1}. Important to note that the yields are different for the two plots but the crop sequences are similar. Plot 39, where a wheat monoculture without a break crop was practised, had a yield of 2.51 t.ha^{-1}. This was accurately estimated by the S_2 mean yield statistic of 2.40 t.ha^{-1}.

Table 4.6 L$_8$ modelled wheat yields (t.ha^{-1})

Plot no.	Min	Max	Mean	Crop sequence	Observed(obs)	(obs-L$_{8mean}$)^2	(obs-L$_{8max}$)^2	(obs-obs$_{mean}$)^2
36	0.16	4.85	3.19	MWMW	3.98	0.62	0.75	0.32
37	2.31	4.25	3.39	McWMcW	2.28	1.23	3.87	1.28
45	0.00	3.59	1.29	LWCW	3.38	4.37	0.05	0.00
46	0.00	2.53	1.34	WWWW,WWCW,CWWW	3.35	4.03	0.67	0.00
39	0.00	1.95	0.50	WWWW	2.51	4.04	0.31	0.82
51	0.00	4.69	2.73	McWMcW	3.32	0.36	1.87	0.01
52	0.00	3.31	0.75	LWCW	3.83	9.49	0.27	0.18
40	0.00	3.39	1.91	LCWW,WLCW,CWLW	3.60	2.86	0.04	0.04
47	0.00	4.89	2.27	MCMW	4.15	3.51	0.56	0.54
57	0.00	5.03	2.47	MWMW	4.10	2.66	0.86	0.47
41	2.89	4.95	4.03	McWMcW	4.22	0.03	0.54	0.64
50	0.00	3.84	2.02	WLCW,LCWW,CWLW	3.55	2.34	0.08	0.02
53	0.00	1.46	0.23	WWCW,CWWW,WWWW	2.86	6.88	1.94	0.31
56	0.00	3.68	1.07	MCMW	3.47	5.72	0.05	0.00
49	0.00	1.31	0.33	WCWW,WWWW	3.01	7.18	2.90	0.16
54	0.26	3.61	2.40	McWMcW	3.01	0.37	0.35	0.16
SUM		57.34	29.93		54.62	55.70	15.11	4.95
RMSE						1.87	0.97	
Mean		3.58	1.87		3.41			
Standard deviation					0.56			
Relative standard deviation					16.30			
Yield$_{Langgewen\_max}$				McWMcW	4.22			
Yield$_{Langgewens\_min}$					2.28			
Range					1.94			

Table 4.7. S_2 modelled wheat yields (t.ha^{-1})

Plot no.	Min	Average	Max	Crop sequences	Observed(obs)	(obs-S$_{2mean}$)^2	(obs_S$_{2max}$)^2	(obs-obs$_{mean}$)^2
36	0.35	5.74	7.18	MWMW	3.98	3.09	10.23	0.32
37	0.00	5.40	7.05	McWMcW	2.28	9.71	22.69	1.28
45	0.00	3.42	6.56	LWCW	3.38	0.00	10.11	0.00
46	0.00	3.40	5.85	WWWW,WWCW,CWWW	3.35	0.00	6.25	0.00
39	0.00	2.40	4.38	WWWW	2.51	0.01	3.53	0.82
51	0.85	5.74	7.10	McWMcW	3.32	5.82	14.25	0.01
52	0.00	2.25	5.49	LWCW	3.83	2.51	2.75	0.18
40	0.00	4.20	6.94	LCWW,WLCW,CWLW	3.60	0.35	11.09	0.04
47	0.00	3.96	7.14	MCMW	4.15	0.03	8.94	0.54
57	0.00	5.43	7.47	MWMW	4.10	1.76	11.37	0.47
41	0.00	5.92	7.25	McWMcW	4.22	2.91	9.20	0.64
50	1.07	3.98	6.89	WLCW,LCWW,CWLW	3.55	0.18	11.16	0.02
53	0.00	1.87	3.71	WWCW,CWWW,WWWW	2.86	0.96	0.74	0.31
56	0.00	2.66	6.23	MCMW	3.47	0.65	7.62	0.00
49	0.00	2.08	4.95	WCWW,WWWW	3.01	0.87	3.74	0.16
54	0.00	4.72	6.37	McWMcW	3.01	2.90	11.29	0.16
Totals		63.15	100.55		54.62	31.76	144.97	4.95
RMSE						1.41	3.01	
Mean		3.95	6.28		3.41			
Yield standard deviation					0.56			
Relative standard deviation %					16.30			
Yield$_{Langgewen\_max}$				McWMcW	4.22			
Yield $_{Langgewens\_min}$				McWMcW	2.28			
Yield Langgewens				WWWW	2.51			
Range					1.93			

The L$_8$ modelled yield for the same plot (39) was 2.00 t.ha^{-1} and 0.50 t.ha^{-1} based on the maximum and mean zonal statistics. Based on this plot level statistics, the S$_2$ sensor mean zonal statistic accuracy is validated.The RMSE analysis was carried out and presented in Table 4.6 and Table 4.7. The Langgewens conservation trials crop codes are outlined in Table 4.8. The crop rotation codes presented in Table 4.8 shows the crop sequences at the Langgewens conservation trials plots.

The cumulative effects of these rotation on wheat yields are discernible in the crop yield data presented in this section.

Table 4.8 Langgewens crop rotation codes

Crop code	Name
W	Wheat
C	Rapeseed Canola
L	Lupins
M	Medicago sp
M/C	Medicago sp clover
+ s	With saltbrush pasture

The Langgewens plot layout was presented overlaid on S_2 based NDVI of the 26th September, 2016 and their relative dimensions can be ascertained based on the inserted scale bar. The plot dimension are 100 by 200m, which can be sampled by 20 S_2 satellite pixels or approximately two L_8 pixels.

The green dots in Figure 4.10 depicts the Langgewens plot wheat yields. The blue and brown marks are the L_8 mean and maximum yields zonal statistics respectively and straddle the green Langgewens actual yields. However the blue are generally all below the actual yields with S_2 mean and maximum L_8 zonal statistics closest to the true values, having 1.865 and 0.971t.ha^{-1} RMSE respectively. The black and red shapes depict the maximum and mean S_2 modelled yield.

These had the largest errors when compared to the observed Langgewens plots' yields. The S_2 maximum and minimum statistic RMSE of 3.010 and 1.408 t.ha^{-1}, respectively, seen in Table 4.9.

Table 4.9 Modelled wheat yield validation

Observed vs Langgewens yields data	RMSE t.ha^{-1}	Mean statistic t.ha^{-1}	RMSE t.ha^{-1}	Maximum statistic t.ha^{-1}
S_2 modelled yields	1.408	5.29	3.010	9.13
L_8 modelled yields	1.865	3.26	0.971	7.23

The S_2 modelled wheat yields-based statistics had the highest overall RMSE using either the mean or maximum statistics. The L_8 modelled yields had lower RMSE whose worst RMSE of 1.8605 t.ha^{-1} was close to the most accurate S_2 mean statistics at 1.408 t.ha^{-1} RMSE. The modelled L_8 yields on the other hand indicated a higher error for the mean statistic of 1.865 that declined to

0.971 t.ha^{-1} with the maximum zonal statistics. Indicating that the L_8 sensor maximum zonal statistic modelled the observed Langgewens yield accurately followed by the S_2 mean zonal statistic value. Note that the model used in the research was based on an empirical relationship derived from MODIS pixels at 250 m spatial resolution (Mashaba et al. 2017).

The study area wide zonal statistics were generated based on the wheat field polygons and extracted into a dbase file in ArcMap. The maximum, average and median metrics of the minimum mean and maximum zonal statistics were calculated in excel and the results are presented in Table 4.10.

Table 4.10 Wheat yield Berg river catchment , 2016

	minimum	mean	maximum
S_{2_medin}	0.35	5.72	7.42
S_{2_mean}	0.98	5.59	7.35
$S_{2\_maximum}$	7.13	7.37	8.52
L_{8_median}	0.08	3.55	4.99
L_{8_mean}	0.81	3.24	4.70
$L_{8\_maximum}$	5.40	5.95	6.42

A graphic depiction of the zonal statistics outlined in Table 4.10 is presented in Figure 4.11.
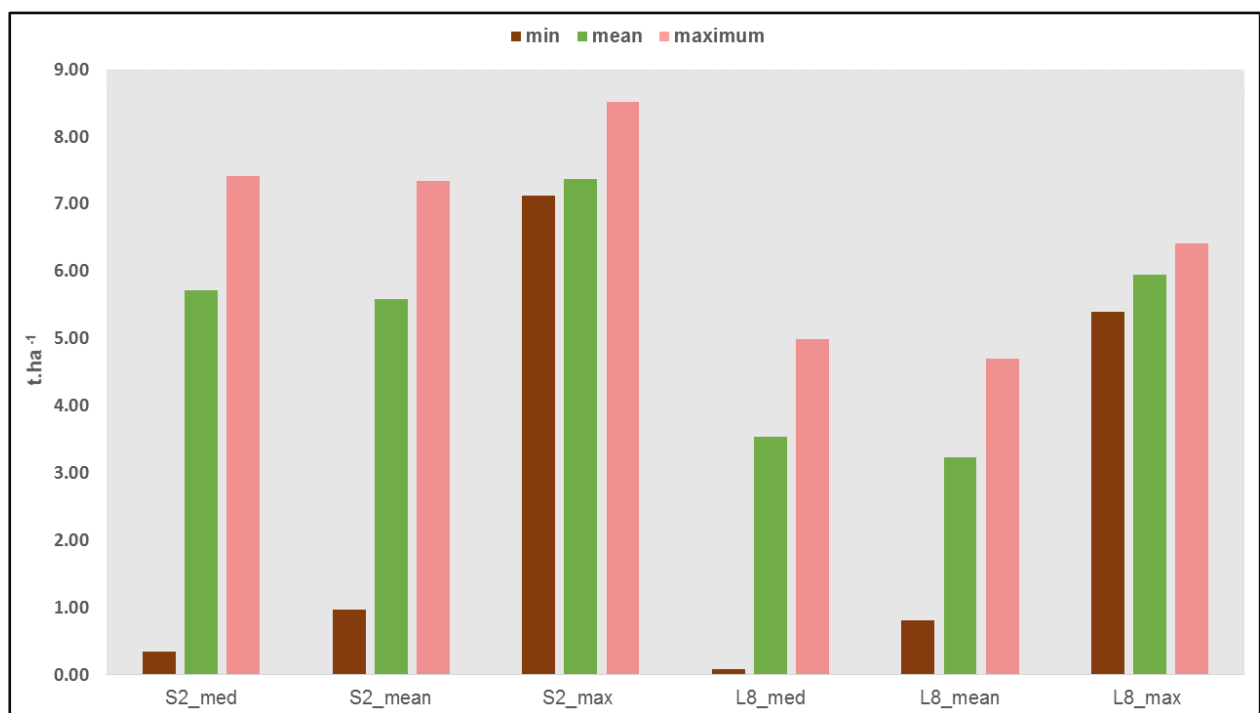

Figure 4.11 Wheat yield Berg river catchment, 2016

The study area modelled yields results indicate dependencies on satellite sensor and spatial resolution with the higher resolution sensor having higher modelled yield values. The modelled

wheat yield results indicated that the S_2 based values were consistently higher yields than the L_8 yield estimates. The highest L_8 based yield statistic had similar yield estimates to the lowest S_2 modelled yield values. The median and mean statistics of the S_2 based yields estimates had near equal values which shows that the S_2 yields had a normal distribution were the mean and median values are close. The S_2 and L_8 based yield median statistics of 5.72 and 3.55 t.ha^{-1} respectively, were determined using the extracted study area wide zonal statistics. The true value yield values would be somewhere in between these two values. The generated statistics indicated a difference between the S_2 and L_8 yield estimates in the order of 2 t.ha^{-1} using the maximum statistics. Although the study did not have the modelled yield differences as an objective it is important to note in quantitative geography analysis that aspects of the MAUP manifests in sampled geographic data. This is true if the sensors have different shapes and sizes. Additionally, sensors with large pixels have been shown to be poor yield estimators' and therefore the results based on the L_8 have uncertainties. The S_2 based yields could have had higher accuracies if the model had been based on a sensor of comparable pixel size than the MODIS with a 250 m footprint. The results indicate that application of the Mashaba et al. (2017) yield modelled were slightly offset from the true value. This implies that accurate results can be obtained if model redesign and validation are carried   out on expanded ground truth data set.

Deriving yield data from farmers was not undertaken in the study given time and resources constraints coupled with fears of invading farmers' privacy. The study indicated that RS based investigation could estimate yield data without undue human contact (Z Munch pers. Com). However, the estimated yields depended on the satellite sensor resolution. District level yield data from farmers although availed, no validation was possible since these data where not geo referenced. The wheat water productivity is presented in the next section.

4.3   WATER PRODUCTIVITY

The wheat crop water productivity (WP) was determined by dividing the modelled S_2 and L_8 wheat yields by the crop water use i.e. ET_{cHS} and ET_{cPM}, at 10 and 30 m spatial resolutions, respectively. The generated WP zonal statistics are presented in Table 4.11 and graphed in Figure 4.12.

Table 4.11 Water productivity (WP)

WP (kg.m^{-3})		Minimum	Mean	Maximum
WP	y_{S2} to ET_{cPMS2}	1.37	1.89	2.29
WP	y_{S2} to ET_{cHSS2}	1.27	1.79	2.16
WP	y_{L8} to ET_{cPML8}	0.30	0.43	0.67
WP	y_{L8} to ET_{cHSL8}	0.27	0.39	0.61
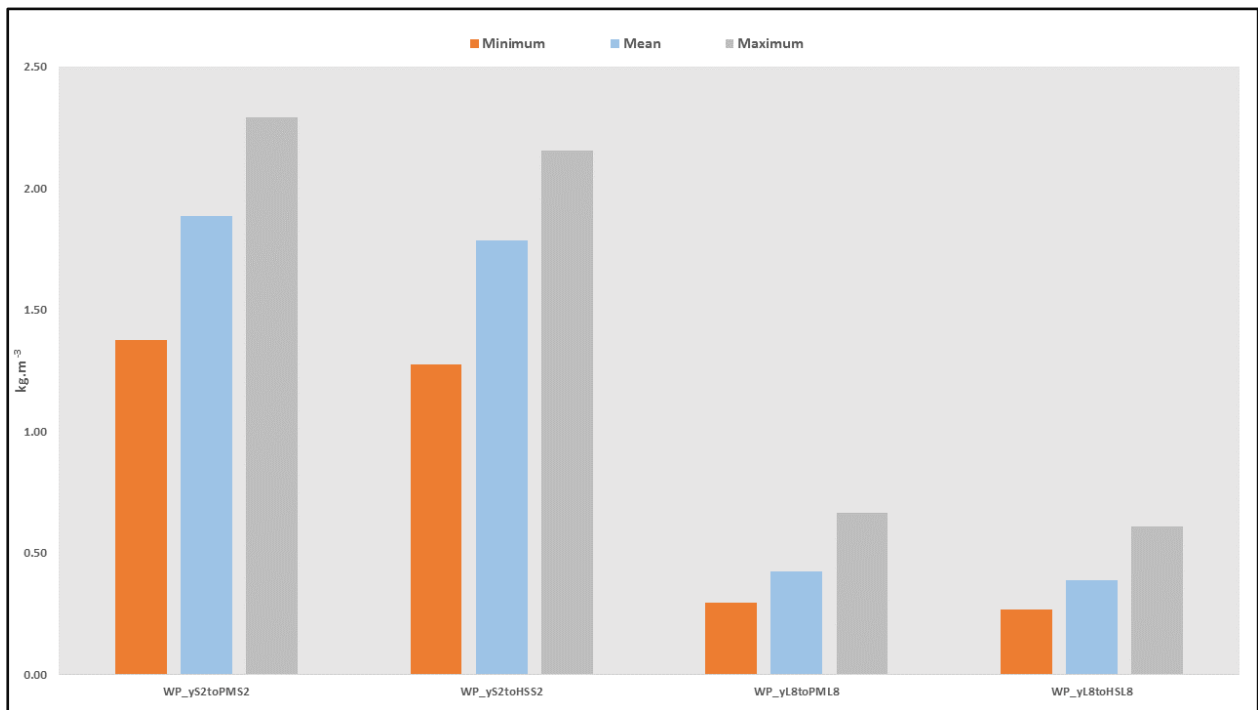
Figure 4.12 Water productivity (wheat), Berg River 2016

There are four water productivity (WP) computations presented in Table 4.11. The S_2 based yields to the ET_{cHS} and ET_{cPM}, and the L_8 based yields to the ET_{cHS} and ET_{cPM}.

The study area wheat fields' polygons comprised 2812 S_2 pixels with the larger L_8 pixels numbering only 1007. The S_2 yield to crop water use ratios had higher values than the L_8 yield to crop water use values. As results indicated in Section 4.2, the S_2 yields had persistently higher values than the L_8 yields seen in Figure 4.10. The S_2 yield to ET_{cPM} and ET_{cHS} at 10 m spatial resolution had comparable mean WP of 0.018 and 0.017 $t.ha^{-1}.mm^{-1}$ or 1.89 and 1.79 $kg.m^{-3}$ respectively seen in Table 4.11. The L_8 based wheat yield to ET_{cPM} and ET_{cHS} at 30m SR had WP of 0.0042 and 0.0038 $t.ha^{-1}.mm^{-1}$ or 0.43 and 0.39 $kg.m^{-3}$ respectively. Remember that the magnitude of the ratios is related to the values in the denominator and numerator.

WP can be expressed as $kg.m^{-3}$ by multiplying the values in Table 4.11 by 100. Expressed as mass per unit volume the S_2 based WP varied from 1.88 to 1.725 $kg.m^{-3}$, and 0.3874 to 0.426 $kg.m^{-3}$ for the L_8 based WP using mean zonal statistics. The L_8 yield based water productivities based on maximum statistics were 0.67 and 0.61 $kg.m^{-3}$ for the ET_{cPML8} and ET_{cHSL8} which indicate large wheat yield gap. The S_2 based WP exceeded the 2 $kg.m^{-3}$ mark which can only be achieved under intense input level scenarios indicating that these values were probably an overestimation. The water productivity frequency tables are presented in Figure 4.13.
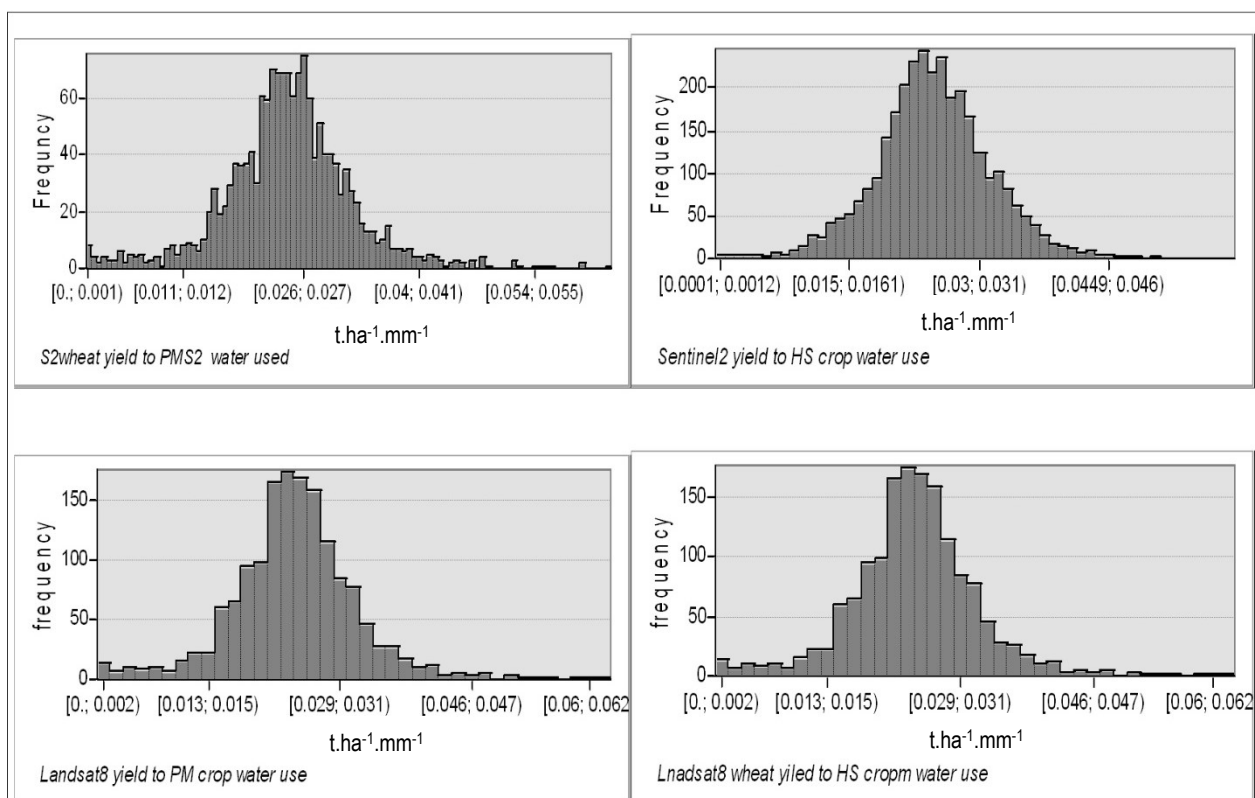
Figure 4.13 Water productivity t.ha^{-1}.mm^{-1}.

The WP distributions suggests that the highest frequencies were obtained in the range 0.012 to 0.04 t.ha^{-1}.mm^{-1}. The difference observed in the frequencies were due to the number of pixels per S_2 images compared to the L_8 image pixels. The L_8 and S_2 yields based on the mean statistics gave comparable results which would appear to suggest very low WP values.

The WP results are subject to uncertainties related to observed differences in S_2 and L_8 modelled yield and ET_{cHS} and ET_{cPM} calculated crop water requirements. The yield gap analysis is presented next.

4.4 YIELD GAP ANALYSIS

The modelled wheat yield data, were extracted from the distributed study area S_2 and L_8 wheat yield maps, shown in Figure 4.8 using zonal statistics based on study area wheat fields' polygons. The mean zonal statistics are presented in Table 4.11 from which the mean values used in Table 4.12 were extracted. The L_8 and S_2 mean yields used in yield gap calculations were based on zonal statistics in Table 4.11 and are presented in Table 4.12. The S_2 modelled wheat statistics had higher mean and 95th percentile values at 5.59 and 7.08 t.ha^{-1}, respectively. The L_8 had comparatively lower values for the mean and 95th percentiles wheat yields at 3.24 and 5.02 t.ha^{-1}, respectively. The differences between the mean and the 95th percentile yield levels gave approximately equal value in both the S_2 and L_8 based wheat yield distributions. The 95th percentile value was

established using a Script A.2.2 that plots the wheat yields vs percentile distribution .The mean statistic of the zonal statistics table was used to determine the within study region yield gap.

Table 4.12 Within study area yield gap (Lobell 2013)

Yield t. ha^{-1}	Average yield	95th Percentile yield	Yield Gap	Median	Yield Gap median based
S$_2$ Wheat yield (y$_{S2}$)	5.59	7.08	1.49	5.72	1.36
L$_8$ Wheat yield (y$_{L8}$)	3.24	5.02	1.78	3.55	1.47

Although the absolute modelled wheat yield values varied according to sensor resolution the difference of 95th percentile wheat yield and the mean yield in the S$_2$ and L$_8$ modelled yields distribution gave similar values of 1.49 and 1.78 t.ha^{-1} with a difference of 28 kg.ha^{-1} in the yield gap estimates. An additional yield gap computed based on the median and the 95th percentile although lower than the mean based yield gap estimates were near identical at 1.36 and 1.47 t.ha-1 for the S$_2$ and L$_8$ data sets respectively. The yield gap benchmarked on countries indicated in Figure 4.14 were calculated as the difference between L$_8$ mean wheat yield value vs actual respective country mean yields (Sosibo et al, 2016).
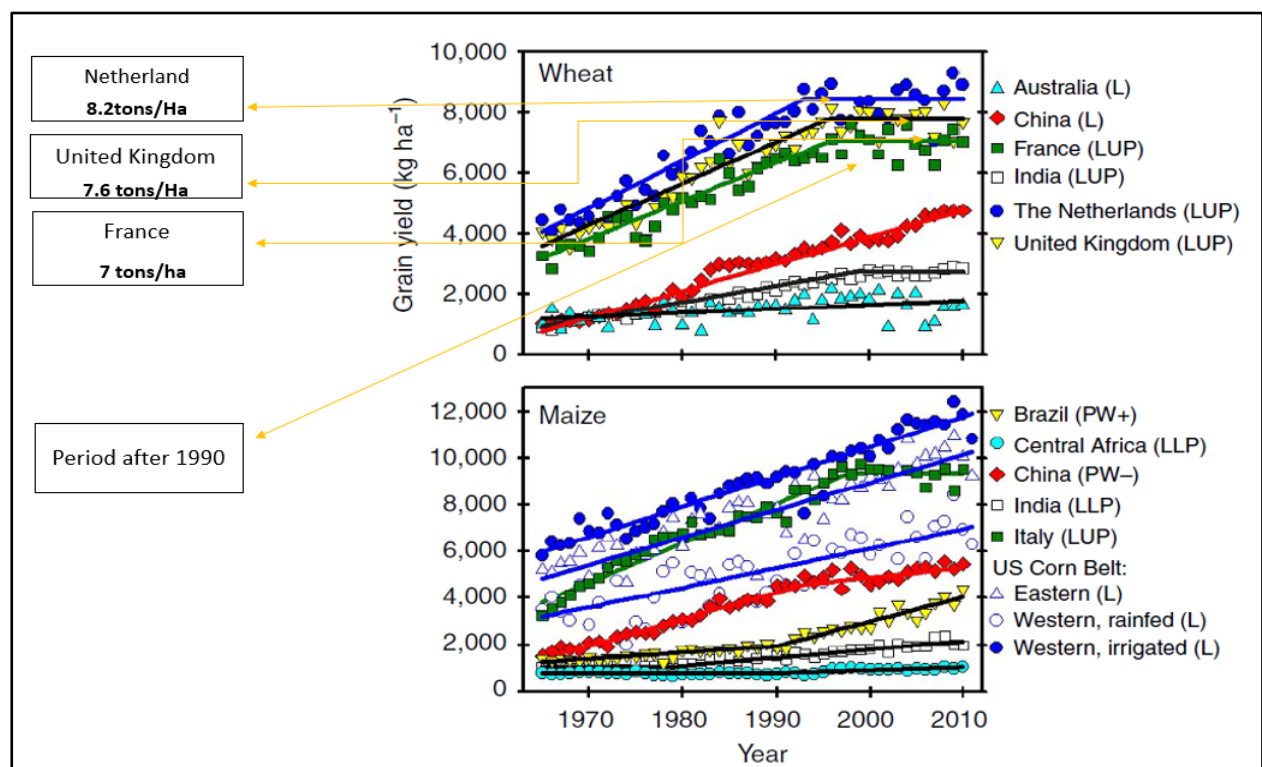
Source: Grassini et al. (2013)

Figure 4.14 Global wheat yield

Figure 4.14 gives the worldwide production rates trajectories for maize and wheat yield for the period 1970 to 2010. Different agro-ecological regions impact wheat yield, in addition input use and crop management widen yield gaps and according to Mueller et al. (2012) yield gaps can be reduced with optimal management. The findings are presented in Table 4.13 below.

Table 4.13 Wheat yield gaps based on global benchmarks

Wheat yields in t.ha-1	Country mean yield (Figure 4.14)	Study area L_8 mean wheat yield	Yield gap L_8 mean based	Study area L_8 median wheat yield	Yield gap L_8 median based
Within study area yield potential seen inTable 4.12			L_8 1.49 S_2 1.78		1.36 1.47
France	7	3.24	3.74	3.55	3.45
Netherlands	8.2	3.24	4.94	3.55	4.65
United Kingdom	7.6	3.24	4.34	3.55	4.05
Australia	2.0	3.24	-1.24	3.55	-1.55
SA irrigated mean 2015/2016	5.94	3.24	2.70	3.55	2.39
SA dryland 2015/2016	2.04	3.24	-1.20	3.55	-1.51
Northern Cape Irrigated	7.2	3.24	3.96	3.55	3.65

The study area wheat yield gap rated at local, regional and global scales were determined as outlined in the Table 4.13 above, where the study area average yield was based on the L_8 maximum zonal statistics value. The L_8 modelled yields estimated Langgewens yields more effectively than the S_2 based yields, with the lowest RMSE of 0.9701 seen in Table 4.9. The global based country wheat mean yield levels presented in Table 4.12 were estimated using the graph presented in Figure 4.14. These yields where attained after the 1990s and represented the technological ceiling depicted by stagnating yields trajectories (Grassini et al. 2013). The results indicated that there is significant yield potential in the study area in the range of 1.49 to 4.94 t.ha^{-1}. In the 2015/16 season the Berg study area, L_8 mean and median wheat modelled yield exceeded the Australian wheat yield by 1.24 and 1.55 t.ha^{-1} respectively. At national level the study area wheat yield was lower

than levels attained under irrigation. The Northern Cape had the highest irrigated wheat yields of 7.2 t.ha^{-1} indicating yield gaps of 3.96 and 3.65 t.ha^{-1}using the mean and median study area statistics respectively. The WC dryland wheat production exceeded the SA national dryland production by more than a tonne in the 2015/16 season (SAGL NPC 2020).

The high yields currently achieved in other regions of the world have been ascribed to nutrient, pesticide and water management and this is expected to be the major drivers to close yield gaps in the developing world especially in Sub Saharan Africa (Muller et al. 2012). The study results area discussion in the next section.

4.5   DISCUSSION

The analysis is based on the extent to which the utilised RS and GIS methodologies and climate data use have contributed to achieving the research objectives. The study aimed to firstly determine a snapshot, study area seasonal distributed wheat crop water use in 2016. The process included the use of GIS software, ArcMap 10.4.1 and PCIGM, and developed Python scripts to process the satellite imagery to ground reflectance and thereafter, computation of NDVI. The computation and compilation of study area daily ET_{0HS} and ET_{0PM}, respectively   from climatic data was carried out followed by the determination of study area ET_{cHS} and ET_{cPM} surfaces at 10 and 30 m SR. The second objective was the determination of seasonal wheat water use based on ET_{0PM} and ET_{0HS} and modelled K_{cL8} and K_{cS2} respectively. The crop water results are discussed in Section 4.5.1.

The 3rd objective was wheat yield modelling. Wheat yield was modelled on a pixel by pixel basis from S_2 and L_8 scenes, respectively, and the results are discussed in Section 4.5.2. The yield validations were carried out based on 2061 Langgewens ARC research plots observed wheat yield data and from literature. Water productivity study objectives aimed to determine wheat yield per unit of water consumed and the results are discussed in Section 4.5.3. The yield gap objective, was intended to estimate the study area wheat crop production potential. The yield gap analysis results are discussed in Section 4.5.4.

According to Huete et al. 2011, large bandwidth reduces NDVI sensitivity and dynamic range. This implied that the use of the B_{8S2} which has 115 nm bandwidth negatively impacted the accuracy of computed NDVI and subsequently the derived products, i.e. wheat K_c and yield estimates. Refer to Table 2.1.The MODIS and L_8 sensors have narrow NIR bandwidths of 35 and 28 nm respectively. The above could explain the relative accuracy of the L_8 modelled products, when compared to the $S_2 B_8$ based K_c, ET_c and wheat yield. Narrower bandwidth are less influenced by atmospheric water vapour than the wider bandwidth.

4.5.1 Crop water use

The computation of the seasonal distributed crop water use surfaces was implemented using developed Python Scripts (Appendix A) in ArcMap as detailed in Section 3.4

4.5.1.1 Reference crop water requirements

The results in Table 4.1 indicate that the ET_{0HS} and ET_{0PM} had similar annual patterns with values of 205.2 and 203.6 mm, respectively for the month of January. The lowest reference crop water requirements for the ET_{0PM} and ET_{0HS} of 43.8 and 46.7 mm respectively, were recorded in June 2016. This is too be expected given that the months June and July are the months in which the lowest temperatures are recorded, The highest ET_{0PM} values of 131.04 mm were recorded at Ideal_pool_Hill climate station and the lowest annual ET_{0PM}, of 104.60 mm recorded at De_Poort climate stations. The annual monthly average ET_{0PM} for Abendruhe was 108.50 mm which indicated that the ET_{0HS} monthly total value was an overestimation at that station. ET_0 results varied according to computation methodologies (Table B 1 and B 2). The JD 140 ET_0 surfaces depicted in

Figure 4.2 gave an insight of ET_0 surface variation for that particular day in 2016. The observed ET_0 values at a given point varied depending on the ET_0 estimation methodology, rather than from map spatial resolution. The distributed ET_0 surfaces indicated that ET_{0HS} had both higher values and lower values, when compared to ET_{0PM} values, seen as the deep green (1.97-2.22 mm.day^{-1}) and the dark red (0.77-1.11 mm.day^{-1}) on the colour legend. The combined effects of the methodology and spatial resolution, contributed to the observed discrepancies in ET_{0PM} and ET_{0HS} surfaces. Additionally this can be attributed to the modifiable area unit problem (MAUP) (Dark &Bram 2007). The performance of the ET_{0HS} methodology was evaluated based on magnitude of differences to the ET_{0PM} which varied with the climate stations and the months, for example the Bokveldskloof climate station had the lowest ET_0 absolute difference to ET_{0PM} in 2016 at less than 20 mm.month^{-1}, indicating that the ET_{0HS} accurately determined the actual study area ET_0.

The HS methodology has been evaluated worldwide due to its appeal in climatic data scarce regions of the world. The overestimation or underestimation ET_0 by the HS methodology was observed throughout the study period and more so and largely in the month of December seen Figure 4.1. Lima et al. (2013) recorded similar ET_0 overestimations while using the HS equation in Brazil during periods of low evaporative demand from May to July. In the WC study area, the HS equation overestimated ET_0 for a longer period stretching from April to November which covers the winter period, through to the beginning of summer. The observed overestimation by the ET_{0HS} could be ascribed to the HS model inability to compute ET_0 under low evaporative scenarios.

This occurred because, in such cases, ET_0 presented would be largely correlated to variables that are missing in the HS equation i.e.vapour pressure deficit and windspeed, and the use of the full PM equation would be unavoidable (Althoff et al. 2019). The HS underestimation of ET_0 as observed in some months including the month of December 2016 in nearly all stations in the study area was also recorded in Iran at Abadan (Shahidian et al. 2012). Under conditions of high evaporative demand, the HS equation failed to calculate ET_0 values above 9 mm when actual ET_0 according to the PM equation exceeded 13mm per day. December of the year 2016 had very high temperature, though precedent, recorded in SA due to the drought of 2015 to 2017 accompanied by low relative humidity therefore increased evapotranspiration (Otto et al. 2018). This result indicated that during the summer period especially in December with low humidity and high temperatures, the HS based ET_0 values are lower than the actual ET_0 and therefore not representative of the true ET_0. Although the absolute deviations of HS to PM ET_0 appear large as seen in Figure 4.1 & Figure 4.2, these differences have low errors (RMSE = 0.426 mm.day^{-1}). The results indicated that the computed ET_{0HS} values approximated the ET_{0PM} especially during the wheat growing season and therefore can be used as a decision support tool in water management studies. Similar observations were made by a number of researchers.

4.5.1.2   Crop coefficient

The S_2 and L_8 modelled crop coefficient values and evolution over the season seen in Figure 4.3 , have confirmed the similarity of these K_c curves to research findings published in the literature. Typical K_c curves start with very low values during crop establishment when crop water use is dominated by evaporation. The K_c values rises during the vegetative phase and plateaus in the mid season. During crop maturation and senescence stages the K_c values decreases. The determined crop coefficient values of 0.185 and 0.236 for the K_{cL8} and K_{cS2} are typical in the early season. Hunsaker et al. 2007 observed similar K_c of 0.2 in the early stages of wheat crop establishment which rose to 1.1 in the mid season stages and declined thereafter to 0.4. In the Indo_Gangetic plains Choudhury et al. 2013 observed high K_c in both the initial, vegetative and mid season and late stages of 0.98-1.06, 1.10-1.14, 1.25-1.26 and 0.46-0.47 for a wheat. These results were observed in the current study if we consider the maximum zonal statistics of S_2 and L_8 based K_c in Table 4.2 and Table 4.3.The estimated $K_{cS2 \text{ values}}$ ranged from 0.761 in the early part of the season to a maximum of 1.157 and thereafter started to decline reaching 1.094. The K_{cS2} zonal statistics indicated a consistent overestimation K_c in the initial and final stages, whereas the mid season estimates are comparable to those reported by Choudhury et al. (2013). Based on the maximum zonal statistic study area K_{cL8} values of 0.76, 1.004 and 0.986 were observed in the initial, mid and late season, respectively for the 2016 wheat crop. The results validate the observations by

Hunsaker et al. (2007) that NDVI based K_c are robust enough even under water stressed conditions. The incidence of pixels having high K_c values suggests that some fields could have been under irrigation or had substantial soil moisture reserves to maintain plant vigour. The typical underestimation of K_c by the L_8 sensor as compared to the S_2 sensor has to do with the differences in spatial resolution, the central band values and band widths used in computing NDVI and finally modelling K_c values. The average study area maximum K_c values of 0.660 and 0.954 were attained for the K_{cL8} and K_{cS2} respectively. The lower average K_c values modelled in the study was mainly due to the drought that occurred in 2016. During the dates when the average study area attained its maximum values, the maximum zonal statistic had K_c values of 1.004 on the 21/9 for the L_8 model and 1.096 on the 26/8 for the S_2 model. These results indicate lower water use rates in the early season, increased water use   in the mid season due to complete ground cover by the crop canopy cover and enhanced photosynthetic activity and reduced water use with crop senescence.The results are comparable to those attained by researchers in the US and India.

4.5.1.3   Crop water use

The crop water use results were impacted by modelled K_c and interpolated ET_0 surfaces. The results indicated that the sensor spatial resolution had an impact on computed ET_c values. The L_8 sensor samples R and NIR at 30 m resolution in comparison to the S_2 sensors at 10 m spatial resolution respectively. In addition, the overestimation of ET_0 by the HS equation magnified the crop water use values as was illustrated in Figure 4.2. Low spatial resolution have scenes characterised by mixed pixels which tend to result in lower vegetation indices in this instances the NDVI $_{L8}$ upon which the K_{cL8} was based.

The NDVI modelled crop coefficient values were presented in Table 4.2 & Table 4.3 for S_2 and L_8 satellites respectively. The results indicate that higher values for K_c were obtained using the S_2 sensor and the study area K_c maximum statistics was above 1.00 except on the 05/08. The maximum of the K_{cL8} mean statistic over the season were below the 1.00 threshold with a study area mean maximum statistic of 0.895 attained on the 21/09.

The meaningful seasonal wheat water use results were based on the maximum zonal statistics using the 10 m SR sensor with total season crop water use estimates of 414.07 and 463.83 mm for the ET_{cPM} and ET_{cHS} methodologies respectively. If we consider the ET_{0PM} as the standard, then the ET_{cHS} had an over estimation of about 50 mm crop water use. The Landsat8 based water use were much lower than the Sentinel2 based crop water use. The season L_8 based water use was 291 versus 317 mm for the PM and HS approaches respectively. This again indicated the overestimation of the HS method by 26 mm. The results indicated that the L_8 based crop water use estimates are lower in the order of 120 mm when compared to the S_2 based estimates. This feature of the results

is clearly illustrated in Figure 4.7. The minimum values below 30 mm per season should not be considered as these are not realistic and might be referring to uncultivated land which were bare of any vegetation during the study period. The computed wheat crop use results indicate that these values although having a wide range are all in within the expected values of wheat water use. Under irrigated conditions and using the SAPWAT model water use values of 665 mm at Orange_Riet WUA were determined while at Orange_Vaal WUA, 748 mm water depth excluding rainfall was, needed for the wheat crop. The wheat crop water use results presented in Table 4.5 has maximum water consumption values of 290 to 463 mm. Researchers suggests that rainfall amounts are indicative of available water that plants loose through evapotranspiration especially in the absence of substantial residual moisture from the preceding periods (French & Schultz 1984). According to indications on the Langgewens website, the station receives an annual average rainfall of 395 mm (https://www.elsenburg.com/research-tags/langgewens). Taking into account the values indicated to ascertain the accuracy of the obtained seasonal crop water use generated in the study the rainfall data indicated in the literature for SA indicates that the estimated crop water use is in the range of expected values.

4.5.2   Wheat yield

A highly sought-after variable in agronomic studies is crop yields (Lobell 2013). The analysis of the wheat yield results are presented in this section. The results obtained demonstrated that the modelled yields were a function of satellite sensor characteristics. The relatively more accurate results were achieved using the L_8 sensor. The S_2 based yields highly overestimated the reported Langgewens wheat yields both the mean or maximum zonal statistics with RMSE of 1.408 and 3.010 t.ha^{-1} respectively. The modelled wheat yield RMSE summary are presented in Table 4.9 .

The lower spatial resolution sensor L_8 at 30 m underestimated the Langgewens wheat yields but with comparably less estimation errors than the S_2 sensors. The most accurate metric was recorded with the L_8 maximum statistic at 0.971 t.ha^{-1} RMSE .This latter statistic was the best indication of the general validity of the Mashaba et al, 2017 yield model. However, the best yield metrics are usually based on the mean or median zonal statistics. The L_8 sensor modelled yield were an underestimation of Langgewens yields as illustrated in Figure 4.10. The results further indicated that the S_2 mean, S_2 maximum and L_8 mean based RMSE had higher values than the L_8 maximum RMSE. Based on the mean zonal statistics only the S_2 sensor modelled yields were relatively more accurate than the corresponding mean L_8 statistic with a 0.457 t.ha^{-1} RMSE difference. One could infer that the S_2 mean statistic indicated the general validity of the S_2 mean statistic in wheat yield modelling albeit with large errors. Large pixels generally record degraded signals, due to low S/N ratio. This is typical of large pixels such as the L_8 and MODIS sensors. The results suggest that

the deflection of modelled yields downwards from the actual yields was related to the larger L_8 pixel. Conversely the high resolution S_2 wheat yields seen in Figure 4.10 scatter plot were above the actual Langgewens yields, indicating an upward estimation bias. Based on RMSE the L_8 sensor was the best overall yield estimator. The S_2 sensor modelled values were expected to outperform the L_8 based yields based on the higher spatial resolution, and as confirmed by the mean statistic RMSE analysis.

The equation developed by Mashaba et al. (2017) based on MODIS pixels which are at 250 m spatial resolution was implemented using 10 and 30 m spatial resolution sensors for the research carried out in the Berg river catchment. The results suggest that in general the modelled yields were in the range of yields obtained at Langgewens across the S_2 and L_8 sensors but with large errors. The significance of the current study established based on the RMSE analysis was that, the L_8 based maximum zonal statistic gave a relatively more accurate results than the S_2 based mean and maximum, and L_8 mean zonal statistics. Furthermore, the S_2 mean zonal statistic had a relatively higher accuracy when compared to the L_8 mean zonal statistic. The results indicated that modelling wheat yields based on empirical formulations might require local recalibration to improve on the mean zonal statistics accuracies, in predicting wheat yields across sensors. Further studies are required to reformulate or validate the used yield model given that in this instance only a smaller data set was used to validate the modelled yields i.e. the observed ARC Langgewens 2016 wheat yields.

Additionally, the ARC Langgewens plot sizes are relatively small, measuring 100 by 200 m^2 ~ about 2 ha and they are adjacent to each other, seen in Figure 4.9. This raises concerns of edge effects, the L_8 at 30 m pixel footprint potentially overlapped the treatment plots resulting in erroneous plot yields estimates. Although no strategy was employed to cater for this it's important to be aware of possible error sources which could have negatively impacted the results. Extra validation was based on SA wheat production statistics spanning from the period 1994/95. These statistics showed that mean SA wheat yields ranged between 1.45 and 3.76 t.ha$^-$1. In the 2015/16 and 2016/2017 yields of 2.99 and 3.76 t.ha^{-1} were reported. These data validate the S_2 and L_8 modelled yields mean zonal statistics of 5.25 and 3.6 t.ha^{-1} respectively, seen in Figure 4.10. For the period 2012/13 to 2017/18 the SA statistics (https://www.grainsa.co.za/report-documents?submited=1&cat=14 & find =) indicates the following mean wheat yield data set: 3.63, 3.63, 3.70, 3.67, 2.99, 3.76, and 3.12 t.ha^{-1} respectively. The FAO STAT data released on 12/08/2019 (http://www.fao.org/faostat/en/#data/QC/visualize), shows a similar range of wheat yield values for the period 2012 to 2017 based on calculated data which gave the following values: 3.75, 3.67, 3.67, 2.99, 3.76 and 3.13 t.ha^{-1} wheat yields in SA for the period. It is clear that the S_2

modelled yield were outside this range whereas the L_8 mean statistic was within the range of cited statistics. These data and results give confidence to researchers to use satellite imagery in yield estimation. Despite the fact that the model was calibrated based on MODIS pixel data at 250 m SR and formulated elsewhere in the Free State province the obtained results and in the absence of model parameters modifications, suggests that the model is effective for any pixel sizes. The bands and bandwidths appear to have an effect on the obtained results. As indicated in the current report recorded signal quality depends to a large extend on the bandwidth. On further scrutiny the accuracies observed due to the L_8 could be ascribed to the narrow 5th Band at 28 nm bandwidth. Conversely the inaccuracies by the S_2 sensor could be ascribed to the wide 8th band at 115 nm. Researchers have discovered that large band width are negatively impacted by atmospheric water vapour. The use of narrower bands have been reported to avoid atmospheric water vapour influences (Huete et al. 2011). Given the above scenario the L_8 maximum zonal statistics wheat yield values were used in wheat yield gap analysis in Section 4.2.4. The use of narrower bands have been reported to avoid negative influences of atmospheric water vapour (Huete et al. 2011) .The central wavelength and bandwidth of the S_2 NIR used in computing NDVI largely differ to those of the corresponding L_8 and MODIS bands which might have led to the modelling errors observed.The detailed MODIS, S_2 and L_8 sensor characteristics were presented in Table 2.1, to expose dynamics of bands and bandwidths effects on NDVI values and subsequently modelled yields and K_c.

4.5.3   Water productivity

The research carried out determined the crop water use in Section 3.3 and the results were presented in Section 4.1.3. The results indicated that the S_2 yield based water productivity had values exceeding those estimated using L_8 yield based WP (Table 4.10). Given that the S_2 sensor-based yields largely overestimated crop yields in relation to the underestimation by the L_8 sensor-based yields, the water productivities results were impacted in a similar manner. Consequently, the S_2 water productivities were higher than those based on L_8 wheat yields as is depicted in Table 4.10. To reduce error impact associated with the modelled yields the discussion presented herein after Section 4.2.4 was restricted to using the L_8 wheat yield maximum zonal statistics water productivity ratios given its lower RMSE value of 0.971 t.ha^{-1} seen in Table 4.9.

The results obtained in the current study were validated by using the 2016, Langgewens wheat yields and quoted literature below. In a tabulation of water productivities for a range of crops, compiled from several researches, 0.2 to 1.2 kg.m^{-3} are the current water productivities range in dryland wheat production (Molden 2010). Araya et al. (2019) reported water transpiration productivities and irrigation water productivities ranges of 15.2 - 16.1 kg.ha^{-1}.mm^{-1} and 0.98 to 1.6

kg.m^{-3} for irrigation at 1.7 mm.day^{-1} depths compared to 14.7 - 15.5 kg.ha^{-1}.mm^{-1} and 0.6 to 1.06 kg.m^{-3}, respectively at 5 mm.day^{-1} irrigation depth applied. Based on the above findings they concluded that irrigation-based wheat WP can potentially be augmented depending on the amounts of water and nitrogen fertilisers applied, respectively and exhibit decreasing marginal returns to increased water inputs. The results by Araya et al. (2019) indicate that WP under irrigation exceeds the figures quoted by Molden et al. (2010) for dryland wheat production. The computed wheat water productivity ratios results of 0.3874 and 0.4262 kg.m^{-3} for the L$_8$ based mean zonal statistic are further confirmatory evidence of research findings validity as they are within the range observed by Molden et al. (2010). In water productivities research comparable results of 0.99 and 1.59 kg.m^{-3} dryland wheat grain yield were obtained in the south and south east of Australia respectively (Sadras & Angus 2006, Sadras & McDonald 2012). Additionally, higher water application does not augment wheat production at constant rates but are subject to diminishing returns implying that water savings can be effected if water use is restricted to high marginal return levels than total yield maximisation per se.

The S$_2$ based water yields had values within the 1.7252 to 1.8883 kgs.m^{-3} range, are comparable to the figures reported by Araya et al. (2019). But given that the S$_2$ modelled yields had large RMSE these pixel values were largely due to wheat yield overestimation. Water productivity varies according to the fertilisation rates which implies therefore that increases in crop water productivity, can in addition to increased water application be accomplished through higher fertiliser inputs, pest and diseases control, and improved water application management (Mueller et al. 2012; Araya et al. 2019).The wheat crop yield potential determination based on yield gap analysis is presented next.

4.5.4   Yield gap

The study area wheat yield characterisation allows for further analyses that determines yield potential based on the yield gap approach (Lobell 2013; van Ittersum 2013). The yield potential research results are discussed in this section. The modelled yields were validated using recorded ARC Langgewens research station yields as defined and implemented in Section 3.4 of the study. The validation analyses confirmed the authenticity of the results more so by the L$_8$ based zonal maximum statistic that had the lowest RMSE of 0.971 t.ha^{-1}. This was the lowest RMSE attained by all possible combinations of S$_2$ and L$_8$ zonal statistics. The extracted wheat yields were subjected to a yield gap analyses that culminated in the within study area wheat yield gap of 1.49 to 1.78 t.ha^{-1} (Table 4.12). The results were interesting in that although the absolute modelled yield vector values were different, with the mean yields at 5.59 and 3.24 t.ha^{-1}, and 95th percentile yields at 7.08 and 5.02 t.ha^{-1}, for the S$_2$ and L$_8$ sensors respectively, the established actual yield

gaps differed by 290 kg.ha^{-1}. These findings implied that although S_2 modelled yields values were an overestimation of the yields, the gap determined equalled the L_8 based value. The L_8 yields despite having the least RMSE using the maximum zonal statistics, still this was too high. Recalibration of the Mashaba et al. (2017) equation to reduce errors across sensors is necessary. The yield gap results indicated that the L_8 based values permits the continued use of the historical archive L_8 imagery in yield research. The within study area yield gaps could be estimated by using either of the two sensors L_8 or S_2 because the results were near identical.

The global based study area wheat production potential was calculated as the difference of the within study area L_8 modelled mean yield and the regional average wheat yields obtained in the countries presented in Figure 4.14 (Grassini et al. 2013, Sosibo et al, 2016) and Table 4.13. The potential wheat yields in physical terms were adequately quantified from the research carried out. The determinants of potential wheat production where neither identified nor quantified explicitly. These required to be characterised so as to direct further research aimed at formulating input levels required and water management requirements. The expected production increases in wheat are not only premised on increased amount of water applied but complimentary inputs that raise water productivities in wheat production (Mueller et al. 2012; Araya et al. 2019)

CHAPTER 5: CONCLUSION

In this chapter yield gap closure proposals are presented in Section 5.1 and research study limitations and recommendations made in Section 5.2 and finally the research study conclusions are presented in Section 5.3.

5.1   YIELD GAP CLOSURE

There are a range of interventions that can contribute to escalation of wheat yields in the study area. These include, effective rainfall management, drastic soil fertility augmentation, efficient irrigation supplementation followed by institutional and economic incentives as encountered in the literature review section. Yield gap closure in the study area can only be achieved sustainably, if the variables pertinent to yield increases are judiciously augmented (Mueller et al. 2012; Snyder et al. 2017). CA practices in wheat production has started in the WC (Kotze 2016) and with increased adoption, yield gap closure in wheat production is expected. Current research results at Langgewens are indicating the existence of viable CA crop rotations that are out yielding the traditional mono cultural wheat production. From the yields reported at Langgewens in the year 2016, the McWMcW rotation gave the highest yield of 4215.04 kg.ha^{-1}, while the mono culture based on continuous wheat had a yield of 2507.00 kg.ha^{-1}. Wheat supplementary irrigation for crop establishment and occasional irrigation in the event of mid season droughts could improve on WC wheat yields. The use of supplementary irrigation in Zimbabwe ensures early establishment of long season maize varieties. The negative impacts of mid-season droughts are avoided by using supplementary irrigation. The WC dryland wheat yields' historical variability has been ascribed to unsteady and highly inconsistent winter rainfall patterns (IPAD 2013). Given that SA is a water scarce country, supplementary irrigation could benefit wheat production in the WC, where winter rainfall is usually delayed which results in late wheat crop establishment and yield. In addition, scientifically based crop water requirements estimation would ensure that only required irrigation amounts are applied leaving enough water for downstream users.   The expanded use of RS and GIS products such as Fruitlook in conjunction with CA are expected to accelerate the sustainable local and regional wheat yield gap closure in the WC and region.

5.2   LIMITATIONS AND FUTURE STUDIES

Quantitative research study results need validation to ensure the integrity of study findings. The snapshot study intended to establish the wheat crop water use, wheat yield, yield potential and wheat water productivities based on climate and satellite imagery data set for the 2016 winter wheat growing season. These data sets serve as benchmarks on which to estimate wheat crop

production intensification potential in a given region and facilitate the viability assessment of projects. The study had two sets of data which were taken as ground truth data, the supplied climate station reference evapotranspiration and Langgewens research station 2016 yield data. For crop water use the validation was partial, covering only climate station reference crop water requirements. For wheat yields, the observed yield data from the ARC research plots at Langgewens was sourced. However, this only represented a small part of the study which might not be representative of the whole study area. For future studies usage of ground truth data should be included to ensure the integrity of research findings and to convince sceptics on the robustness of GIS in agricultural production facilitation. The mean wheat yield statistic for purposes of a full scale irrigation feasibility study should be determined for a longer periods of time preferably exceeding three years to capture the temporal and spatial study area yields variability. The year 2016 was a drought year and hence the obtained metrics might not be representative of the average study area wheat yield mean values. Despite the above observations   the yields recorded where similar to those in the wheat production statistics for the WC. Temporal and spatial yields variation are expected to be high under dryland conditions given the variability in rainfall or water availability in the soil. The study generated daily distributed ET_0 surfaces from climate data and integrated these data with remotely sensed data sets to determine study area distributed crop water use surfaces. The validation of the ET_0 research results was based on the availed $ET_{0\,PM}$ from the ARC climate station network excel data base. The ET_{0HS} reference crop evapotranspiration were calculated using Python scripts and map algebra in ArcMap. In the absence of an independent ET_c data sets, validation of generated ET_c surfaces becomes an issue as the two steps of, K_c generation from satellite vegetation indices and computing the distributed ET_0 surfaces had no corresponding data sets for verification/validation. The modelling of K_c from NDVI and using climate station derived ET_0 was the study novelty as this yields accurate ET_c values as compared to the theoretical K_c values (Allen et al 1998, Hunsaker et al.2007). The vegetation indices e.g. NDVI is a more realistic crop coefficient determination methodology as it is based on actual plant photosynthetic activity, than the theoretical based approach that assumes non limited water availability, which is difficult to attain under practical field conditions. The major limitation to using K_c based from NDVI was the cloud cover prevalence that reduced the number of usable study area satellite imagery database from which to model NDVI. The use of other regions of the electromagnetic spectrum to model K_c should be investigated e.g. SWIR, including direct ET_c methodologies as used in ETLook, SEBAL and METRIC among other approaches. The research used the "big leaf "approach which uses a one crop coefficient (K_{cb}) approach. However other researchers advocate for the use of the two crop coefficient approach (Allen et al. 1998). According to Lobell (2013)

crop production characterisation should be accompanied by the identification of the factors contributing to the observed metrics.

The current study was limited to the establishment of wheat yield gaps without a required concurrent determination of limitations to yield growth and water productivity (Lobell 2013; van Ittersum 2013). The known crop yields determinants, include soil fertility, pests and diseases control, fertiliser inputs and improved water application need to be quantified to enable focussed intervention strategies (Molden et al. 2010; Mueller et al .2012). The yield gap analysis was based on a single image modelled yield data set and not the physically based Monteith (1972, 1977) methodology which is reputed as the standard yield estimating procedure. A comparison of different yield estimation methodologies coupled with independent data sets of crop water use and yields would have improved on accuracy assessment of water productivity and reduced uncertainties on the conclusion made. To enable the assessment of irrigation potential in wheat production, feasibility report data requirements as indicated in the literature section, must be met. These will be addressed in future research and include, the characterization of study soils and water resources, their physical and chemical properties, landform for irrigation infrastructure planning and formulation of viable cropping program based on available project area resources. The proposed advanced level study will include increased utilisation of automated procedures to speed up data acquisition, processing and analysis. Detailed irrigation designs will be carried out to ascertain the current contemporary costs of irrigation development and facilitate the economic appraisal of irrigation-based crop intensification intervention. Additionally, study area soils carbon sequestration potential and effect on sustainability need investigation. The irrigation appraisal will expose further the potential complimentary utility of GIS and RS to address the concerns raised above including reduction of environmental costs in food production intensification strategies and mitigation of global climate change. The socio-economic environment can negatively impact wheat production if prizes offered are not competitive. These aspects can be exposed in a fully fledged financial an economic project appraisal of irrigation-based crop intensification projects.

5.3 CONCLUSION

The current chapter seeks to ascertain whether the research study achieved its stated goals and provides a summary of the findings and suggestions for future research. The study aimed to determine the study area wheat crop water related performance characteristics for the Berg river catchment. The performance variables data were determined based on the processing and analyses of RS and climate data sets in a GIS platform. The daily wheat crop water use were determined using climate data based reference crop evapotranspiration (ET_0) and the single crop coefficient as practised by agriculturalists (Jensen 1998; Allen et al.1998) and depicted in Figure 1.1. The

research novelty involved the determination of study area seasonal wheat crop water use based on satellite NDVI modelled K_c and daily distributed interpolated ET_0 surfaces (ET_{0PM} and ET_{0HS}) at 10 and 30m SR. The process was implemented based on extensive and intensive usage of Python scripts in ArcMap, the used python scripts are presented Appendix A.

The characteristic ET_{cHS} overestimation and underestimation of ET_c under conditions of extreme weather conditions were presented in Section 4.1 and Section 4.5.The results indicated that the ET_{cHS} errors were very low during the period May to September, which covers the wheat growing period. Given the above the HS methodology can be used in computing study area ET_0 for wheat crop water use. Furthermore these recorded ET_{0HS} , low annual RMSE values shows that in regions, in and around specific climate stations these ET_0 estimates are representative of true reference crop evapotranspiration and can be used for both feasibility and irrigation scheduling e.g. at Abendruhe , Ashanti and Bokveldskloof, (Table B 3 &). The ET_{0HS} was with 20 % RD of the ET_{0PM} indicating further that the ET_{0HS} is valid to use for ET_0 and ET_c calculations. The stations which had higher discrepnce levels like Zuurvalkate are outside the study area and are located at high altitudes above 1000 m.a.s.l where the HS fails to give accurate results. In general, HS methodology should be taken as a rough estimate of ETc and its use restricted to pre-feasibility and feasibility studies where the levels of accuracy can be substantially lower than required in precision irrigation scheduling. However, where conditions permit and it can also be used in water scheduled. Viable seasonal L_8 and S_2 satellite imagery database to model crop coefficients, was negatively impacted by prevalence of cloudy conditions. This could be overcome by using coarse daily MODIS NDVI data to estimate wheat K_c and then ET_{cHS}. The redundancy in daily ET_0 surfaces generated from climate station data counterpoised the low frequency of viable L_8 and S_2 satellite images used to model crop coefficients.

Wheat yields were successfully modelled within acceptable levels of accuracy from satellite imagery, except for the systematic yield overestimation and underestimation by the S_2 and L_8 sensors, respectively. Based on the maximum zonal statistics, the L_8 based estimates outperformed the L_8 average statistics including all the S_2 based yield estimates with a RMSE of 0.971 (Table 4.9). It is therefore recommended that to facilitate the use of S_2 satellite data, the Mashaba et al. (2017) equation has to recalibration and validated. Alternatively, the use of S_{2B8A} should be investigated in future studies and determination made on whether this improves on the $S_{2 B8}$ in NDVI calculation. However, this will entail the scaling up of the B_{8A} from 20 to 10 m SR. It is hypothesied that the B_{8A} based NDVI will not be negatively impcted with water vapour effects and hence reduce the RMSE across the S_2, L_8 and MODIS estimates (Table 2.1 and Table 4.9).

Modelling historical wheat yields based on L_8 archived data sets using the Mashaba et al. (2017) equation is recommended for irrigation appraisal purposes. The use of S_2 modelled yield values should be restricted to the mean zonal statistics and with caution given the large RMSE recorded when compared to the Langgewens yields. The observed dynamics of the S_2 and L_8 modelled yields and the zonal statistics interplay indicates that caution on use of satellite-based yields estimate is critical.

The yield gap analysis however demonstrated the potential utility of using the S_2 and L_8 sensors in determining the wheat yield potential. Based on the L_8 and S_2 sensor data and using the Mashaba et al. (2017) equation a yield gap of 1.78 and 1.49 t.ha^{-1} were determined, respectively (Table 4.12). The determined yield gaps constituted the within study area wheat production intensification potential that can be attained if the Mueller et al. (2012) and Araya et al. (2019) recommendations are implemented. The regional based yield potential using average wheat yields in north western European countries of France, Netherlands and United Kingdom indicated wheat yield gaps of 3.74 to 4.34 t.ha^{-1} (seen in Table 4.13) indicating that WC wheat yields could be doubled. The Nothern Cape based yield gap of 3.65 t.ha^{-1} indicated the irrigation wheat production of the WC. The study findings indicated that if wheat production intensification programmes are implemented in the study area, yields would be doubled. In addition, the current low wheat water productivities of 0.3874 and 0.4262 kg.m^{-3} seen in Table 4.11 based on L_8 zonal statistics illustrated the potential in wheat production intensification to 2.00 kg.m^{-3} or 20 kg.ha^{-1}.mm^{-1} water yield levels i.e. quadrupling of water productivity. The study determined the crop water use, yield potential and water productivities which all indicated the existence of wheat production intensification opportunities in the study area. It is noteworthy that the entire study relied on models established by literature search. This indicates that the current body of knowledge in modelling and GIS technology if judiciously implemented even without recalibration reasonable estimates of ET_0, ET_c and wheat yield can be made.

The contemporary agricultural settings of increasing non-agricultural water demand, escalating food requirements based on affluence and population increases, and environmental concerns implies that there is a need to escalate crop production. To ensure sustainable crop production intensification, research studies should include analysis of all relevant physical variables pertinent to yield augmentation. Therefore the dynamics of soils, water, climate, ecosystems services, sustainable cropping programs formulation, complimented by integrated livestock production (e.g. fisheries) as suggested by Mueller et al. (2013) should be understood. The platform where many themes can be integrated and analysed concurrently, for optimal resources use design will increasingly be on GIS platforms, using RS data complemented with ancillary tabular data sets.

The current study has demonstrated the utility of GIS to integrate RS and tabular data sets to establish wheat crop yield, water use, water productivity and wheat yield production potential in the Berg river catchment. Further research that include soils resources characterisation with respect to soil carbon content (SCC), soil physical and chemical attribute are suggested so as to spatially and temporally facilitate the design of optimal intensification strategies in wheat production while mitigating the negative impacts of climate change. Historical reference crop water requirements characterisation and analyses using ET_{0HS} in SADC regions having limited climate station data is envisaged to facilitate the science-based water development planning and use in irrigated agriculture. Remote sensing of soils would facilitate the physical and chemical soil properties temporal and spatial profiling which is necessary for the design of CA. The SCC and soil parent materials are critical parameters in soil fertility and salinity risks ranking respectively. Furthermore, CA generally and SCC in particular when coupled with scientific based water management are set to augment water productivities under irrigated and rainfed systems thus ensuring food production self-sufficiency now and in the future. RS and GIS technologies-based studies are expected to facilitate the design of sustainable agricultural production intensification programmes.

REFERENCES

Alexandratos N & Bruinsma J 2012. World agriculture towards 2030/2050: the 2012 revision. Agricultural Development Economics Division, *Food and agriculture organization of the United Nations*. Available from http://ageconsearch.umn.edu/record/288998/files/a-ap106e.pdf [Accessed 3 Feb 2020].

Allen R, Kilic A & Huntington J 2015. Google earth engine evapotranspiration Flux-EEFlux. Landsat science team meeting. *EROS*. Available from https://landsat.usgs.gov/sites/default/files/documents/Allen_UNL_DRI_UI_EEFlux_update_LST_meeting_July_8_2015c.pdf [Accessed 3 Feb 2020].

Allen R, Pereira L, Raes D & Smith M 1998. Crop evapotranspiration – guidelines for computing crop water requirements. *FAO irrigation and drainage paper 56*. Food and agriculture organization of the United Nations: Rome, Italy. Available from https://appgeodb.nancy.inra.fr/biljou/pdf/Allen_FAO1998.pdf [Accessed 3 Feb 2020].

Allen RG, Morse A, Tasumi M, Bastiaanssen W, Kramber W & Anderson H 2001. Evapotranspiration from Landsat (SEBAL) for water rights management and compliance with multi-state water compacts. *Geoscience and remote sensing symposium IGARSS '01*. IEEE International. Available from https://ieeexplore.ieee.org/stamp/stamp.jsp?tp=&arnumber=976651 [Accessed 3 Feb 2020].

Allen RG, Pereira LS, Smith M, Raes D & Wright JL 2005. FAO-56 dual crop coefficient method for estimating evaporation from soil and application extensions. *ASCE Journal of irrigation and drainage engineering* 131: 2-13.

Allen RG, Tasumi M & Trezza R 2007. Satellite-based energy balance for mapping evapotranspiration with internalized calibration (METRIC): Model. *ASCE Journal of irrigation and drainage engineering* 133 (4): 380-394.

Allen RG, Irmak A, Trezza R, Hendrickx JM, Bastiaanssen W & Kjaersgaard J 2011. Satellite-based ET estimation in agriculture using SEBAL and METRIC. *Hydrological processes* 25:4011-4027.

Althoff D, Argolo dos Santos R, Bazame H C, França da Cunha F & Filgueiras R 2019. Improvement of Hargreaves–Samani reference evapotranspiration estimates with local calibration. *MDPI Water journal* 11:2272.

Anderson HE, Reutebuch SE & McGaughey 2006. Active remote sensing. *Computer applications in sustainable forest management.* Springer Netherlands. Available from

https://link.springer.com/chapter/10.1007%2F978-1-4020-4387-1_3[Accessed 15 Feb 2020]

Angus DE & Watts PJ 1984. Evapotranspiration - how good is the Bowen ratio. *Agricultural Water Management* 8:133-150.

Archer E, Landman W, Malherbe J, Tadross M & Pretorius S 2019. South Africa's winter rainfall region drought: A region in transition? *Climate risk management* 25:1-8.

Araya A, Prasad PVV, Gowda PH, Kisekk I & Foster AJ 2019. Yield and water productivity of winter wheat under various irrigation capacities. *Journal of the American water resources association* 55(1):24-37.

Atzberger C 2013. Advances in remote sensing of agriculture: Context description, existing operational monitoring systems and major information needs. *Remote Sensing* 5:949-981.

Basso B, Cammarano D & De Vita P 2004. Remotely sensed vegetation indices: Theory and applications. *Rivista Italiana di Agrometeorologia*. Available from http://eww.agrometeorologia.it/documenti/rivista9_1/Basso2004_1.pdf [Accessed on 15 Feb 2020]

Bastiaanssen WGM, Menenti M, Feddes RA & Holtslag AAM 1998a. A remote sensing surface energy balance algorithm for land (SEBAL), 1 Formulation. *Journal of hydrology* 212–213: 198–212.

Bastiaanssen WGM & Bos MG 1999. Irrigation performance indicators based on remotely sensed data: a review of literature. *Irrigation and drainage systems* 13: 291–311.

Bastiaanssen WGM, Noordman EJM, Pelgrum H, Davids G, Thoreson BP & Allen RG 2005. SEBAL model with remotely sensed data to improve water-resources management under actual field conditions. *ASCE Journal of irrigation and drainage engineering* 131(1): 85–93.

Bastiaanssen WGM, Cheema MJM, Immerzeel WW, Miltenburg IJ & Pelgrum H 2012. Surface energy balance and actual evapotranspiration of the transboundary Indus Basin estimated from satellite measurements and the ETLook model. *Water resources research* 48:1-16.

Baum WC 1978. The Project cycle. *Finance and development* 15 (4):10-17.

Bjorneberg DL 2013. Irrigation Methods. *USDA Agricultural research services*. Available from https://eprints.nwisrl.ars.usda.gov/1568/1/1524.pdf [Accessed on 4 Jan 2020].

Blatchford ML, Mannaerts CM, Zeng Y, Nouri H & Karimi P 2019. Status of accuracy in remotely sensed and in-situ agricultural water productivity estimates: A review. *Remote sensing of environment* 234:111413.

Blaney HF & Criddle DW 1949. Consumptive use of water the irrigated areas of the Upper Colorado River basin. *USDA Soil conservation services*. Available from https://books.google.co.za/books?hl=en&lr=&id=U8VQ1VI-aMC&oi=fnd&pg=PA1&dq=Blaney+H+F+%26+Criddle+D+W+1949.+Consumptive+use+of+water+the+irrigated+areas+of+the+Upper+Colorado+River+Basin.+USDA+Soil+conservation+services.+Editor+Clyde+D+G.&ots=4qAyHEb3V4&sig=A6b-Q9DfkbDpyANWYLqodtL3rOU&redir_esc=y#v=onepage&q&f=false [Accessed 3 Feb 2020].

Blaney HF & Criddle WD 1964. Determining water requirements for settling water disputes. *Resources journal* 4:29-41.

Bodner G, Nakhforoosh A & Kaul HS 2015. Management of crop water under drought: a review. *Agronomy for sustainable development* 35(2):401-442.

Boelee E & Madse H 2006. Irrigation and schistosomiasis in Africa: Ecological aspects. *IWMI Research report 99*. Available from https://core.ac.uk/reader/6405130 [Accessed 11 Feb 2020]

Boogaard H, Wolf J, Supit I, Niemeyer S & van Ittersum M 2013. A regional implementation of WOFOST for calculating yield gaps of autumn-sown wheat across the European Union. *Field crops research* 143:130-142.

Butterworth BJ & Else BGT 2018. Dried, closed-path eddy covariance method for measuring carbon dioxide flux over sea ice. *Atmospheric measurement techniques* 11: 6075–6090.

Cahn DM & Johnson FL 2017. New approaches to irrigation scheduling of vegetables. *Horticulturae* 3:1-20.

Calera A, Campos I, Osann A, D'Urso G & Menenti M 2017. Remote sensing for crop water management: From ET modelling to services for the end users. *Sensors* 17 (5):1-25.

Chansyk DS & Naeth MA 1996. Field measurement of soil moisture using neutron probes. *Canadian journal of soil science* 76:317-323.

Childs C 2004. Interpolating surfaces in ArcGIS spatial analyst. ESRI Education services. Available from https://www.esri.com/news/arcuser/0704/files/interpolating.pdf [Accessed 15 Feb 2020].

Choudhury B U, Sing A K, Pradhan S 2013. Estimation of crop coefficients of dry-seeded irrigated rice–wheat rotation on raised beds by field water balance method in the Indo-Gangetic plains, *Agricultural Water Management* 123:20– 31.

Clark M & Tilman D 2017. Comparative analysis of environmental impacts of agricultural production systems, agricultural input efficiency, and food choice. *Environmental research letters* 12(064016):1-12.

Cleland J 2013. World population growth; past present and future. *Environmental Resources Economics* 55:543-554.

Davidson L, Mills JP, Haynes I, Augarde C, Bryan P & Douglas M 2019. Airborne to UAS Lidar: an analysis of UAS Lidar ground control targets. *The International archives of the photogrammetry, remote sensing and spatial information sciences* 2(13):255-262

Dark S J & Bram D 2007. The modifiable areal unit problem in physical geography. *Progress in Physical Geography* 31(5): 471–479.

DEADP 2012b. Western Cape sustainable water management plan. Department of environmental affairs and development planning. Available from https://www.greencape.co.za/assets/Water-Sector-Desk-Content/WC-DEAP-DWS-Western-Cape-sustainable-water-management-plan-2012.pdf [Accessed 2 Jan 2020].

DEADP 2013. Annual report 12/13. *Department of environmental affairs and development planning*. Available from

https://www.environment.gov.za/sites/default/files/docs/environmental_affairs2012_2013_annualreport.pdf[Accessed 2 Jan 2020].

De Bruin HAR 1983. A model for the Priestley –Taylor parameter. *Journal of climate and applied meteorology* 22:572-578.

Descheemaeker K, Stuart W, Bunting SW, Bindraban P, Muthuri C, Molden D, Beveridge M, van Brakel M, Herrero M, Clement F, Boelee E & Jarvis DI 2013. Increasing water productivity in agriculture. *Managing water and agroecosystems for food security*. Available from http://www.iwmi.cgiar.org/Publications/CABI_Publications/CA_CABI_Series/Managing_Water_and_Agroecosystems/chapter_8-increasing_water_productivity_in_agriculture.pdf [Accessed 3 Feb 2020].

De Villiers MC, Nell J P, Barnard RO & Henning A 2003. Salt-affected soils: South Africa. *FAO contract paper number PR 26897*. Available from

https://www.researchgate.net/publication/271836352_Saltaffected_soils_South_Africa [Accessed 11 Feb 2020]

De Villiers S 2007. The deteriorating nutrient status of the Berg River, South Africa. *Water SA* 33 (5): 659-664.

Dhungel S & Barber ME 2018. Estimating calibration variability in evapotranspiration derived from a satellite-based energy balance model. *Remote sensing* 10(1695):1-25.

Doorenbos J & Pruitt WO1977. Guidelines for predicting crop water requirements. Crop water requirements. *Food and agriculture organization of the United Nations*. Available from http://www.fao.org/3/a-f2430e.pdf [Accessed 4 Jan 2020].

Droogers P & Allen RG 2002. Estimating reference evapotranspiration under inaccurate data conditions. *Irrigation and drainage systems* 16: 33-45.

Du Plessis J & Schloms A 2017. An investigation into the evidence of seasonal rainfall pattern shifts in the Western Cape, South Africa. *Journal South Africa institutes of civil engineers* 59 (4): 48-55.

DWAF 2004. National water resource strategy. *Department of Water Affairs and Forestry*. Available from https://cer.org.za/wp-content/uploads/2017/10/NWRS-2004.pdf [Accessed 2 Jan 2020].

DWAF 2007. Berg river baseline monitoring programme. *Department of Water Affairs and Forestry* Available from http://www.fewlbnexus.uct.ac.za/sites/default/files/image_tool/images/91/DWAF%20VOLUME5_Synthesis_Berg%20River%20Baseline%20Monitoring%20Programme.pdf [Accessed 4 Jan 2020].

DWAF 2013. Strategic overview of the water sector in South Africa. *Department of Water Affairs and Forestry.* Available from http://nepadwatercoe.org/wp-content/uploads/Strategic-Overview-of-the-Water-Sector-in-South-Africa-2013.pdf [Accessed 4 Jan 2020].

Dzikiti S,Volschenk T, Midgley SJ, ELötze E, Taylor NJ,Gush MB, Ntshidi Z,Zirebwa SF, Doko Q, Schmeisser M, Jarmain C,Steyn WJ &Pienaar HH, 2018. Estimating the water requirements of high yielding and young apple orchards in the winter rainfall areas of South Africa using a dual source evapotranspiration model. *Agricultural Water Management, Elsevier* .208:152-162.

Edreira JIR, Guilpart N, Sadras V, Cassman KG, van Ittersum MK, Schils RLM & Grassini P 2018. Water productivity of rainfed maize and wheat: A local to global perspective. *Agricultural and forest meteorology* 259: 364-373.

Esser KB 2017. Water infiltration and moisture in soils under conservation and conventional agriculture in agro-ecological Zone IIa, Zambia. *Agronomy*. Available from http://www.mdpi.com/journal/agronomy [Accessed 20 Jan 2020].

Euser T, Luxemburg WMJ, Everson CS, Mengistu MG, Clulow AD & Bastiaanssen WGM 2014. A new method to measure the Bowen ratios using high-resolution vertical dry and wet bulb temperature profiles, *Hydrology of the earth systems sciences* 18:2021-2032.

Farahani H J, Howell TA, Shuttleworth WJ & Bausch WC 2007. Evapotranspiration: Progress in measurement and modelling in agriculture. *Transaction of the American society of agricultural and biological engineer*s 50 (5): 1627-1638.

FAO STAT 2020 Wheat crop statistics 2012 to 2017. *Food and Agricultural Organisations of the United Nations*. Available from http://www.fao.org/faostat/en/#data/QC/visualize [Accessed 20 Sept 2020]

Faurès JM, Hoogeveen J & Bruinsma J 2002. The FAO irrigated area forecast for 2030. *Food and Agriculture Organisation of the United Nations*. Available from http://www.fao.org/3/I9278EN/i9278en.pdf [Accessed 4 Jan 2020].

French R J & Schultz J E 1984. Water use efficiency of wheat in a Mediterranean-type environment. Some limitations to efficiency. *Australian Journal Agricultural Research* 35:765-775.

Fritschen LJ 1965. Accuracy of the evapotranspiration determination by the Bowen ratio. *Hydrological sciences journal* 10(2):38-48

Gibson LA, Jarmain C, Su Z & Eckard FE 2013. Estimating evapotranspiration using remote sensing and the surface energy balance system – A South African perspective. *Water SA* 39:477- 482.

Gitelson AA, Gritz Y & Merzlyak MN 2003. Relationship between leaf chlorophyll content and spectral reflectance algorithms for non-destructive chlorophyll assessment in higher plant leaves. *Journal of plant physiology* 160:271-282.

Gitelson AA 2004. Wide dynamic range vegetation index for remote quantification of biophysical characteristics of vegetation. *Journal of plant physiology* 161 (2):165-173.

Gittinger JP 1984. Economic analysis of agricultural projects. *Economic development institute, the World Bank.* Available from https://pdfs.semanticscholar.org/67f7/ 6b673ef244f061801facadcd83757bc43b27.pdf? ga=2.150960949.229838968.1578172427-309761345.1570307005 [Accessed 4 Jan 2020].

Glecer EM, Fraisse CW & Sentelhas PC 2010. Evaluation of methodologies to estimate reference evapotranspiration in Florida. *Proceedings Florida state horticultural society* 123:189-195.

Gleason CP 1982. Large area yield estimation and forecasting using plant process models, Paper No 82-4569. *American society of agricultural engineers.* Available from https://pdfs.semanticscholar.org/05b8/f57d3c62e5f69551cb4922aa6577c0d56d69.pdf [Accessed 4 Jan 2020].

Glenn EP, Neale CMU, Hunsaker DJ & Nagler PL 2011. Vegetation index-based crop coefficients to estimate evapotranspiration by remote sensing in agricultural and natural ecosystems. *Hydrological Processes* 25:4050-4062.

Gowda PH, Chávez JL, Howell TA, Marek TH & New LL 2008. Surface energy balance based evapotranspiration mapping in the Texas high plains. *Sensors* 8:5186-5201.

Gowda PH, Chávez JL, Colaizzi PD, Evett SR, Howell TA & Tolk JA 2007. Remote sensing based energy balance algorithms for mapping ET: Current status and future challenges. *American society of agricultural and biological engineers* 50:1639-1644.

Görgens AHM & de Clercq WP 2005. Research on Berg river water management. Summary on water quality information system and soil quality studies. WRC Report No. TT 252/05. Available from http://www.fewlbnexus.uct.ac.za/sites/default/files/image_tool/images/91/Research%20on%20Berg%20River%20Water%20Management%20WRC%202005.pdf [Accessed 4 Jan 2020].

Grain SA 2020. Wheat yield 2012 - 2018 report. Available online at https://www.grainsa.co.za/report-documents?submited=1&cat=14 & find = [accessed on 29 Sept 2020]

Grassini P, Kent M, Eskridge KM & Cassman KG 2013. Distinguishing between yield advances and yield plateaus in historical crop production trends. *Nature communications* 4, 2918 [online] Available from https://doi.org/10.1038/ncomms3918 [Accessed4 Jan 2020].

Hargreaves GH & Allen RG 2003. History and evaluation of the Hargreaves evapotranspiration equation. *Journal of irrigation and drainage engineering* 129:53-63.

Harman GE & Uphoff N 2019. Symbiotic root-endophytic soil microbes improve crop productivity and provide environmental benefits. *Scientifica (Cairo)*. Available from https://www.ncbi.nlm.nih.gov/pubmed/31065398 [Accessed 20 Jan 2020].

Hatfield JL & Prueger JH 2010. Value of using different vegetative indices to quantify agricultural crop characteristics at different growth stages under varying management practices. *Remote sensing* 2:562-578.

Hermans K, Verburg P, Stehfest E & Müller C 2010. The yield gap of global grain production: A spatial analysis. *Agricultural systems* 103:316-326.

Hoogeveen J, Faurès JM & van de Giessen N 2009.Increased biofuel production in the coming decade: To what extend will it affect global freshwater resources? *Irrigation and drainage* 58: 148-160.

Huete A, Didan K, Miura T, Rodriguez EP, Gao X & Ferreira LG 2002. Overview of the radiometric and biophysical performance of the MODIS vegetation indices. *Remote sensing of environment* 831:95-213.

Huete A, Didan K, Miura T & Van Leeuwen W J D 2011. MODIS vegetation indices. Available online at https://www.researchgate.net/publication/226279239_MODIS_vegetation_indices

[Accessed on 14 Sept 2020]

Hunsaker DJ, Fitzgerald GJ, French AN, Clarke TR, Ottman MJ & Pinter PJ 2007a. Wheat irrigation management using multispectral crop coefficients. I. Crop evapotranspiration prediction. *Transactions of the ASABE* 50:2017-2033.

Hunsaker DJ, Fitzgerald GJ, French AN, Clarke TR, Ottman MJ & Pinter PJ 2007b. Wheat irrigation management using multispectral crop coefficients. II. Irrigation scheduling performance, grain yield, and water use efficiency. *Transactions of the ASABE* 50:2035-2050.

IPAD 2013. South Africa's 2013/14. Available from https://ipad.fas.usda.gov/highlights/2013/08/SouthAfricaWheat/ [Accessed 10 Aug 2019].

Irmak S 2008. Evapotranspiration - Introduction the hydrologic cycle and ET -ET Terminology. *University of Nebraska-Lincoln extension, journal series No.* 1037:1432-1438.

Jacobs AFG & de Bruin HAR 1998. Makkink's equation for evapotranspiration applied to unstressed maize. *Hydrological processes* 12:1063-1066.

Jacobsen T & Adams MR 1958. Salt and silt in ancient Mesopotamian agriculture. *Science new series* 128:1251-1258.

Jarmain C, Van Niekerk A & Goudriaan R 2016. Remote sensing applications for sustainable agriculture in South Africa. *Proceedings of the SPIE 9998*. Available from https://doi.org/10.1117/12.2241860 [Accessed 4 Jan 2020].

Jensen ME 1968. Water consumption by agricultural plants, Chapter 1. *Water deficits and plant growth 2*:1-22.

Jensen ME, Wright JL & Pratt BJ 1971. Estimating soil moisture depletion from climate, crop and soils data. *Transactions of ASAE* 14:954-959.

Jensen ME 2010. Historical evolution of ET estimations methods. A century of progress. *CSU/ARS Evapotranspiration workshop, Fort Collins*. Available from https://coagmet.colostate.edu/ET_Workshop/ET_Jensen/ET_history.pdf [Accessed 10 Aug 2018].

Johnson L F & Trout T J 2012. Satellite NDVI Assisted Monitoring of Vegetable Crop Evapotranspiration in California's San Joaquin Valley. *Remote Sensing*. 4: 439-455

Jones SB, Wraith JM & Or D 2002. Time domain reflectometry measurement principles and applications. *Hydrological processes* 16:141-153.

Kalma DJ, McVicar RT & McCabe FM 2008. Estimating land surface evaporation: A review of methods using remotely sensed surface temperature data. *Survey geophysics* 29:421-469.

Kumar L & Mutanga O 2018. Google earth engine applications since inception: Usage, trends, and potential. *Remote sensing* 10 (1509):1-15.

Kotzé P 2016. Water and Agriculture. Conservation agriculture: Farming for the future. *The Water wheel* March/April Available from https://www.arc.agric.za/Economic%20News%20articles/ Conservation%20agriculture%20is%20proving%20well%20worth%20(The%20Water%20W heel,%20March-April%202016,%20pp%2012-15).pdf [Accessed 10 Sep 2019].

Lamm FR & Rogers DH 2014. SDI. For Corn production – A Brief review of 25 years of KSU research. *Proceedings of 26th Annual Central plains irrigation conference, Kansas*. Available from http://www.ksre.ksu.edu/sdi/ [Accessed 4 Jan 2020].

Letsebe K 2018. Fruitlook helps drought-stricken Cape farmers to save water. *Business Technology Media Company*. Available from https://www.itweb.co.za/content/KA3WwMdY2bNqrydZ [Accessed 6 Jan 2020].

Ling B, Lehman D, Kinyangi J, Grossman J, O'Neil & Thies J 2006. Black carbon increases cation exchange capacity in soils. *Soil science society of America Journal* 70:1719-1730.

Light DL 1990. Photogrammetric engineering & remote sensing. *American society for photogrammetry and remote sensing* 56 (12):1613-1623.

Lillesand TM & Kiefer RW 1994. *Remote sensing and image interpretation*. 3rd Ed. New York John Wiley & Sons. Available from

https://ui.adsabs.harvard.edu/abs/1995GeoM..132..248D/abstract [Accessed 15 Feb 2020]

Lima JRS, Antonino ACD, de Souza ES, Hammecker C, Montenegro SMGL & Lira CABO 2013. Calibration of Hargreaves-Samani equation for estimating reference evapotranspiration in sub-humid region of Brazil. *Journal of water resource and protection* 5: 1-5.

Lobell DB, Azzari G, Burke M, Gourlay S, Jin Z, Kilic T & Murray S 2020. Eyes in the sky, boots on the ground: assessing satellite- and ground-based approaches to crop yield measurements. *American journal of agricultural economics.* Available from https://doi.org/10.1093/ajae/aaz051 [Accessed 4 Jan 2020].

Lobell DB 2013. The use of satellite data for crop yield gap analysis. *Field crops research* 143: 56-64.

Lobell DB, Asner GP, Ortz-Monasterio & Benning TL 2003. Remote sensing of regional crop production in the Yaqui Valley Mexico: estimates and uncertainties. *Agriculture, ecosystems and environment* 94:205-220.

Lori M, Symnaczik S, Ma¨der P, De Deyn G & Gattinger A 2017. Organic farming enhances soil microbial abundance and activity - A meta-analysis and meta-regression. *PLoS ONE* 12 (7): 1-25.

Losgedaragh S Z & Rahimzadegan M 2018. Evaluation of SEBS, SEBAL and METRIC models in estimation of the evaporation from the freshwater lakes. Case study of Amirkabir dam, Iran. *Journal of hydrology* 561:523–531.

Maluleke I 2018. Grain SA 2017/2018's Wheat Market Trends. Available from https://www.grainsa.co.za/2017/2018s-wheat-market-trends [Accessed 4 Jan 2020].

Mashaba Z, Chirima G, Botai J O, Combrinck L, Munghemezulu C & Dube E 2017. Forecasting winter wheat yields using MODIS NDVI data for the Central Free State region. *South African journal of science* 113(11/12):1-6.

Maune DF 2011. Digital elevation model (DEM) Whitepaper. NRCS High Resolution Elevation Data. *USDA* Natural Resources Conservation Service. *National geospatial management center.* Available from https://www.nrcs.usda.gov/Internet/FSE_DOCUMENTS/ stelprdb1047930.pdf [Accessed 4 Jan 2020].

Mazareanu E 2019. Number of satellites by country 2019. *Statista web page.* Available from https://www.statista.com/statistics/264472/number-of-satellites-in-orbit-by-operating-country/ [Accessed 12 Jan 2020].

McCurdy M, Davies EO, Gunaratnan A, Grafton M, Bishop P & Jeyakumar P 2019. Instrumentation of a bank of lysimeters: Sensors and sensibility. Conference chemical mega trends and the elements. *International Year of the periodic table.* Available from https://www.researchgate.net/publication/336287792 [Accessed 3 Feb 2020].

McMahon TA, Peel MC, Lowe L, Srikanthan R & McVicar TR 2013. Estimating actual, potential reference crop and pan evaporation using standard meteorological data: a pragmatic synthesis. *Hydrology and earth system sciences* 17: 1331-1363.

Meyer F, Davids T, Gouse M, van der Westhuizen D, van der Burg G, Delport M & Trapnell L 2015. An assessment of the drivers influencing wheat production in South Africa. *Bureau for Food and Agricultural Policy BFAP.* University of Pretoria. Conference paper. Available from

https://www.researchgate.net/profile/Tracy_Davids/publication/317332694_An_assessment_of_t he_drivers_influencing_wheat_production_in_South_Africa/links/5932b85e0f7e9beee7997a2 f/An-assessment-of-the-drivers-influencing-wheat-production-in-South-Africa.pdf?origin=publication_detail [Accessed 17 August 2020]

Mitasova H & Mitas L 1993.Interpolation by regularized Spline with Tension. Theory and implementation. *Mathematical Geology* 25:641-655.

Mitas L & Mitasova H 2005. Spatial interpolation. *Geographic information system, principles, techniques, management and applications*. Available from

https://www.scirp.org/(S(351jmbntvnsjt1aadkposzje))/reference/ReferencesPapers.aspx?Refer enceID=2061139   [Accessed 15 Feb 2020]

Mkhwanazi MM & Chávez JL 2013. Mapping Evapotranspiration with the Remote Sensing ET algorithms METRIC and SEBAL. Hydrology days. Available from

https://pdfs.semanticscholar.org/9e68/78d0efd19e36a5a8f7187a8b200e550174fb.pdf [Accessed 3 Feb 2020]

Molden D, Oweis T, Steduto P, Bindraban P, Hanjra MA & Kijne J 2010. Improving agricultural water productivity: Between optimism and caution. *Agricultural water management* 97:528-535.

Monteith JL 1977. Climate and the efficiency of crop production in Britain. *Philosophical transactions of the royal society of London* 281:277-294.

Monteith JL 1972. Solar Radiation and Productivity in Tropical Ecosystems. *British ecological society* 9:747-766.

Monteith JL 1985. Evaporation from land surfaces: Progress in analysis and prediction since 1948. Advances in Evapotranspiration, Proceedings of the national conference on advances in evapotranspiration. *American society of agricultural engineers* 14-85:4-12.

Mouton A 2019. Getting ahead of Salinization. Scientists utilise satellites images for early detection, *Fresh Quarterly Newspaper* 6. Available from http://www0.sun.ac.za/cga/wp-content/uploads/2019/09/201909_Fresh-Quarterly-issue-6_Salinization-research.pdf [Accessed 4 Jan 2020].

Moeletsi ME, Walker S & Hamandawana H 2013. Comparison of the Hargreaves and Samani equation and the Thornwaite equation for estimating dekadal evapotranspiration in the Free State Province of South Africa. *Physics and chemistry of the earth* 66:4-15.

Mueller ND, Gerber JS, Johnston M, Ray DK, Ramankutty N & Foley JA 2012. Closing yield gaps through nutrient and water management. *Nature* 490:254-257.

Nagler PM, Glenn EP, Nguyen U, Scott LR & Doody T 2013. Estimating riparian and agricultural actual evapotranspiration by reference evapotranspiration and MODIS Enhanced Vegetation Index. *Remote sensing* 5:3849-3871.

Nelson A, Reuter HI & Gessler P 2009. DEM Production Methods and Sources. *Developments in soil science* 3:0166- 2481.

Neumann K, Verburg HJ, Stehfest E & Müller C 2010 The yield gap of global grain production: A spatial analysis: *Agricultural systems* 103:316-326.

OGA 2015. South Africa Wheat. Highlights. Available from http://www.pecad.fas.usda.gov/highlights/2013/08/SouthAfricaWheat/ editor [Accessed 16 Dec 2019].

Penman H L 1948. Natural evaporation from open water, bare soil, and grass. *Proceedings royal society of London* 193:120-146

Pelgrum H, Miltenburg JI, Cheema MJM, Klaasse A & Bastiaanssen WGM 2010. ETlook: a novel evapotranspiration algorithm. *Remote sensing and hydrology*. Available from https://www.researchgate.net/publication/290698119_ET_Look_A_novel_continental_evapot ranspiration_algorithm[accessed 15 Jan 2020].

Phocaides A 2007. Handbook on pressurized irrigation techniques. *Food and Agriculture Organization.* ISBN 978-92-5-105817-6. Available online at http://www.fao.org/3/a1336e/a1336e.pdf [Accessed 4 Jan 2020].

Priestly C H B & Taylor R J 1972. On the Assessment of Surface Heat Flux and Evaporation Using Large-Scale Parameters. *Monthly weather review* 100 (2):81 -92.

Rahimzadeh-Bajgiran P, Berg AAP, Champagne C & Omasa K 2013. Estimation of soil moisture using optical/thermal infrared remote sensing in the Canadian Prairies. *ISPRS Journal of photogrammetry and remote Sensing* 8:94-103.

Ramoelo et al. 2014. Validation of global evapotranspiration product (MOD16) using flux tower data in the African savannah. Available from https://www.mdpi.com/2072-4292/6/8/7406/htm [Accessed 22Sept 2020].

Renault D & Wallender WW 2000. Nutritional water productivity and diets: From "Crop per Drop" towards: "Nutrition per drop". *Agricultural water management* 45:275-296.

Rensburg van LD, de Clercq W P, Barnard JH & du Preez CC 2011. Salinity guidelines for irrigation: Case studies from Water Research Commission projects along the Lower Vaal, Riet, Berg and Breede Rivers. *Water SA* 37 5.

Reinders FB 2011. Irrigation methods for efficient water application: 40 years of South African research excellence. *Water SA* 37 (5):765-770.

Reis S 2008. Analysing land use/land cover changes using remote sensing and GIS in Rize, North-East Turkey. *Sensors* 8:6188-6202.

Reyes-González A, Kjaersgaard J, Trooien T, Hay C & Ahiablame L 2018. Estimation of Crop evapotranspiration using satellite remote sensing-based vegetation index. Advances in meteorology. Available from http://downloads.hindawi.com/journals/amete/2018/4525021.pdf [Accessed 16 Feb 2020]

Reynold SG 1970. The Gravimetric method of soil moisture determination Part III. An examination of factors influencing soil moisture variability. *Journal of hydrology* 11: 288-300.

Richards M 2017. pyeto *Documentation Release 02*. Available from https:// readthedocs.org/projects/ pyeto/downloads/ pdf/latest [Accessed 4 Jan 2020].

Richards L A & Neal O R 1936. Some field observations with tensiometers. *Soil Science Society of America Proceedings* 1: 71.

Rouse JW, Haas RH, Jr Schell JA & Deering D W 1974. Monitoring vegetation systems in the Great Plains with ERTS. NASA SP-351. *Third ERTS-1 Symposium NASA Washington DC* 1: 309–317.

Rowland J, Wood E & Tieszen LL 2007. Review of remote sensing needs of and applications in Africa. *USGS Centre for earth resources observation and science (EROS).* Available from https://www.researchgate.net/publication/282650020 [Accessed 3 Feb 2020].

SABI 2017 Norms for the design of irrigation systems. *South African irrigation institute*. Available from https://www.sabi.co.za/0-pdf/SABI%20norms%202017.pdf [Accessed 4 Jan 2020].

Sadras V O & Angus JF 2006. Benchmarking water use efficiency of rainfed wheat in dry environments. *Australian journal of agricultural research* 57:847-856.

Sadras V O & McDonald G 2012. Water use efficiency of grain crops in Australia: principles, benchmarks and management. *Grains Research and Development Corporation. Australian Government*. Project Code: DAS00089.

Savva AP & Frenken K 2001. Planning, development monitoring and evaluation of irrigated agriculture with farmer participation. *FAO Irrigation manual*. Available from http://www.fao.org/3/a-ai597e.pdf [Accessed 4 Jan 2020].

Savva AP & Frenken K 2002. Crop water requirements and irrigation scheduling. *FAO Irrigation manual volume 4.* Available from http://www.fao.org/tempref/docrep/fao/010/ai593e/ai593e00.pdf [Accessed on 4 Jan 2020].

Schauberger B, Ben-ari T, Makowoski D, Kato T, Kato H & Ciais P 2018. Yield trends, variability and stagnation analysis of major crops in France over more than a century. *Scientific reports* 8 (16865):1-12.

Schierhorn F, Faramarzi M, Prishchepov AV, Koch F & J Müller 2014. Quantifying yield gaps in wheat production in Russia. *Environmental Research letters* 9:1-12.

Schulze RE 2016. On Observations, Climate Challenges, the South African Agriculture Sector and Considerations for an Adaptation Handbook. Section A: *Agriculture and climate change in South Africa*. Available from

https://www.nda.agric.za/doaDev/sideMenu/forestry/docs/Handbook%20Part%201.pdf [Accessed 12 Oct 2019].

Schulze R E &Taylor M A 2016. Environmental impacts of irrigation on water resources in South Africa and climate change: The case of surface water and deep percolation losses from irrigated areas. *Handbook for farmers, officials and other stakeholders on adaptation to climate change in the agriculture sector within South Africa. Chapter H3*. Available from

https://www.nda.agric.za/doaDev/sideMenu/forestry/docs/Booklet%2013%20Irrigation.pdf [Accessed 12 Oct 2019]

Sellers JP 1987. Canopy reflectance, photosynthesis, and transpiration. The Role of biophysics in the linearity of their interdependence. *Remote sensing of the environment* 21:143-183.

Seyler H 2015. Water as a constraint on economic development. 2014-2015 Research Project Progress Report. *Green cape sector development agency*. Available from https://greencape.co.za/assets/GreenCape-Water-Project-2014-2015-Report-excl-AppendicesSec1011.1.pdf [Accessed 10 Oct 2019].

Sibley AM, Grassini P, Thomas EN, Cassman GK & Lobell BD 2014. Testing remote sensing approaches for assessing yield variability among maize fields. *Agronomy journal* 106:24-32.

Siebert S, Doll P, Hoogeveen J, Faures JM, Frenken K & Feick S 2005. Development and validation of the global map of irrigation areas. *Hydrology and earth system sciences discussions* 2: 1299-1327.

Sing M, Kumar R, Sharma A, Sing B, Mishra PK & Sharma K 2013. Evaluation of yield monitoring system installed on indigenous grain combine harvester for rice crop. *Agricultural engineering international* 15 (3):148-153.

Shahidian S, Serralheiro R, Serrano J, Teixera J, Haie N & Santos F 2012. Hargreaves and Other Reduced-Set Methods for Calculating Evapotranspiration. *Evapotranspiration remote sensing and modelling.* Available from http://www.intechopen.com/books/evapotranspiration-remote-sensing-and-modeling/hargreaves-and-otherreduced-set-methods-for-calculating-evapotranspiration [Accessed 15 Aug 2019].

Shelestov A, Lavreniuk M, Kussul N, Novikov A & Skakun S 2017. Exploring Google Earth Engine Platform for Big Data Processing: Classification of multi-temporal satellite imagery for crop mapping. *Frontiers in earth science* 5(17):1-10.

Shuttleworth WJ 2007. Putting the 'vap' into evapotranspiration. *Hydrology and earth system sciences* 11:210-244.

Sosibo N Z, Muchaonyerwa P, Visser L, Barnard A, Dube E & Tsilo TJ 2016. Soil fertility constraints and yield gaps of irrigation wheat in South Africa. *South African journal of science.*113 (1/2):1-9.

South African Grain laboratory 2020. Wheat Report 2015.2016 season. Available online at https://sagl.co.za/wp-content/uploads/Reports/Wheat/2015.2016/PAGE-4.pdf [Accessed on 29 Sept 2020].

Spiliotopoulos M, Holden NM & Loukas A 2017. Mapping evapotranspiration coefficients in a Temperate Maritime Climate using the METRIC Model and Landsat TM. *Water* 9 (23):1-15.

Stanhill G, Worthington E B & Angus D E 1986. Irrigation in arid lands. *Philosophical transactions of the royal society of London* 316:261-273

Su Z 2002. The Surface Energy Balance Systems (SEBS) for estimation of turbulent heat fluxes. *Hydrology and earth systems sciences* 6 (1):85-99.

Su B & Wang L 2013. Practical session instructions. Surface energy balance systems. *University of Twente Faculty of Geo-information science and earth observation.* Available from https://earth.esa.int/documents/10174/643007/D5P1c-1_SEBS_LTC2013.pdf [Accessed 20 Aug 2019].

Tasumi M 2019. Estimating evapotranspiration using METRIC model and Landsat data for better understandings of regional hydrology in the western Urmia Lake Basin. *Agricultural water management* 226:1-11.

Tasumi M, Allen RG & Trezza R 2006. Calibrating satellite-based vegetation indices to estimate evapotranspiration and crop coefficients. *Researchgate.* Available from https://www.researchgate.net/publication/265261183_Calibrating_Satellite Based_Vegetation_Indices_to_Estimate_Evapotranspiration_and_Crop_Coefficients[Accessed 20 July 2019]

Tasumi M, Trezza R, Allen RG & Wright JL 2003. U.S. Validation tests on the SEBAL Model for evapotranspiration via satellite. International committee on irrigation and drainage (ICID) *Workshop on remote sensing of ET for large regions.* Available from https://pdfs.semanticscholar.org/86f2/8c435ad67929a2ac0b3dd135fdc7cdbd090b.pdf [Accessed 15 Nov 2018].

Tilman D, Cassman KG, Matson P , Naylor R & Polasky S 2002. Agricultural sustainability and intensive production practices. *Nature* 418:671-677.

Thierfelder CT & Wall PC 2009. Effects of conservation agriculture techniques on infiltration and soil water content in Zambia and Zimbabwe. *Soil and tillage research* 105 (2):217-227.

Toth C & Józ´ków G 2016. Remote sensing platforms and sensors: A survey. *ISPRS Journal of photogrammetry and remote sensing* 115:22–36.

Tucker CJ 1979. Red and photographic infrared linear combinations for monitoring vegetation. *Remote sensing of the environment* 8:127-150.

Otto FEL, Wolski P, Lehner F, Tebaldi C, van Oldenborgh GJ, Hogesteeger S, Singh R, Holden P, Fučkar NS, Odoulami RC & New M 2018. Anthropogenic influence on the drivers of the Western Cape drought 2015–2017. *Environmental resources letters* 13 (124010):1-10.

USDA 2018. Sub-Saharan Africa drives growth in Global wheat imports. *Grain: World markets and trade.* Available from https://www.tralac.org/images/docs/12936/grain-world-markets-and-trade-usda-april-2018.pdf [Accessed 1 May 2018].

Van Heerden P S, Crosby C T & Crosby C P 2001. Using SAPWAT to estimate water requirements of crops in selected irrigation managed by Orange-Vaal and Orange - Riet water user associations. *Water Research Commission.* Report No: TT 163/01

Van Ittersum KM, Cassman G, Grassini P, Wolf J, Tittonell P & Hochman Z 2013. Yield gap analysis with local to global relevance. *Field crops research* 143:4-17.

Van Niekerk A, Jarmain C, Goudriaan R, Muller SJ, Ferreira F, Münch Z, Pauw T, Stephenson G & Gibson L 2018. *An earth observation approach towards mapping irrigated areas and quantifying water use by irrigated crops in South Africa.* Report WRC and DAFF Republic of SA. Available from https://www.researchgate.net/publication/326128157 [Accessed 20 Oct 2019].

Van Niekerk A, Stephenson G, Muller J & Pauw T 2019. Earth observation for monitoring salt accumulation and water logging. *PositionIT*. Available from https://www.ee.co.za/article/earth-observation-for-monitoring-salt-accumulation-and-waterlogging.html [Accessed 20 Oct 2019].

van Wart J, Kersebaum C, Peng S, Milner M, Kenneth G, Cassman KG & Lobell DB 2013. The use of satellite data for crop yield gap analysis. *Field crops research* 143:56-64.

Venturini V, Rodriguez L & Bisht G 2011. A comparison among different modified Priestley and Taylor equations to calculate actual evapotranspiration with MODIS data. *International journal of remote sensing* 32 (5):1319-1338.

Vicente-Serrano SM, Lanjeri S & Lopez-Moreno JI 2007. Comparison of different procedures to map reference evapotranspiration using geographical information systems and regression-based techniques. *International journal of climatology* 27:1103-1118.

Vink N & Tregurtha N 2005. Western Cape Agricultural Sector; Structure, Performance and Future Prospects, An overview. Department of agricultural economics Stellenbosch University. Available from https://www.westerncape.gov.za/other/2005/10/ agri_final_first_paper_overview.pdf [Accessed 4 Jan 2020].

Vogeler JC & Cohen WB 2016. A review of the role of active remote sensing and data fusion for characterizing forest in wildlife habitat models. REVISTA DE TELEDETECCIÓN *Spanish association of remote sensing* 45:1-14.

Walhan EF 1939. Use of tensiometers for soil moisture measurement in ecological research. *Ecological society of America* 20 (3):403- 412.

Walter A, Finger R, Huberb R & Buchmann N 2017. Smart farming is key to develop in sustainable agriculture. *Proceedings of the national academy of sciences of the USA* 14:6148-6150.

Walker WR 1989. Guidelines for designing and evaluating surface irrigation systems. FAO 45 Irrigation and Drainage Paper. Rome, 1989. Available from http://www.fao.org/3/t0231e/t0231e00.htm [Accessed 20 Oct 2020].

Ward W A, Deren B J & D'Silva H E 1991. The Economics of project analysis. A practionner's guide. Available from https://books.google.co.za/books?id=QxretNCgto0C&pg=PA296 &lpg=PA296&dq=Economic+Appraisal++by+Ward+JD&source=bl&ots=dS2wxmoy0Z&sig =ACfU3U1VD3NP_4wsxFLoG_K00e8pjCkUIA&hl=en&sa=X&ved=2ahUKEwjly5KZqcD nAhXqzoUKHUAlAzUQ6AEwFHoEC [Accessed 20 Oct 2019].

WaterWheel 2008. Berg river dam: Designed with rivers in mind. Available from http://www.wrc.org.za/wp-content/uploads/mdocs/ [Accessed 2 Jan 2020].

Water R, Allen R, Tasumi M, Trezza R & Bastiaanssen W 2002. SEBAL Surface energy balance algorithm for land Idaho Implementation. Advanced Training and User Manuals. Available from http://www.posmet.ufv.br/wp-content/uploads/ [Accessed 15 Jan 2020].

Wang K & Dickinson RF 2012. A review of global terrestrial evapotranspiration: Observation, modelling climatology and climatic variability. *Reviews of geophysics* 50:1-54.

Wensley A 2013. Strategic Overview of the water sector in South Africa. Department of water affairs and forestry. Available from https://nepadwatercoe.org/wp-content/uploads/Strategic-Overview-of-the-Water-Sector-in-South-Africa-2013.pdf [Accessed 15 Oct 2019].

Westerhof RS 2018. Using uncertainty of Penman and Penman-Monteith methods in combined satellite and ground-based evapotranspiration estimates. *Remote sensing of environment* 169: 102-112.

Wiegand CL, Richardson AJ, Escobar DE & Gerbermann AH 1991. Vegetation indices in crop assessments. *Remote Sensing of Environment* 35(2-3):105-119.

Wright D 2010. The current space debris situation. Global security program. Union of concerned scientists. Conference paper presented at 2010 Beijing orbital debris mitigation workshop. Available from https://swfound.org/media/99971/wright-space-debris_situation.pdf [Accessed 12 Jan 2020].

Yang R, Rossiter DG, Liu F, Lu Y, Yang F, Yang F, Zhao Y, Li D & Zhang G 2015. Predictive mapping of topsoil organic carbon in an alpine environment aided by Landsat TM. *PLoS One* 10 (0139042):1-20.

Youker R 1989. Managing the project cycle for time, cost and quality: lessons from World Bank experience. *The World Bank*. Available from https://www.pm4dev.com/resources/documents-and-articles/105-managing-the-project-cycle-robert-youker/file.html [Accessed on 04 Jan 2020].

Zaussinger F, Dorigo W, Gruber A, Tarpanelli A, Filippucci P & Brocca L 2019. Estimating irrigation water use over the contiguous United States by combining satellite and reanalysis soil moisture data. *Hydrology and earth systems sciences* 23:897-923.

Zeiske K 2004. Surveying made easy. Leica Geosystems. Available from https://www.aps.anl.gov/files/APS-Uploads/DET/Detector-Pool/Beamline-Components/Lecia_Optical_Level/Surveying_en.pdf [Accessed 10 Oct 2019].

Zhu L, Suomalainen J, Liu J, Hyyppä J, Kaartinen H & Haggren H 2018. A review: remote sensing sensors. Multi-purpose application of geospatial data. Available from http://dx.doi.org/10.5772/intechopen.71049 [Accessed 15 Feb 2020]

Zotarelli L, Dukes M D, Romero CC, Migliaccio K W & Morgan K T 2010. Step by Step calculation of the Penman-Monteith evapotranspiration *Food Agriculture Organisation 56*. Available from https://edis.ifas.ufl.edu/pdffiles/AE/AE45900.pdf [Accessed on 4 Feb 2020].

Zwart SJ & Bastiaanssen WGM 2004. Review of measured crop water productivity values for irrigated wheat, rice, cotton and maize. *Agricultural water management* 69:115-133.

Zwart SJ & Leclert LMC 2009. A remote sensing-based irrigation performance assessment: a case study of the Office du Niger in Mali. *Irrigation science* 28:371-385.

APPENDICES

APPENDIX A. **SCRIPTS**

Script A.1.1 $ET_{0\,HS}$ computation based on climate station data

```python
import os
import pandas as pd
dataroot = ("U:/PyETo-master")
os.chdir(dataroot)
import datetime, pyeto
xl = pd.ExcelFile("U:/pratizing_Pyeto/STUDY_CLIMATIC_DATA.xlsx")
current_sheet ="KOPERFONTEIN"
df =xl.parse(current_sheet)
current_altitude = 61
lat= pyeto.deg2rad(-33.1)
day_of_year =[]
for i in range (0, len(df[Tx])):
    dummy = datetime.date(df["Year"][i],df["Month"][i], df['Day']['i'].timetuple().tm_yday)
    day_of_year.append(dummy)
#print(day_of_year)
sol_dec = []  #solar declination angle
for i in range (0, len(df["Tx"])):
    dummy = pyteo.sol_dec(day_of_year[i])
    sol_dec.append(dummy)
#print(sol_dec)
sha = []
for i in range (0, len(df['Tx'])):
    dummy =pyeto.sunset_hour_angle(lat,sol_dec[i])
    sha.append(dummy)
#print
ird = []
for i in range(0,len(df["Tx"])):
    dummy = pyeto.inv_rel_dist_earth_sun(day_of_year[i])
    ird.append(dummy)
et_rad = []
for i in range(0, len(df['Tx'])):
    dummy=pyteo.et_rad(lat,sol_dec[i],sha[i],ird[i])
    et_rad.append(dummy)
ET0_HS = []
for i in range(0, len(df["Tx"])):
    dummy =pyeto.hargreaves(df["Tn"][i],df['Tx'][i],(df['Tn'][i]+df['Tx'][i])/2,et_rad[i])
    ET0_HS.append(dummy)
import numpy as np
current_sheet= pd.DataFrame(np.column_stack([sol_dec,sha,ird,et_rad,ET0_HS]),index=
day_of_year,columns =["Solar declination angle",
"Sunset_HourA","IRD_EarthSun","Extra_TerRadiation","RefET_HS"])
XLL = current_sheet.T
writer = pd.ExcelWriter("/Hargreaves_Samani_ET0/KOPERFONTEIN.xlsx")
writer.to_excel(writer, sheet_name = "KOPERFONTEIN_HS_REFet")
writer.save()
```

Script A.1.2 $ET_{0\,HS}$ database indexed by Julian day

```python
# Script develops the ET0HS csv data frame indexed by JD
import os
import pandas as pd
import numpy as np
import csv
import datetime
xl = pd.ExcelFile("/Hargreaves_Samani_ETo/HS_REFETO.xlsx")
current_sheet = "ALL_STATIONS"
df = xl.parse(current_sheet)
#print(day_of_year)
#print(day_of_year)
ABENDRUHE       = np.array(df["ABENDRUHE"])
ASHANTI         = np.array(df["ASHANTI"])
BELLEVUE        = np.array(df["BELLEVUE"])
BOKVELDSKLOOF   = np.array(df["BOKVELDSKLOOF"])
DE_POORT        = np.array(df["DE_POORT"])
FAIRVIEW        = np.array(df["FAIRVIEW"])
HLS_BOLAND      = np.array(df["HLS_BOLAND"])
Ideal_pool_Hill = np.array(df["Ideal_pool_Hill"])
KOPERFONTEIN    = np.array(df["KOPERFONTEIN"])
LANDAU          = np.array(df["LANDAU"])
LANGGEWENS      = np.array(df["LANGGEWENS"])
MOORREESBURG    = np.array(df["MOORREESBURG"])
```

```
NEDERBURG      = np.array(df["NEDERBURG"])
PORTERVILLE    = np.array(df["PORTERVILLE"])
Riviera        = np.array(df["Riviera"])
SCHAAPKRAAL    = np.array(df["SCHAAPKRAAL"])
ZUURVLAKTE     = np.array(df["ZUURVLAKTE"])
day_of_year
current_sheet = pd.DataFrame(np.column_stack([ABENDRUHE,ASHANTI,BELLEVUE,BOKVELDSKLOOF,DE_POORT,
FAIRVIEW,HLS_BOLAND,Ideal_pool_Hill,KOPERFONTEIN,LANDAU,LANGGEWENS,MOORREESBURG,NEDERBURG,PORTERV
ILLE,Riviera,SCHAAPKRAAL,ZUURVLAKTE ]),index = day_of_year, columns = [
"Abendruhe","Ashanti","Bellevue","Bokveldskloof", "De poort","Fairview","Hls
Boland","Ideal_pool_Hill","Koperfontein","Landau","Langgwens","Moorreesburg","Nederburg","Porterv
ille","Riviera","Schaapkraal","Zuurvlakte"])
#print(current_sheet)
XLL = current_sheet.T
#print(XLL)
#XLL.drop([0,0])
#print(XLL)
writer =pd.ExcelWriter("/Hargreaves_Samani_ETo/HS_ETO_current.xlsx")
XLL.to_excel(writer, sheet_name = "sheet_1")
writer.save()
#save the file as  comma seperated values
XLL.to_csv("/Hargreaves_Samani_ETo/CSV/HS_ETO_All.csv")
```

Script A.1.3 Interpolation ET$_{0HS}$ at 10 m resolution

```
#The script uses the spline with tension interpolation scheme in ArcMap to compute the daily
distributed ET0HS surfaces
import arcpy
import numpy as numpy
from arcpy import env
from arcpy.sa import *
env.workspace   = "/Hargreaves_Samani_ETo/CSV"
fieldlist = arcpy.ListFields("HS_ALL_STATIONS.shp")
fields = fieldlist[7:]
inPointFeatures   =  "HS_ALL_STATIONS.shp"
cellSize = 10
power = 2
searchRadius = 1000
env.overwriteOutput = True
day_of_year = 0
for i  in  fields:
   day_of_year += 1
   #print day_of_year
   outSpline = Spline(inPointFeatures,i.name, cellSize,"TENSION",4)
 outSpline.save("/Hargreaves_Samani_ETo/HS_10_Year2016_ETo/{0}".format(day_of_year))
```

Script A.1.4 Interpolation ET$_{0HS}$ at 30 m resolution

```
#The script uses the spline with tension interpolation scheme in ArcMap to compute the daily
distributed ET0HS surfaces at 30 m SR
Script
import arcpy
import numpy as numpy
from arcpy import env
from arcpy.sa import *
env.workspace   = "/Hargreaves_Samani_ETo/CSV"
fieldlist = arcpy.ListFields ("HS_ALL_STATIONS.shp")
fields = fieldlist [7:]
InPointFeatures   =  "HS_ALL_STATIONS.shp"
cellSize = 30
power = 2
searchRadius = 1000
env.overwriteOutput = True
day_of_year = 0
for i  in  fields:
   day_of_year += 1
   #print day_of_year
   outSpline = Spline (inPointFeatures,i.name, cellSize,"TENSION", 4)
outSpline.save("/Hargreaves_Samani_ETo/HS_30_Year2016_ETo/{0}".format(day_of_year))
```

Script A.2.1 ET_{0PM} into Excel csv file database

```
#Script develops the climate station ET0PM Excel csv data frame indexed by JD.
import os
import pandas as pd
import numpy as np
import csv
import datetime
xl = pd.ExcelFile("/PM_ET0/PM_ETO.xlsx")
current_sheet = "Sheet1"
df = xl.parse(current_sheet)
#print(df.head())
#date string format for the days in year for easy of identifying the day of year when matching
Kc maps to reference ETo
ymd = []
for i in range (0,len(df["YEAR"])):
    dummy = datetime.date(df["YEAR"][i],df["MONTH"][i],df["DAY"][i]).isoformat()
    ymd.append(dummy)
#print(ymd)
day_of_year = []
for i in range(0,len(df["YEAR"])):
    dummy = datetime.date(df['YEAR'][i],df['MONTH'][i],df['DAY'][i]).timetuple().tm_yday
    day_of_year.append (dummy)

#print(day_of_year)
#print(day_of_year)
ABENDRUHE       = np.array(df["ABENDRUHE"])
ASHANTI         = np.array(df["ASHANTI"])
BELLEVUE        = np.array(df["BELLEVUE"])
BOKVELDSKLOOF   = np.array(df["BOKVELDSKLOOF"])
DE_POORT        = np.array(df["DE_POORT"])
FAIRVIEW        = np.array(df["FAIRVIEW"])
HLS_BOLAND      = np.array(df["HLS_BOLAND"])
Ideal_pool_Hill = np.array(df["Ideal_pool_Hill"])
KOPERFONTEIN    = np.array(df["KOPERFONTEIN"])
LANDAU          = np.array(df["LANDAU"])
LANGGEWENS      = np.array(df["LANGGEWENS"])
MOORREESBURG    = np.array(df["MOORREESBURG"])
NEDERBURG       = np.array(df["NEDERBURG"])
PORTERVILLE     = np.array(df["PORTERVILLE"])
Riviera         = np.array(df["Riviera"])
SCHAAPKRAAL     = np.array(df["SCHAAPKRAAL"])
ZUURVLAKTE      = np.array(df["ZUURVLAKTE"])
day_of_year
current_sheet = pd.DataFrame(np.column_stack([ABENDRUHE,ASHANTI,BELLEVUE,BOKVELDSKLOOF,DE_POORT,
FAIRVIEW,HLS_BOLAND,Ideal_pool_Hill,KOPERFONTEIN,LANDAU,LANGGEWENS,MOORREESBURG,NEDERBURG,PORTERV
ILLE,Riviera,SCHAAPKRAAL,ZUURVLAKTE ]),index = day_of_year
,columns = [ "Abendruhe","Ashanti","Bellevue","Bokveldskloof", "De poort","Fairview","Hls
Boland","Ideal_pool_Hill","Koperfontein","Landau","Langgwens","Moorreesburg","Nederburg","Porterv
ille","Riviera","Schaapkraal","Zuurvlakte"])
print(current_sheet)
XLL = current_sheet.T
#print(XLL)
#XLL.drop([0,0])
print(XLL)
writer =pd.ExcelWriter("/PM_ET0/TranS_PM_ET0_ALL.xlsx")
XLL.to_excel(writer, sheet_name = "sheet_1")
writer.save()
#save the file as  comma seperated values
XLL.to_csv("/PM_ET0/CSV/PM_ET0_All.csv")
# reading a comma seperated file syntax
# by default it only reads  the first five columns
```

Script A.2.2 Interpolation ET_{0PM} at 10 m spatial resolution

```
# Script computes the distributed study area ET0PM surfaces at 10m SR
import arcpy
import numpy as numpy
from arcpy import env
from arcpy.sa import *
env.workspace   = "/PM_ET0/CSV"
fieldlist = arcpy.ListFields("PM_ALL_ET0.shp")
fields = fieldlist[7:]
inPointFeatures   =  "PM_ALL_ET0.shp"
cellSize = 10
power = 2
searchRadius = 1000
env.overwriteOutput = True
```

```
day_of_year = 0
for i  in  fields:
    day_of_year += 1
    #print day_of_year
    outSpline = Spline(inPointFeatures,i.name, cellSize,"TENSION",4)
outSpline.save("/PM_ET0/2016_PM_10_img/{0}.img".format(day_of_year))
```

Script A.2.3 Interpolation ET$_{0PM}$ at 30 m spatial resolution

```
# Script computes the distributed study area ET0PM surfaces at 10m SR
import arcpy
import numpy as numpy
from arcpy import env
from arcpy.sa import *
env.workspace   = "/PM_ET0/CSV"
fieldlist = arcpy.ListFields("PM_ALL_ET0.shp")
fields = fieldlist[7:]
inPointFeatures   =  "PM_ALL_ET0.shp"
cellSize = 10
power = 2
searchRadius = 1000
env.overwriteOutput = True
day_of_year = 0
for i  in  fields:
    day_of_year += 1
    #print day_of_year
    outSpline = Spline(inPointFeatures,i.name, cellSize,"TENSION",4)
    outSpline.save("/PM_ET0/2016_PM_10_img/{0}.img".format(day_of_year))
```

Script A.2.4 Computing ET$_{cPM}$ at 10 m spatial resolution

```
#Scripts computes seasonal ETcPM10
import arcpy, math
from arcpy import env
from arcpy.sa import *
ws1 = r"X:\Users\Postgrad\Joseph\MSC_data_sets\PM_ET0\2016_PM_10_img"
arcpy.env.workspace = ws1
arcpy.env.scratchWorkspace = ("X:/Users/Postgrad/Joseph/S2.gdb")
arcpy.env.overwriteOutput = True
dummy = 0
kc74  = ("X:/Users/Postgrad/Joseph/Sentinel_Re_Copy/S2_cl_nkc_0/s2ckc_0_7_4")
kc264 = ("X:/Users/Postgrad/Joseph/Sentinel_Re_Copy/S2_cl_nkc_0/s2ckc_0_26_4")
kc175 = ("X:/Users/Postgrad/Joseph/Sentinel_Re_Copy/S2_cl_nkc_0/kc_0_17_5")
kc66  = ("X:/Users/Postgrad/Joseph/Sentinel_Re_Copy/S2_cl_nkc_0/s2ckc_0_6_6")
kc267 = ("X:/Users/Postgrad/Joseph/Sentinel_Re_Copy/S2_cl_nkc_0/s2ckc_0_26_7")
kc58  = ("X:/Users/Postgrad/Joseph/Sentinel_Re_Copy/S2_cl_nkc_0/s2ckc_0_5_8")
kc268 = ("X:/Users/Postgrad/Joseph/Sentinel_Re_Copy/S2_cl_nkc_0/s2ckc_0_26_8")
kc239 = ("X:/Users/Postgrad/Joseph/Sentinel_Re_Copy/S2_cl_nkc_0/s2ckc_0_23_9")
kc2310 = ("X:/Users/Postgrad/Joseph/Sentinel_Re_Copy/S2_cl_nkc_0/s2ckc_0_23_10")
kc139 = ("X:/Users/Postgrad/Joseph/Sentinel_Re_Copy/S2_cl_nkc_0/s2ckc_0_13_9")


dummy  += Raster(kc74)*(Raster("89.img")+Raster("90.img")+ Raster("91.img") +
Raster("92.img")+Raster("93.img")+Raster("94.img")+Raster("95.img")+Raster("96.img")
+Raster("97.img")+Raster("98.img")+ Raster("99.img")+ Raster("100.img")+Raster("101.img") +
Raster("102.img") + Raster("103.img")+ Raster("104.img")+Raster("105.img")
+Raster("106.img")+Raster("107.img"))
dummy  += Raster(kc264)*(Raster("108.img")+Raster("109.img")+Raster("110.img")+ Raster("111.img")
+ Raster("112.img")+ Raster("113.img")+ Raster("114.img")+ Raster("115.img")
+Raster("116.img")+Raster("117.img")+Raster("118.img")+Raster("119.img")+Raster("120.img")+Raster
("121.img")+Raster("122.img")+Raster("123.img")+Raster("124.img")
+Raster("125.img")+Raster("126.img") +Raster("127.img")+Raster("128.img"))
dummy  +=
Raster(kc175)*(Raster("129.img")+Raster("130.img")+Raster("131.img")+Raster("139.img")+Raster("14
0.img")+Raster("141.img")+Raster("142.img")+Raster("143.img")
+Raster("144.img")+Raster("145.img")+Raster("146.img")+Raster("147.img")+Raster("148.img")+Raster
("149.img"))
dummy  +=
Raster(kc66)*(Raster("150.img")+Raster("151.img")+Raster("152.img")+Raster("153.img")+Raster("154
.img")+Raster("155.img")+Raster("156.img")+Raster("157.img")
+Raster("158.img")+Raster("159.img")+Raster("160.img")+Raster("161.img")+Raster("162.img")+Raster
("163.img")+Raster("164.img")+Raster("165.img")+Raster("166.img")+Raster("167.img")+Raster("168.i
mg"))
```

```
dummy  +=
Raster(kc267)*(Raster("169.img")+Raster("170.img")+Raster("171.img")+Raster("172.img")+Raster("17
3.img")+Raster("174.img")+Raster("175.img")+Raster("176.img")
+Raster("177.img")+Raster("178.img")+Raster("179.img")+Raster("180.img")+Raster("181.img")+Raster
("182.img")+Raster("183.img")+Raster("184.img")+Raster("185.img")+Raster("186.img")
+Raster("187.img")+Raster("189.img")+Raster("190.img")+Raster("191.img")+Raster("192.img")+Raster
("193.img")+Raster("194.img")+Raster("195.img")+Raster("196.img")
+Raster("197.img")+Raster("198.img")+Raster("199.img")+Raster("200.img")+Raster("201.img")+Raster
("202.img")+Raster("203.img")+Raster("204.img")+Raster("205.img")+Raster("206.img")
+Raster("207.img")+Raster("208.img")+Raster("209.img")+Raster("210.img")+Raster("211.img")+Raster
("212.img"))
dummy  +=
Raster(kc58)*(Raster("213.img")+Raster("214.img")+Raster("215.img")+Raster("216.img")+Raster("217
.img")+Raster("218.img")+Raster("219.img")+Raster("220.img")+Raster("221.img")
+Raster("222.img")+Raster("223.img")+Raster("224.img")+Raster("225.img")+Raster("226.img")+Raster
("227.img"))
dummy  +=
Raster(kc268)*(Raster("228.img")+Raster("229.img")+Raster("230.img")+Raster("231.img")+Raster("23
2.img")+Raster("233.img")+Raster("234.img")+Raster("235.img")+Raster("236.img")
+Raster("237.img")+Raster("238.img")+Raster("239.img")+Raster("240.img")+Raster("241.img")+Raster
("242.img")+Raster("243.img")+Raster("244.img")+Raster("245.img")+Raster("246.img")+Raster("247.i
mg"))
dummy  +=
Raster(kc239)*(Raster("262.img")+Raster("263.img")+Raster("264.img")+Raster("265.img")+Raster("26
6.img")+Raster("267.img")+Raster("268.img")+Raster("269.img")+Raster("270.img")
+Raster("271.img")+Raster("272.img")+Raster("273.img")+Raster("274.img")+Raster("275.img")+Raster
("276.img")+Raster("277.img")+Raster("278.img")+Raster("279.img")+Raster("280.img")
+Raster("281.img")+Raster("282.img"))
dummy  +=
Raster(kc2310)*(Raster("283.img")+Raster("284.img")+Raster("285.img")+Raster("286.img")+Raster("2
87.img")+Raster("288.img")+Raster("289.img")+Raster("290.img")
+Raster("291.img")+Raster("292.img")+Raster("293.img")+Raster("294.img")+Raster("295.img")+Raster
("296.img")+Raster("297.img")+Raster("298.img")+Raster("299.img")+Raster("300.img"))
dummy  +=
Raster(kc139)*(Raster("248.img")+Raster("249.img")+Raster("250.img")+Raster("251.img")+Raster("25
2.img")+Raster("253.img")+Raster("254.img")+Raster("255.img")
+Raster("256.img")+Raster("257.img")+Raster("258.img")+Raster("259.img")+Raster("260.img")+Raster
("261.img"))
# save the  computation as PM_10_S2_nETc
# PM = Penman Monteinth
# 10 = 10 m spatial resolution
# S2 = Sentinal 2 based  crop  factor
# n  = crop factor derived from S2 image and the normalised difference vegetation indice

dummy.save("/PM_ET0/ETc_PM10M_S2/PM10S2n0ETc")
```

Script A.2.4.1 Kc Landsat8 NDVI based

```
###Script computes Kc from Landsat8 NDVI and WDRVI please ignore the WDRVI computation
import arcpy
from arcpy import env
from arcpy.sa import *
env.overwriteOutput  = True
ndvi = Raster("/Landsat8data/Processed_Landsat8_/2016_04_30/APAR_WDRVI_Kc_L8/ndvi_30_4")
wdrvi = Raster("/Landsat8data/Processed_Landsat8_/2016_04_30/APAR_WDRVI_Kc_L8/15wdrvi_30_04")
kc_ndvi = 1.46*(ndvi)-0.26
kc_wdrvi = 1.46*(wdrvi)-0.26
kc_ndvi.save("/Landsat8data/Processed_Landsat8/kc_ndvi_f/30_04.img")
kc_wdrvi.save("/Landsat8data/Processed_Landsat8_/kc_wdrvi_f/30_04.img")
ndvi = Raster
("X:/Users/Postgra/Joseph/MSC_data_sets/Landsat8data/Processed_Landsat8_/2016_05_16/APAR_WDRVI_Kc
_L8/ndvi_16_5")
wdrvi =
Raster("X:\Users\Postgrad\Joseph\MSC_data_sets\Landsat8data\Processed_Landsat8_\2016_05_16\APAR_W
DRVI_Kc_L8/15wdrvi_16_5")
kc_ndvi = 1.46*(ndvi)-0.26
kc_wdrvi = 1.46*(wdrvi)-0.26
kc_ndvi.save("/Landsat8data/Processed_Landsat8/kc_ndvi_f/16_05.img")
kc_wdrvi.save("/Landsat8data/Processed_Landsat8_/kc_wdrvi_f/16_05.img")
ndvi  = Raster("/Landsat8data/Processed_Landsat8_/2016_06_01/APAR_WDRVI_Kc_L8/ndvi_1_6")
wdrvi  = Raster("/Landsat8data/Processed_Landsat8_/2016_06_01/APAR_WDRVI_Kc_L8/15wdrvi_1_6")
kc_ndvi = 1.46*(ndvi)- 0.26
kc_wdrvi = 1.46*(wdrvi)- 0.26
kc_ndvi.save("/Landsat8data/Processed_Landsat8/kc_ndvi_f/01_06.img")
kc_wdrvi.save("/Landsat8data/Processed_Landsat8_/kc_wdrvi_f/01_06.img")
ndvi  = Raster("/Landsat8data/Processed_Landsat8_/2016_07_03/APAR_WDRVI_Kc_L8/ndvi_3_7")
```

```
wdrvi =  Raster("/Landsat8data/Processed_Landsat8_/2016_07_03/APAR_WDRVI_Kc_L8/15wdrvi_3_7")
kc_ndvi = 1.46*(ndvi)- 0.26
kc_wdrvi = 1.46*(wdrvi)- 0.26
kc_ndvi.save("/Landsat8data/Processed_Landsat8/kc_ndvi_f/03_07.img")
kc_wdrvi.save("/Landsat8data/Processed_Landsat8_/kc_wdrvi_f/03_07.img")
ndvi = Raster ("/Landsat8data/Processed_Landsat8_/2016_08_04/APAR_WDRVI_Kc_L8/ndvi_04_08")
wdrvi = Raster ("/Landsat8data/Processed_Landsat8_/2016_08_04/APAR_WDRVI_Kc_L8/15wdrvi_04_08")
kc_ndvi = 1.46*(ndvi)- 0.26
kc_wdrvi = 1.46*(wdrvi)- 0.26
kc_ndvi.save("/Landsat8data/Processed_Landsat8/kc_ndvi_f/04_08.img")
kc_wdrvi.save("/Landsat8data/Processed_Landsat8_/kc_wdrvi_f/04_08.img")
ndvi = Raster("/Landsat8data/Processed_Landsat8_/2016_09_21/APAR_WDRVI_Kc_L8/ndvi_21_9")
wdrvi = Raster
("X/Users/Postgrad/Joseph/MSC_data_sets/Landsat8data/Processed_Landsat8_/2016_09_21/APAR_WDRVI_Kc
_L8/15wdrvi_21_9")
kc_ndvi = 1.46*(ndvi)- 0.26
kc_wdrvi = 1.46*(wdrvi)- 0.26
kc_ndvi.save("/Landsat8data/Processed_Landsat8/kc_ndvi_f/21_09.img")
kc_wdrvi.save("/Landsat8data/Processed_Landsat8_/kc_wdrvi_f/21_09.img")
ndvi = Raster("/Landsat8data/Processed_Landsat8_/2016_10_23/APAR_WDRVI_Kc_L8/ndvi_23_10")
wdrvi = Raster("/Landsat8data/Processed_Landsat8_/2016_10_23/APAR_WDRVI_Kc_L8/15wdrvi_23_10")
kc_ndvi = 1.46*(ndvi)- 0.26
kc_wdrvi = 1.46*(wdrvi)- 0.26
kc_ndvi.save("/Landsat8data/Processed_Landsat8/kc_ndvi_f/23_10.img")
kc_wdrvi.save("/Landsat8data/Processed_Landsat8_/kc_wdrvi_f/23_10.img")
```

Script A.2.4.2 Kc Sentinel2 NDVI based

```
#Script compute the Crop coefficient from ndvi
import arcpy
from arcpy import env
from arcpy.sa import *
"ndvi_07_04" = ("X:/Users/Postgrad/Joseph/Sentinel_Re-Copy/S2A_R121_20160407T220359_dd/VI/ndvi")
"ndvi_26_04" = ("X:/Users/Postgrad/Joseph/Sentinel_Re-
Copy/S2A_R121_20160426T180046_dd/VI/ndvi_26_04")
"ndvi_17_05" = ("X:/Users/Postgrad/Joseph/Sentinel_Re-
Copy/S2A_R121_20160517T024617_dd/VI/ndvi_17_5")
"ndvi_06_06" = ("X:/Users/Postgrad/Joseph/Sentinel_Re-
Copy/S2A_R121_20160606T231257_dd/VI/ndvi_6_6")
"ndvi_26_07" = ("X:/Users/Postgrad/Joseph/Sentinel_Re-
Copy/S2A_R121_20160726T114955_dd/VI/ndvi_26_7")
"ndvi_05_08" = ("X:/Users/Postgrad/Joseph/Sentinel_Re-
Copy/S2A_R121_20160805T224516_dd/05_08_2016/VI/ndvi_516")
"ndvi_26_08" = ("X:/Users/Postgrad/Joseph/Sentinel_Re-
Copy/S2A_R121_20160826T114421_dd/26_08_2016/VI/ndvi_10300006")
"ndvi_13_09" = ("X:/Users/Postgrad/Joseph/Sentinel_Re-
Copy/S2A_R121_20160913accept/13_09_2016_2/VI/ndvi_WDRVI/ndvi")
"ndvi_23_09" = ("X:/Users/Postgrad/Joseph/Sentinel_Re-
Copy/S2A_R121_20160923T164311_dd/ATCOR_23_09_2016/ndvi")
"ndvi_23_10" = ("X:/Users/Postgrad/Joseph/Sentinel_Re-
Copy/S2A_R121_20161023T223528/Oct_23_2016_1/New Folder/ndvi2")
"ndvi_03_10" = ("X:/Users/Postgrad/Joseph/Sentinel_Re-
Copy/S2A_R121_20161003T172326_ddp/ATCOR_03_10_2016/ndvi_3_10")

fields =
["ndvi_03_10","ndvi_23_10","ndvi_23_09","ndvi_13_09","ndvi_26_08","ndvi_05_08","ndvi_26_07","ndvi
_06_06","ndvi_17_05","ndvi_26_04","ndvi_07_04"]
env.workspace   = "X:/Users/Postgrad/Joseph/Sentinel_Re-Copy/Senti_ndvi_kc"
for field in fields:
    ndvi = 1.46*(Raster(field))- 0.26
    outname = "X:/Users/Postgrad/Joseph/Sentinel_Re-Copy/Senti_ndvi_kc/{0}.img".format(field)
    env.overwriteOutput  = True
    ndvi.save(outname)
```

Script A.2.5 Computing ET$_{cPM30}$ at 30 m spatial resolution

```
#script computes ET_CPM30SR
import arcpy, math
from arcpy import env
from arcpy.sa import *
ws1 = r"X:\Users\Postgrad\Joseph\MSC_data_sets\PM_ET0\2016_PM_30_1img"
arcpy.env.workspace = ws1
arcpy.env.scratchWorkspace = ("X:/Users/Postgrad/Joseph/SS2.gdb")
```

```
arcpy.env.overwriteOutput = True
dummy = 0
##############################################################################
##########
# landsat 8 based Kc using NDVI  at 30 resulotion
##############################################################################
#############
kcl8304  = ("/Landsat8data/L8_cl_nkc_0/l8ckc_0_30_4")
kcl816   = ("/Landsat8data/L8_cl_nkc_0/l8ckc_0_01_6")
kcl837   = ("/Landsat8data/L8_cl_nkc_0/l8ckc_0_3_7")
kcl848   = ("/Landsat8data/L8_cl_nkc_0/l8ckc_0_4_8")
kcl8165  = ("/Landsat8data/L8_cl_nkc_0/l8ckc_0_16_5")
kcl8219  = ("/Landsat8data/L8_cl_nkc_0/l8ckc_0_21_9")
kcl82310 = ("/Landsat8data/L8_cl_nkc_0/l8ckc_0_23_10")
dummy  += Raster(kcl8304)*(Raster("89.img")+Raster("90.img")+ Raster("91.img") +
Raster("92.img")+Raster("93.img")
+Raster("94.img")+Raster("95.img")
+Raster("96.img")+Raster("97.img")+Raster("98.img")+ Raster("99.img")+
Raster("100.img")+Raster("101.img") + Raster("102.img") + Raster("103.img")
+
Raster("104.img")+Raster("105.img")+Raster("106.img")+Raster("107.img")+Raster("108.img")+Raster(
"109.img")+Raster("110.img")+ Raster("111.img")
+ Raster("112.img")+ Raster("113.img")+ Raster("114.img")+
Raster("115.img")+Raster("116.img")+Raster("117.img")+Raster("118.img")+Raster("119.img")
+Raster("120.img")+Raster("121.img")+Raster("122.img")+Raster("123.img")+Raster("124.img")+Raster
("125.img")+Raster("126.img")+Raster("127.img")
+Raster("128.img")+Raster("129.img"))
dummy  +=
Raster(kcl8165)*(Raster("130.img")+Raster("131.img")+Raster("139.img")+Raster("140.img")+Raster("
141.img")+Raster("142.img")+Raster("143.img"
)+Raster("144.img")+Raster("145.img"))
dummy  +=
Raster(kcl816)*(Raster("146.img")+Raster("147.img")+Raster("148.img")+Raster("149.img")+Raster("1
50.img")+Raster("151.img")+Raster("152.img")
+Raster("153.img")+Raster("154.img")+Raster("155.img")+Raster("156.img")+Raster("157.img")+Raster
("158.img")+Raster("159.img")+Raster("160.img")+Raster("161.img"))
dummy  +=
Raster(kcl82310)*(Raster("290.img")+Raster("291.img")+Raster("292.img")+Raster("293.img")+Raster(
"294.img")+Raster("295.img")+Raster("296.img")
+Raster("297.img")+Raster("298.img")+Raster("299.img")+Raster("300.img"))
dummy  +=
Raster(kcl8219)*(Raster("234.img")+Raster("235.img")+Raster("236.img")+Raster("237.img")+Raster("
238.img")+Raster("239.img")+Raster("240.img")
+Raster("241.img")+Raster("242.img")+Raster("243.img")+Raster("244.img")+Raster("245.img")+Raster
("246.img")+Raster("247.img")+Raster("248.img")+Raster("249.img")
+Raster("250.img")+Raster("251.img")+Raster("252.img")+Raster("253.img")+Raster("254.img")+Raster
("255.img")+Raster("256.img")+Raster("257.img")+Raster("258.img")
+Raster("259.img")+Raster("260.img")+Raster("261.img")+Raster("262.img")+Raster("263.img")+Raster
("264.img")+Raster("265.img")+Raster("266.img")+Raster("267.img")
+Raster("268.img")+Raster("269.img")+Raster("270.img")+Raster("271.img")+Raster("272.img")+Raster
("273.img")+Raster("274.img")+Raster("275.img")+Raster("276.img")
+Raster("277.img")+Raster("278.img")+Raster("279.img")+Raster("280.img")+Raster("281.img")+Raster
("282.img")+Raster("283.img")+Raster("284.img")+Raster("285.img")
+Raster("286.img")+Raster("287.img")+Raster("288.img")+Raster("289.img"))
dummy  +=
Raster(kcl837)*(Raster("162.img")+Raster("163.img")+Raster("164.img")+Raster("165.img")+Raster("1
66.img")+Raster("167.img")+Raster("168.img")+ Raster("169.img")
+Raster("170.img")+Raster("171.img")+Raster("172.img")+Raster("173.img")+Raster("174.img")+Raster
("175.img")+Raster("176.img")+Raster("177.img")+Raster("178.img")
+Raster("179.img")+Raster("180.img")+Raster("181.img")+Raster("182.img")+Raster("183.img")+Raster
("184.img")+Raster("185.img")+Raster("186.img")+Raster("187.img")
+Raster("189.img")+Raster("190.img")+Raster("191.img")+Raster("192.img")+Raster("193.img")+Raster
("194.img")+Raster("193.img")+Raster("196.img")+Raster("197.img")
+Raster("198.img")+Raster("199.img")+Raster("200.img")+ Raster("201.img"))
dummy  +=
Raster(kcl848)*(Raster("202.img")+Raster("203.img")+Raster("204.img")+Raster("205.img")+Raster("2
06.img")+Raster("207.img")+Raster("208.img")+Raster("209.img")
+Raster("210.img")+Raster("211.img")+Raster("212.img")+Raster("213.img")+Raster("214.img")+Raster
("215.img")+Raster("216.img")+Raster("217.img")+Raster("218.img")
+Raster("219.img")+Raster("220.img")+Raster("221.img")+Raster("222.img")+Raster("223.img")+Raster
("224.img")+Raster("225.img")+Raster("226.img")+Raster("227.img")
+Raster("228.img")+Raster("229.img")+Raster("230.img")+Raster("231.img")+Raster("232.img")+Raster
("233.img"))
# save the  computation as PM_30_l8_nETc_0
# HS = Hargreaves Samani
# located in this instance at
X:\Users\Postgrad\Joseph\MSC_data_sets\Hargreaves_Samani_ETo\HS_10_Year2016_ETo
# 10 = 10 m spatial resolution
# S2 = Sentinal 2 based  crop  factor
# w = crop factor derived from S2 image and the normalised difference  vegetation indice
```

```
dummy.save("/PM_ET0/ETc_PM30M_L8/PM30L8n0ETc")
```

Script A.2.6 Computing ET$_{cHS30}$ mm

```
#Script computes ETcHS at 30 m Spatial Resolution
import arcpy, math
from arcpy import env
from arcpy.sa import *
ws1 = r"X:\Users\Postgrad\Joseph\MSC_data_sets\Hargreaves_Samani_ETo\HS_30_Year2016_ETo"
arcpy.env.workspace = ws1
arcpy.env.scratchWorkspace = ("X:/Users/Postgrad/Joseph/SS2.gdb")
arcpy.env.overwriteOutput = True
dummy = 0
###############################################################################################
###########
# Landsat 8 based Kc using NDVI at 30 resolution
###############################################################################################
#############
kcl8304 = ("X: /Users/Postgrad/Joseph/MSC_data_sets/Landsat8data/L8_cl_nkc_0/l8ckc_0_30_4")
kcl816  = ("X: /Users/Postgrad/Joseph/MSC_data_sets/Landsat8data/L8_cl_nkc_0/l8ckc_0_01_6")
kcl837  = ("X: /Users/Postgrad/Joseph/MSC_data_sets/Landsat8data/L8_cl_nkc_0/l8ckc_0_3_7")
kcl848  = ("/Landsat8data/L8_cl_nkc_0/l8ckc_0_4_8")
kcl8165 = ("/Landsat8data/L8_cl_nkc_0/l8ckc_0_16_5")
kcl8219 = ("/Landsat8data/L8_cl_nkc_0/l8ckc_0_21_9")
kcl82310 = ("/Landsat8data/L8_cl_nkc_0/l8ckc_0_23_10")
###############################################################################################
###############################################################################################
################
dummy  += Raster(kcl8304)*(Raster("89")+Raster("90")+ Raster("91") +
Raster("92")+Raster("93")+Raster("94")+Raster("95")+Raster("96")+Raster("97")+Raster("98")+
Raster("99")+ Raster("100")+Raster("101") + Raster("102") + Raster("103")+
Raster("104")+Raster("105")+Raster("106")+Raster("107")+Raster("108")+Raster("109")+Raster("110")
+ Raster("111") + Raster("112")+ Raster("113")+ Raster("114")+
Raster("115")+Raster("116")+Raster("117")+Raster("118")+Raster("119")+Raster("120")+Raster("121")
+Raster("122")+Raster("123")+Raster("124")+Raster("125")+Raster("126")
+Raster("127")+Raster("128")+Raster("129"))
dummy  +=
Raster(kcl8165)*(Raster("130")+Raster("131")+Raster("139")+Raster("140.")+Raster("141")+Raster("1
42.")+Raster("143")+Raster("144")+Raster("145"))
dummy  +=
Raster(kcl816)*(Raster("146")+Raster("147")+Raster("148")+Raster("149")+Raster("150")+Raster("151
")+Raster("152")+Raster("153")+Raster("154")+Raster("155")+Raster("156")+Raster("157")+Raster("15
8")+Raster("159")+Raster("160")+Raster("161"))
dummy  +=
Raster(kcl837)*(Raster("162")+Raster("163")+Raster("164")+Raster("165")+Raster("166")+Raster("167
")+Raster("168")+
Raster("169")+Raster("170")+Raster("171")+Raster("172")+Raster("173")+Raster("174")+Raster("175")
+Raster("176")+Raster("177")+Raster("178")+Raster("179")+Raster("180")+Raster("181")+Raster("182"
)+Raster("183")+Raster("184")+Raster("185")+Raster("186")+Raster("187")+Raster("189")+Raster("190
")+Raster("191")+Raster("192")+Raster("193")+Raster("194")+Raster("193")+Raster("196")+Raster("19
7")+Raster("198")+Raster("199")+Raster("200")+ Raster("201"))
dummy  +=
Raster(kcl848)*(Raster("202")+Raster("203")+Raster("204")+Raster("205")+Raster("206")+Raster("207
")+Raster("208")+Raster("209")+Raster("210")+Raster("211")+Raster("212")+Raster("213")+Raster("21
4")+Raster("215")+Raster("216")+Raster("217")+Raster("218")+Raster("219")+Raster("220")+Raster("2
21")+Raster("222")+Raster("223")+Raster("224")+Raster("225")+Raster("226")+Raster("227")+Raster("
228")+Raster("229")+Raster("230")+Raster("231")+Raster("232")+Raster("233"))
dummy  +=
Raster(kcl8219)*(Raster("234")+Raster("235")+Raster("236")+Raster("237")+Raster("238")+Raster("23
9")+Raster("240")+Raster("241")+Raster("242")+Raster("243")+Raster("244")+Raster("245")+Raster("2
46")+Raster("247")+Raster("248")+Raster("249")+Raster("250")+Raster("251")+Raster("252")+Raster("
253")+Raster("254")+Raster("255")+Raster("256")+Raster("257")+Raster("258")+Raster("259")+Raster(
"260")+Raster("261")+Raster("262")+Raster("263")+Raster("264")+Raster("265")+Raster("266")+Raster
("267")+Raster("268")+Raster("269")+Raster("270")+Raster("271")+Raster("272")+Raster("273")+Raste
r("274")+Raster("275")+Raster("276")+Raster("277")+Raster("278")+Raster("279")+Raster("280")+Rast
er("281")+Raster("282")+Raster("283")+Raster("284")+Raster("285")+Raster("286")+Raster("287")+Ras
ter("288")+Raster("289"))
dummy  +=
Raster(kcl82310)*(Raster("290")+Raster("291")+Raster("292")+Raster("293")+Raster("294")+Raster("2
95")+Raster("296")+Raster("297")+Raster("298.")+Raster("299")+Raster("300"))

# save the  computation as HS_30_S2_nETc
# HS = Hargreaves Samani
# located in this instance at
X:\Users\Postgrad\Joseph\MSC_data_sets\Hargreaves_Samani_ETo\HS_10_Year2016_ETo
# 30 =  30 m spatial resolution
```

```
# l8 = landsat8 based  crop  factor from ndvi
# ndvi = crop factor derived from S2 image and the normalised difference  vegetation indice

dummy.save("/Hargreaves_Samani_ETo/HSl8_ETc")
```

Script A.2.7 Computing ET_{cHS10} mm

```
#Script computes ETcHS at 10 m SR
import arcpy, math
from arcpy import env
from arcpy.sa import *
ws1 = r"X:\Users\Postgrad\Joseph\MSC_data_sets\Hargreaves_Samani_ETo\HS_10_ETc_S2_0"
arcpy.env.workspace = ws1
arcpy.env.scratchWorkspace = ("X:/Users/Postgrad/Joseph/default_gdb/testing2.gdb")
dummy = 0
kc_ndvi74  = ("X:/Users/Postgrad/Joseph/Sentinel_Re_Copy/S2_cl_nkc_0/s2ckc_0_7_4")
kc_ndvi264 = ("X:/Users/Postgrad/Joseph/Sentinel_Re_Copy/S2_cl_nkc_0/s2ckc_0_26_4")
kc_ndvi175 = ("X:/Users/Postgrad/Joseph/Sentinel_Re_Copy/S2_cl_nkc_0/s2ckc_0_17_5")
kc_ndvi66  = ("X:/Users/Postgrad/Joseph/Sentinel_Re_Copy/S2_cl_nkc_0/s2ckc_0_6_6")
kc_ndvi267 = ("X:/Users/Postgrad/Joseph/Sentinel_Re_Copy/S2_cl_nkc_0/s2ckc_0_26_7")
kc_ndvi58  = ("X:/Users/Postgrad/Joseph/Sentinel_Re_Copy/S2_cl_nkc_0/s2ckc_0_5_8")
kc_ndvi268 = ("X:/Users/Postgrad/Joseph/Sentinel_Re_Copy/S2_cl_nkc_0/s2ckc_0_26_8")
kcndvi239  = ("X:/Users/Postgrad/Joseph/Sentinel_Re_Copy/S2_cl_nkc_0/s2ckc_0_23_9")
kcndvi2310 = ("X:/Users/Postgrad/Joseph/Sentinel_Re_Copy/S2_cl_nkc_0/s2ckc_0_23_10")
kc_ndvi139 = ("X:/Users/Postgrad/Joseph/Sentinel_Re_Copy/S2_cl_nkc_0/s2ckc_0_13_9")

dummy  += Raster(kc_ndvi74)*(Raster("89")+Raster("90")+ Raster("91") +
Raster("92")+Raster("93")+Raster("94")+Raster("95")+Raster("96")+Raster("97")+Raster("98")+
Raster("99")+ Raster("100")+Raster("101") + Raster("102") + Raster("103")+
Raster("104")+Raster("105")+Raster("106")+Raster("107"))
dummy  += Raster(kc_ndvi264)*(Raster("108")+Raster("109")+Raster("110")+ Raster("111") +
Raster("112")+ Raster("113")+ Raster("114")+
Raster("115")+Raster("116")+Raster("117")+Raster("118")+Raster("119")+Raster("120")+Raster("121")
+Raster("122")+Raster("123")+Raster("124")+Raster("125")+Raster("126")
+Raster("127")+Raster("128"))
dummy  +=
Raster(kc_ndvi175)*(Raster("129")+Raster("130")+Raster("131")+Raster("139")+Raster("140.")+Raster
("141")+Raster("142.")+Raster("143")+Raster("144")+Raster("145")+Raster("146")+Raster("147")+Rast
er("148")+Raster("149"))
dummy  +=
Raster(kc_ndvi66)*(Raster("150")+Raster("151")+Raster("152")+Raster("153")+Raster("154")+Raster("
155")+Raster("156")+Raster("157")+Raster("158")+Raster("159")+Raster("160")+Raster("161")+Raster(
"162")+Raster("163")+Raster("164")+Raster("165")+Raster("166")+Raster("167")+Raster("168."))
dummy  +=
Raster(kc_ndvi267)*(Raster("169")+Raster("170")+Raster("171")+Raster("172")+Raster("173")+Raster(
"174")+Raster("175")+Raster("176")+Raster("177")+Raster("178")+Raster("179")+Raster("180")+Raster
("181")+Raster("182")+Raster("183")+Raster("184")+Raster("185")+Raster("186")+Raster("187")+Raste
r("189")+Raster("190")+Raster("191")+Raster("192")+Raster("193")+Raster("194")+Raster("193")+Rast
er("196")
+Raster("197")+Raster("198")+Raster("199")+Raster("200")+Raster("201")+Raster("20")+Raster("203")
+Raster("204")+Raster("205")+Raster("206")+Raster("207")+Raster("208")+Raster("209")+Raster("210"
)+Raster("211")+Raster("212"))
dummy  +=
Raster(kc_ndvi58)*(Raster("213")+Raster("214")+Raster("215")+Raster("216")+Raster("217")+Raster("
218")+Raster("219")+Raster("220")+Raster("221")+Raster("222")+Raster("223")+Raster("224")+Raster(
"225")+Raster("226")+Raster("227"))
dummy  +=
Raster(kc_ndvi268)*(Raster("228")+Raster("229")+Raster("230")+Raster("231")+Raster("232")+Raster(
"233")+Raster("234")+Raster("235")+Raster("236")+Raster("237")+Raster("238")+Raster("239")+Raster
("240")+Raster("241")+Raster("242")+Raster("243")+Raster("244")+Raster("245")+Raster("246")+Raste
r("247"))
dummy  +=
Raster(kcndvi239)*(Raster("262")+Raster("263")+Raster("264")+Raster("265")+Raster("266")+Raster("
267")+Raster("268")+Raster("269")+Raster("270")+Raster("271")+Raster("272")+Raster("273")+Raster(
"274")+Raster("275")+Raster("276")+Raster("277")+Raster("278")+Raster("279")+Raster("280")+Raster
("281")+Raster("282"))
dummy  +=
Raster(kcndvi2310)*(Raster("283")+Raster("284")+Raster("285")+Raster("286")+Raster("287")+Raster(
"288")+Raster("289")+Raster("290")+Raster("291")+Raster("292")+Raster("293")+Raster("294")+Raster
("295")+Raster("296")+Raster("297")+Raster("298.")+Raster("299")+Raster("300"))
dummy  +=
Raster(kc_ndvi139)*(Raster("248")+Raster("249")+Raster("250")+Raster("251")+Raster("252")+Raster(
"253")+Raster("254")+Raster("255")+Raster("256")+Raster("257")+Raster("258")+Raster("259")+Raster
("260")+Raster("261"))
# save the  computation as HS_10_S2_nETc
# HS = Hargreaves Samani
```

```
# located in this instance at
X:\Users\Postgrad\Joseph\MSC_data_sets\Hargreaves_Samani_ETo\HS_10_Year2016_ETo
# 10 = 10 m spatial resolution
# S2 = Sentinal 2 based  crop  factor
# w = crop factor derived from S2 image and the normalised difference  vegetation indice

dummy.save("/Hargreaves_Samani_ETo/HS_10_ETc_S2_0/first")
```

Script A.3 Raw NDVI rescaled to commence from zero upwards

```
#Script sets values in image space below zero upto zero , to zero np.putmask(arr, arr <= 0, 0)
import arcpy
import numpy as np
from  arcpy.sa import *
from arcpy import env
env.overwriteOutput = True
ws1 = r"/New_folder"
arcpy.env.workspace = ws1
arcpy.env.scratchWorkspace = ("X:/Users/Postgrad/Joseph/testing.gdb")
#############################################################################################
inrast = "U:/New_Folder/ndvi2"
#s2ckc_26-4 stands for sentinel two (s2) , clipped crop coefficient (ckc) the 26th of April
(_26_4)
inRas = arcpy.Raster(inrast)
# readin .. extract the raster metadata
lowerLeft = arcpy.Point(inRas.extent.XMin,inRas.extent.YMin)
cellSize = inRas.meanCellWidth
dsc = arcpy.Describe(inRas)
sr = dsc.SpatialReference
ext =dsc.Extent
ll = arcpy.Point(ext.XMin,ext.YMin)
arr = arcpy.RasterToNumPyArray(inRas, nodata_to_value = 99999)
#####################################################################
#use the putmask numPy function to set  values of the input raster e.g s2ckc_26_4  below zero to
zero
#retrieved from the internet 13_9_2018:  "yield_23_10"
#####################################################################
#step one ndvi ranges from -1 to 1 and we want to use the ranges above zero that represent
vegetation
np.putmask(arr, arr <= 0, 0)
#step two use np.nditer to compute the Yields   from ndvi using the formulae
#  only done if you start with the raw ndvi values in this case this stage was done before 1.46
*ndvi- 0.26
############################################################################
#for x in np.nditer(arr, op_flags = ['readwrite']):
#      x[...] = 12.11 * x - 2.7307
####################################################################
# masking the product of the emperical relationship of VI and Kc
#np.putmask(arr, arr<= 0,0)
#####################################################################
newraster = arcpy.NumPyArrayToRaster(arr,lowerLeft,cellSize, value_to_nodata= 99999)
outrast = "U:/New_folder/ndvi_s0_S2"
newraster.save(outrast)
arcpy.DefineProjection_management(outrast,sr)
```

Script A.3.1 95th Percentile yield computation

```
import numpy as np
a = np.array ([vector of S₂ or L₈ modelled wheat yield values])
p = np.percentile (a, 95) # return 95ᵗʰ percentile value data value for each distribution
```

Script A.3.2 Arcpy L$_8$ wheat yield

```
import arcpy
import numpy as np
from  arcpy.sa import *
from arcpy import env
```

```
env.overwriteOutput = True
ws1 = r"/New_folder"
arcpy.env.workspace = ws1
arcpy.env.scratchWorkspace = ("X:/Users/Postgrad/Joseph/testing.gdb")
#####################################################################################
#arcpy.env.mask = "/study_area/study_area_extent"

inrast = "/Landsat8data/Processed_Landsat8_/2016_10_23/APAR_WDRVI_Kc_L8/ndvi_23_10"
#landast8 ndvi image whole scene
inRas = arcpy.Raster(inrast)
# readin .. extract the raster metadata
lowerLeft = arcpy.Point(inRas.extent.XMin,inRas.extent.YMin)
cellSize = inRas.meanCellWidth
dsc = arcpy.Describe(inRas)
sr = dsc.SpatialReference
ext =dsc.Extent
ll = arcpy.Point(ext.XMin,ext.YMin)
arr = arcpy.RasterToNumPyArray(inRas, nodata_to_value = 99999)
###########################################################################
#use the putmask numPy function to set  values of the input raster e.g s2ckc_26_4  below zero to
zero
#retrieved from the internet 13_9_2018:  "yield_23_10"
###########################################################################
#step one ndvi ranges from -1 to 1 and we want to use the ranges above zero that represent
vegetation
#np.putmask(arr, arr <= 0, 0)
#step two use np.nditer to compute the Yields   from ndvi using the formulae

#  only done if you start with the raw ndvi values in this case this stage was done before 1.46
*ndvi- 0.26
###############################################################################
for x in np.nditer(arr, op_flags = ['readwrite']):
     x[...] = 12.1136 * x - 2.7307
###########################################################################
# masking the product of the emperical relationship of VI and Kc
np.putmask(arr, arr<= 0,0)

###########################################################################
newraster = arcpy.NumPyArrayToRaster(arr,lowerLeft,cellSize, value_to_nodata= 99999)
outrast = "/Landsat8data/Yield_L8_23_10/23_10_30m"
#23_10_30m stands for 30 m spatial resolution L8 landsat8 imagery of 23_10_2016
newraster.save(outrast)
arcpy.DefineProjection_management(outrast,sr)
```

Script A.3.3 Arcpy S$_2$ wheat yield

```
The Script computes wheat yields based on the Mashaba et al.2017 Equation using Sentinel 2
imagery NDVI
import arcpy
import numpy as np
from  arcpy.sa import *
from arcpy import env
env.overwriteOutput = True
ws1 = r"/New_folder"
arcpy.env.workspace = ws1
arcpy.env.scratchWorkspace = ("X:/Users/Postgrad/Joseph/testing.gdb")
#####################################################################################
arcpy.env.mask = "/study_area/study_area_extent"
inrast = "/Landsat8data/Yield_L8_23_10/L8w_23_10_"
#landast8 ndvi image whole scene
inras = arcpy.Raster(inrast)
# readin .. extract the raster metadata
lowerLeft = arcpy.Point(inras.extent.XMin,inras.extent.YMin)
cellSize = inras.meanCellWidth
dsc = arcpy.Describe(inras)
sr = dsc.SpatialReference
ext =dsc.Extent
ll = arcpy.Point(ext.XMin,ext.YMin)
arr = arcpy.RasterToNumPyArray(inras, nodata_to_value = 99999)
###########################################################################
#use the putmask numPy function to set  values of the input raster e.g s2ckc_26_4  below zero to
zero
#retrieved from the internet 13_9_2018:  "yield_23_10"
###########################################################################
#step one ndvi ranges from -1 to 1 and we want to use the ranges above zero that represent
vegetation
#np.putmask(arr, arr <= 0, 0)
```

```
#step two use np.nditer to compute the Yields   from ndvi using the formulae

#  only done if you start with the raw ndvi values in this case this stage was done before 1.46
*ndvi- 0.26
###############################################################################
#for x in np.nditer(arr, op_flags = ['readwrite']):
#      x[...] = 12.11 * x - 2.7307
############################################################################
# masking the product of the emperical relationship of VI and Kc
np.putmask(arr, arr<= 0,0)


#########################################################################
newraster = arcpy.NumPyArrayToRaster(arr,lowerLeft,cellSize, value_to_nodata= 99999)
outrast = "/Landsat8data/Yield_L8_23_10/23_10_30m_0"
#23_10_30m stands for 30 m spatial resolution L8 landsat8 imagery of 23_10_2016
newraster.save(outrast)
arcpy.DefineProjection_management(outrast,sr)
```

APPENDIX B. **TABLES**

Table B 1 ET$_{0HS}$

MONTH	JANUARY	FEBRUARY	MARCH	APRIL	MAY	JUNE	JULY	AUGUST	SEPTEMBER	OCTOBER	NOVEMBER	DECEMBER	AVERAGE
ABENDRUHE	210.76	172.46	137.48	97.53	71.28	48.27	51.38	77.34	95.63	151.06	179.27	207.56	125.00
ASHANTI	210.40	170.59	135.15	97.24	70.52	47.66	52.27	77.15	97.47	153.52	179.20	201.43	124.39
BELLEVUE	208.73	170.27	132.38	96.81	69.64	47.57	53.17	77.50	99.31	155.95	179.76	193.85	123.75
BOKVELSKLOOF	205.80	171.05	130.94	95.19	68.40	47.83	52.94	78.62	102.07	154.79	182.81	186.46	123.08
DE POORT	204.00	170.98	128.01	94.78	66.73	48.44	52.67	80.60	104.32	153.01	184.16	180.77	122.37
FAIRVIEW	203.41	168.98	125.89	94.93	65.38	47.51	53.78	80.19	107.28	152.97	187.55	172.65	121.71
HLS BOLAND	203.48	168.54	124.15	93.68	65.34	46.42	54.47	80.85	107.84	154.84	189.17	165.91	121.22
IDEAL_POOL_HILL	204.73	166.45	124.02	91.38	66.31	45.35	54.90	81.77	108.63	156.74	190.41	158.99	120.81
KOPERFONTEIN	204.91	163.97	123.50	89.72	66.66	43.83	55.94	81.94	109.33	159.30	190.95	152.63	120.22
LANDAU	204.85	162.17	122.76	86.70	66.82	44.14	56.72	81.75	110.87	160.80	188.97	148.87	119.62
LANGGEWENS	204.09	159.94	122.71	84.12	65.85	45.35	57.65	81.50	112.61	161.76	189.56	142.47	118.97
MOORESBURG	202.58	158.74	121.90	82.97	64.86	45.80	58.18	82.47	112.30	164.22	191.44	134.80	118.35
NEDERBURG	201.68	157.71	120.38	81.30	64.90	46.04	57.65	83.97	113.31	164.74	192.85	128.78	117.78
PORTERVILLE	199.81	157.13	119.85	79.45	64.76	46.56	57.13	86.15	114.84	163.77	195.79	121.48	117.23
RIVIERA	198.66	158.13	117.84	77.58	63.93	47.59	56.66	88.64	116.91	163.93	197.14	113.87	116.74
SCHAAPKRAAL	197.64	158.21	116.81	76.26	62.50	47.71	57.66	89.05	118.42	167.35	195.95	107.43	116.25
ZUURVLAKTE	195.48	157.68	115.57	75.32	60.71	48.22	58.99	88.22	120.43	169.76	196.76	100.07	115.60

Table B 2 ET$_{0PM}$

MONTH	JANUARY	FEBRUARY	MARCH	APRIL	MAY	JUNE	JULY	AUGUST	SEPTEMBER	OCTOBER	NOVEMBER	DECEMBER	AVERAGE
IDEAL_POOL_HILL	243.32	158.58	148.71	103.26	65.40	48.80	44.90	70.61	97.00	150.08	205.46	236.34	131.04
PORTERVILLE	227.41	157.01	133.64	98.69	65.46	50.49	49.37	67.96	93.76	145.25	174.20	212.65	122.99
KOPERFONTEIN	212.16	189.53	130.01	88.69	79.48	44.46	47.01	68.06	87.97	136.34	168.72	189.34	120.15
ASHANTI	239.88	150.90	139.85	93.95	59.48	42.92	44.50	69.91	85.09	134.39	174.65	196.11	119.30
BOKVELDSKLOOF	195.87	153.71	132.00	88.50	59.31	48.65	50.61	82.95	94.37	138.00	172.51	202.79	118.27
RIVIERA	193.74	168.53	126.99	91.38	79.02	46.29	50.92	72.49	89.44	132.81	167.41	189.54	117.38
FAIRVIEW	227.64	137.25	132.65	88.67	64.40	44.06	46.21	67.78	84.15	137.22	171.88	193.33	116.27
HLS_BOLAND	202.72	171.09	126.30	84.75	63.55	43.06	46.79	67.22	86.76	136.45	171.77	188.55	115.75
MOORREESBURG	207.62	159.56	119.24	84.53	70.44	45.05	44.91	62.70	90.74	133.05	168.27	193.61	114.98
NEDERBURG	207.29	158.81	123.23	83.30	64.91	41.39	44.05	68.13	87.21	137.15	170.79	187.04	114.44
SCHAAPKRAAL	199.47	161.97	127.14	86.24	67.91	41.75	46.38	68.11	89.57	129.09	164.03	180.81	113.54
LANGGEWENS	202.70	147.93	127.21	88.62	63.32	46.33	45.76	68.39	85.04	133.96	165.70	186.09	113.42
BELLEVUE	199.31	181.68	120.78	77.46	69.24	39.14	41.38	64.19	80.47	128.34	158.42	177.44	111.49
LANDAU	185.41	164.55	118.90	82.19	66.39	41.11	44.62	66.54	97.49	127.80	152.71	173.70	110.12
ABENDRUHE	190.13	150.90	119.35	76.42	59.48	38.89	41.87	63.32	84.57	131.93	162.39	182.78	108.50
ZUURVLAKTE	181.01	160.06	114.48	79.57	64.14	43.00	44.08	72.31	77.58	121.32	152.58	177.26	107.28
DE_POORT	172.71	166.09	105.10	74.99	71.46	39.25	39.87	68.28	73.68	121.79	153.11	168.85	104.60

Table B 3 ET$_{0PM}$ less ET$_{0HS}$

MONTH	January	February	March	April	May	June	July	August	September	October	November	December
ABENDRUHE	-20.63	-21.56	-18.13	-21.11	-11.8	-9.38	-9.51	-14.02	-11.06	-19.13	-16.88	-24.782
ASHANTI	29.48	-19.69	4.7	-3.29	-11.04	-4.74	-7.77	-7.24	-12.38	-19.13	-4.55	-5.32
BELLEVUE	-9.42	11.41	-11.6	-19.35	-0.4	-8.43	-11.79	-13.31	-18.84	-27.61	-21.34	-16.412
BOKVELDSKLOOF	-9.93	-17.34	1.06	-6.69	-9.09	0.82	-2.33	4.33	-7.7	-16.79	-10.3	16.33
DE_POORT	-31.29	-4.89	-22.91	-19.79	4.73	-9.19	-12.8	-12.32	-30.64	-31.22	-31.05	-11.924
FAIRVIEW	24.23	-31.73	6.76	-6.26	-0.98	-3.45	-7.57	-12.41	-23.13	-15.75	-15.67	20.678
HLS_BOLAND	-0.76	2.55	2.15	-8.93	-1.79	-3.36	-7.68	-13.63	-21.08	-18.39	-17.4	22.636
IDEAL_POOL_HILL	38.59	-7.87	24.69	11.88	-0.91	3.45	-10	-11.16	-11.63	-6.66	15.05	77.35
KOPERFONTEIN	7.25	25.56	6.51	-1.03	12.82	0.63	-8.93	-13.88	-21.36	-22.96	-22.23	36.71
LANDAU	-19.44	2.38	-3.86	-4.51	-0.43	-3.03	-12.1	-15.21	-13.38	-33	-36.26	24.835
LANGGEWENS	-1.39	-12.01	4.5	4.5	-2.53	0.98	-11.89	-13.11	-27.57	-27.8	-23.86	43.618
MOORREESBURG	5.04	0.82	-2.66	1.56	5.58	-0.75	-13.27	-19.77	-21.56	-31.17	-23.17	58.805
NEDERBURG	5.61	1.1	2.85	2	0.01	-4.65	-13.6	-15.84	-26.1	-27.59	-22.06	58.263
PORTERVILLE	27.6	-0.12	13.79	19.24	0.7	3.93	-7.76	-18.19	-21.08	-18.52	-21.59	91.173
RIVIERA	-4.92	10.4	9.15	13.8	15.09	-1.3	-5.74	-16.15	-27.47	-31.12	-29.73	75.666
SCHAAPKRAAL	1.83	3.76	10.33	9.98	5.41	-5.96	-11.28	-20.94	-28.85	-38.26	-31.92	73.384
ZUURVLAKTE	-14.47	2.38	-1.09	4.25	3.43	-5.22	-14.91	-15.91	-42.85	-48.44	-44.18	77.194

Table B 4 Study average montly ET$_{0PM}$ and ET$_{0HS}$

MONTH	ET$_{0PM}$	Standard deviation ET$_{0PM}$	ET$_{0HS}$	Standard deviation ET$_{0HS}$
January	205.2	19.20	203.6	16.09
February	161.1	12.03	164.3	23.34
March	126.2	9.73	124.7	25.21
April	86.5	7.38	87.9	31.84
May	66.7	5.73	66.2	10.87
June	43.8	3.37	46.7	5.74
July	45.5	2.91	55.4	9.52
August	68.8	4.41	82.2	15.39
September	87.3	6.26	108.9	29.02
October	133.8	7.04	159.3	22.77
November	167.9	11.84	188.9	24.54
December	190.4	15.49	154.0	133.80
Average		8.78		29.06

Table B 5 Relative difference [ET0PM-ET0HS]/ET0PM as %

A-ABENDRUHE; B-ASHANTI; C-BELLEVUE; D-BOKVELDSKLOOF; E-DE_POORT; F-FAIRVIEW; G-HLS_BOLAND; H-Ideal_Hill_Pools; I-KOPERFONTEIN;J-LANDAU; K-LANGGEWENS; L-MOORREESBURG; M-NEDERBURG; N-PORTERVILLE; O-Riviera; P-SCHAAPKRAAL; Q-ZUURVLAKTE

MONTH	A	B	C	D	E	F	G	H	I	J	K	M	N	N	O	P	Q	ALL
Jan	-10.85	12.29	-4.73	-5.07	-18.12	10.64	-0.38	15.86	3.42	-10.48	-0.69	2.43	2.71	12.14	-2.54	0.92	-8.00	7.13
Feb	-14.29	-13.05	6.28	-11.28	-2.95	-23.12	1.49	-4.96	13.49	1.44	-8.12	0.51	0.69	-0.07	6.17	2.32	1.49	6.57
March	-15.19	3.36	-9.60	0.80	-21.79	5.09	1.70	16.60	5.01	-3.25	3.54	-2.23	2.32	10.32	7.21	8.12	-0.95	6.89
April	-27.63	-3.51	-24.98	-7.56	-26.39	-7.06	-10.53	11.50	-1.16	-5.49	5.08	1.85	2.40	19.49	15.10	11.58	5.35	10.98
May	-19.83	-18.56	-0.58	-15.33	6.61	-1.52	-2.81	-1.39	16.13	-0.65	-4.00	7.93	0.02	1.07	19.10	7.97	5.34	7.58
June	-24.12	-11.05	-21.55	1.68	-23.41	-7.82	-7.79	7.06	1.41	-7.37	2.12	-1.66	-11.24	7.79	-2.81	-14.26	-12.15	9.72
July	-22.71	-17.47	-28.50	-4.61	-32.10	-16.39	-16.40	-22.27	-19.00	-27.12	-25.98	-29.55	-30.87	-15.71	-11.27	-24.32	-33.83	22.24
Aug	-22.14	-10.36	-20.73	5.22	-18.04	-18.30	-20.27	-15.80	-20.40	-22.86	-19.18	-31.54	-23.25	-26.76	-22.27	-30.74	-22.00	20.58
Sept	-13.08	-14.55	-23.41	-8.16	-41.58	-27.49	-24.29	-11.99	-24.28	-13.72	-32.42	-23.76	-29.92	-22.48	-30.71	-32.21	-55.23	25.25
Oct	-14.50	-14.24	-21.51	-12.17	-25.64	-11.48	-13.48	-4.44	-16.84	-25.82	-20.75	-23.43	-20.12	-12.75	-23.43	-29.64	-39.93	19.42
Nov	-10.39	-2.61	-13.47	-5.97	-20.28	-9.11	-10.13	7.32	-13.18	-23.74	-14.40	-13.77	-12.91	-12.39	-17.76	-19.46	-28.96	13.87
Dec	-13.56	-2.71	-9.25	8.05	-7.06	10.70	12.01	32.73	19.39	14.30	23.44	30.37	31.15	42.87	39.92	40.59	43.55	22.45
RD %	14.57	7.84	12.62	6.36	16.16	10.15	8.71	9.50	10.94	9.90	11.09	11.42	11.17	13.01	15.38	16.41	17.92	